TECHNISCHE UNIVERSITÄT BERGAKADEMIE FREIBERG

B. Merkel, Ch. Wolkersdorfer, A. Hasche (Hrsg.)

Trace Elements and Isotopes in Geochemistry – Fluids and Solids

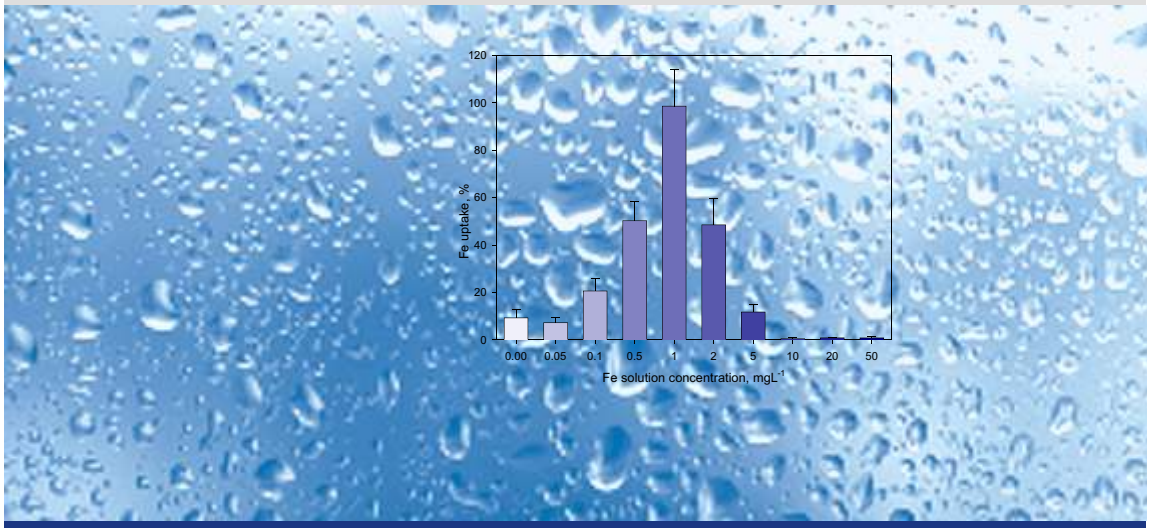

Wissenschaftliche Mitteilungen

INSTITUT FÜR GEOLOGIE

24

Freiberg

2003

TU BERGAKADEMIE FREIBERG

54. Berg- und Hüttenmännischer Tag

Workshop

"Trace Elements and Isotopes in Geochemistry – Fluids and Solids"

20. Juni 2003

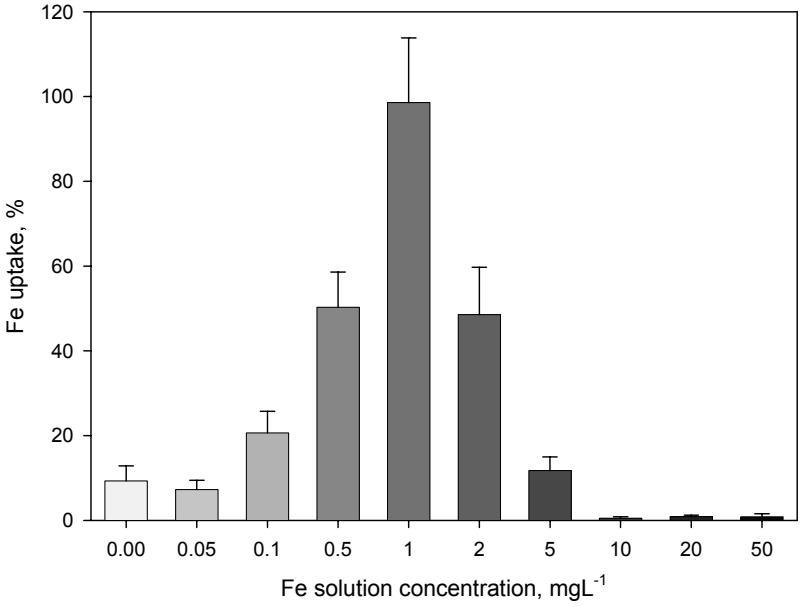

Lehrstuhl für Hydrogeologie

Prof. Dr. Broder Merkel
Dr. Christian Wolkersdorfer
Dipl.-Geol. Andrea Hasche


BERGAKADEMIE
TECHNISCHE
UNIVERSITÄT
FREIBERG

TECHNISCHE UNIVERSITÄT BERGAKADEMIE FREIBERG
Institut für Geologie

Wissenschaftliche Mitteilungen

24

Freiberg
2003

B. Merkel, Ch. Wolkersdorfer, A. Hasche (Hrsg.)

Trace Elements and Isotopes in Geochemistry – Fluids and Solids

Proceedingsband zum Workshop am Geologischen Institut der TU Bergakademie Freiberg am 20. Juni 2003

13 Beiträge, 97 Seiten, 55 Abbildungen, 17 Tabellen, 165 Literaturstellen

Herausgeber: Technische Universität Bergakademie Freiberg
Institut für Geologie

Förderkreis Freiberger Geologie

Internet: http://www.geo.tu-freiberg.de/publikationen/wiss_mitteilungen.html

Redaktion und Manuskriptannahme: TU Bergakademie Freiberg
Institut für Geologie
Dr. P. G. Dietrich
Gustav-Zeuner-Straße 12
09596 Freiberg
☎ +49(0)3731/39-2789
Fax +49(0)3731/39-2720
E-Mail dietrip@geo.tu-freiberg.de

Vertrieb: Akademische Buchhandlung
Inh. B. Hackel
Merbachstraße
Postfach 1445
09599 Freiberg
☎ +49(0)3731/22198
Fax +49(0)3731/22644

ISSN 1433-1284

Gesamtherstellung: Medienzentrum der TU Bergakademie Freiberg

Printed in Germany

Inhaltsverzeichnis


BERGAKADEMIE
TECHNISCHE
UNIVERSITÄT
FREIBERG

Vorwort

Spurensuche am Tatort – wer kennt dieses Szenario nicht? Aber nicht nur in der Kriminologie, sondern auch in der Umweltforschung bedienen wir uns in zunehmenden Maß innovativer Technologien, um Spurenbestandteile bis hin zu Einzelmolekülen in einer Matrix (z.B. Gestein, Wasser, Bioproben) zu identifizieren. Statt Sporen setzen wir beispielsweise industriell gefertigte Mikrosphären aus der Medizintechnik als Tracer in aquatischen Systemen ein, DNA-Analysen geben uns Hinweise auf Mikroorganismen und deren Stoffwechselprodukte, Selten-Erd-Elemente können mittels ICP-MS bis in den pg/L-Bereich bestimmt werden und liefern uns Hinweise auf Fließwege von Wasser im Untergrund.

Im Rahmen des Freiberger Forschungsforums / 54. Berg- und Hüttenmännischer Tag 2003 soll das Kolloquium 1 mit dem Titel „Trace Elements and Isotopes in Geochemistry – Fluids and Solids“ einen kleinen Beitrag leisten, die Vielfalt der analytischen Möglichkeiten moderner Geo-Technologien aufzuzeigen und zu diskutieren.

Vorliegende Proceedings fassen die Beiträge in alphabetischer Auflistung der Autoren zusammen. Ein weites Spektrum an Wissenschaftlern aus den Geowissenschaften, der Physik, Chemie und Archäometrie hat sich zusammengefunden, um über aktuelle Ergebnisse aus der Forschung im Wasser, im Boden und der Luft zu berichten. Dabei zeigt sich, wie schon in den vergangenen Jahren, dass der Spurenelementanalytik mit der ICP-MS eine immer größere Bedeutung zukommt. Möglicherweise werden sich dank dieser leicht verfügbaren Technik neben den Selten-Erd-Elementen künftig noch andere Spurenelemente als geeignete Tracer in den Kompartimenten Wasser, Boden und Luft erweisen.

Wir bedanken uns bei allen Fachkollegen aus dem In- und Ausland für ihre wissenschaftlichen Beiträge und bei den Organisatoren der Tagung für ihr Engagement.

Freiberg/Sachsen, den 6.6.2003

Prof. Dr. Broder J. Merkel Dr. Ch. Wolkersdorfer

Hydrogeologische Probenahme im Bergwerksstollen.


BERGAKADEMIE
TECHNISCHE
UNIVERSITÄT
FREIBERG

Heavy metals in water - suspended matter system in the Odra River

Ewa Adamiec, Edeltrauda Helios–Rybicka

University of Mining and Metallurgy, Faculty of Geology, Geophysics and Environmental Protection, Al. Mickiewicza 30, Kraków

The extensive investigations of total and mobile heavy metals concentrations in water and suspended matter (SPM) of the upper and middle Odra river were carried out over the years 1997 – 2000. The highest metal pollution of the Odra river spm was found with cadmium, zinc, lead and arsenic. The levels of water pollution vary in the wide ranges, depending on metal. Highest Cd, Cu and Zn concentrations in water were observed particularly in middle part of the Odra River at the Lubin - Legnica Cu-mining and processing region. Such high metals concentration is caused mainly due to agricultural and industrial activities such as: petrochemicals, petroleum refining, steel works foundries and non-ferrous metal-works (ADAMIEC, HELIOS–RYBICKA & BEHRENS 2000; HELIOS–RYBICKA 1996).

From all metals studied in suspended matter, Cd, Zn and As appear to be of particular concern because of the high level, that appear to be bioavailable, and their high mobility. The exchangeable and carbonatic fractions of Cd and Zn reached up to 50 % of their total amount.

1 Introduction

The study area covered about 70 % of the total Odra catchment area. At the upper and middle Odra river catchment area, industrial – mainly coal and copper mining and processing activity, as well as agricultural, intensive crop production are the most important sources of contaminations.

The objectives of the study were: (1) to measure concentrations of heavy metals (Cd, Zn, Pb, Cu, Ni, Cr, Mn, Fe and As) for water and suspended matter in the upper and middle Odra river system. (2) To assess the level of contamination by comparison with the river solids classification or geochemical background standards, and to identify any need for monitoring (3) To estimate the mobility and potential bioavailability of metals in the river suspended matter.

2 Sampling and Methods

Totally over 100 samples were collected from both, water and suspended matter, from the upper and middle Odra river (516 km), in five samplings from November 1997 to May 2001. The Odra river suspended matter samples have been separated from the river water on the membrane filters with porous of 0.45 μm diameter and its concentration was established. The obtained samples were undergone an analytical procedure described earlier (HELIOS–RYBICKA & KNÖCHEL 2000).

In order to assess the mobility and potential bioavailability of the metals in the suspended matter, the exchangeable and carbonatic bound metal fraction was estimated, using chemical extraction method proposed by KERSTEN & FÖRSTNER (1986). Metal concentrations were determined using ICP-MS and/or TXRF methods.

3 Data quality control

The analyses were subject to sampling and analytical quality program to describe random errors by Robust Analysis of Variance, with ROB2 program application (RAMSEY 1993). During sampling in May 2000, the filed duplicates of water and spm samples were taken. These samples were analysed twice as analytical duplicates. Robust analysis of variance was applied to estimate the precision (sampling and analytical variances) in comparison to geochemical variances.

For most elements measured in water samples (except arsenic) data quality control was satisfying. In a case of suspended matter, results of Cd, Ni, Cr, Cu measurements indicates an excellent precision. The analytical precision for Cd, Pb and particularly for Ni is not enough satisfying.

In order to estimate accuracy of the analytical method, reagent blanks and certified reference materials (Lake Sediment LSKD-4, riverin water 1643d) were used to assure criteria related to quality of the analytical results. Unambiguous of ICP-MS technique was confirmed in case of suspended matter by TXRF.

4 Results and discussion

The heavy metals concentration in the Odra river water vary in the wide ranges. The statistical parameters are showen in table 1.

In order to estimate the Odra river water contamination with heavy metals, obtained results were assessed by LAWA classification for water (IRMER 2000). The results are presented in figure 1 (ADAMIEC & HELIOS–RYBICKA 2002a).

Highest values of arsenic in water were measured in samples taken in May 98, particularly in the upper Odra river at Krapkowice (8.10 µg/L), as well as at Brzeg Dolny and Nietków sampling points, at the Cu-mining and processing region.

Most of the samples are moderately to strongly and/or very strongly contaminated with Cd (fig.1). Taking into account four sampling campaigns, the Odra river water is characterized by slightly decreased with Cd contamination. Highest concentrations of Cd were observed in the water samples taken near Nietków and Krosno Odrzańskie.

Observed concentrations of Cr in water were rather stable (µg/L): 3.43 in May 98, 3.25 in November 98, 3.80 in June 99 and 4.35 in May 2000. Most of the samples can be classified from unpolluted to moderately polluted with Cr - classes I to II (fig. 1).

The level of contamination with Pb increased during the period 1998 – 2000. Highest concentrations of Pb in the Odra river water were detected in May 98 (7.84µg/L) at Nietków and in samples taken in November 98 in Brzeg Głogowski (5.67 µg/L) and in Obrzyca (5.40 µg/L).

Generally most of the water samples are moderately contaminated with Cu – LAWA class II.

The concentration of Ni in water is getting higher and higher taking into consideration following sampling campaigns. Highest concentration of Ni was measured in samples taken in November 98 in tributaries Osobłoga 36, 99 µg/L.

Concentration of Zn in water shows that average values of the individual sampling campaigns is rather high and vary in narrow ranges from 40.02 µg/L in June 99 up to 48.26 µg/L in November 98. Most of the samples are strongly contaminated. Samples taken in Cu-mining and smelting region are strongly and very strongly contaminated with Zn and highest concentrations were found in water samples taken in May 98.

Table 1: Statistical parameters of metals content in water of the upper and middle Odra River.

Parameters	As	Cd	Cr	Cu	Ni	Pb	Zn	Fe	Mn
n=85					µg/L				
Minimum	0.376	<0.02	<0.21	0.550	0.259	<0.1	12.4	16.2	5.91
Maximum	8.10	0.867	12.7	54.6	27.2	7.84	535	1861	353
arithmetical average	2.33	0.140	4.78	8.24	5.34	1.77	55.4	250	73.3
geometrical average	1.91	0.075	3.74	5.81	4.01	1.41	45.9	165	55.2
median	1.75	0.082	3.93	5.65	4.20	1.45	43.0	154	54.5
std. deviation	1.70	0.186	3.00	8.64	4.34	1.26	57.6	298	58.5

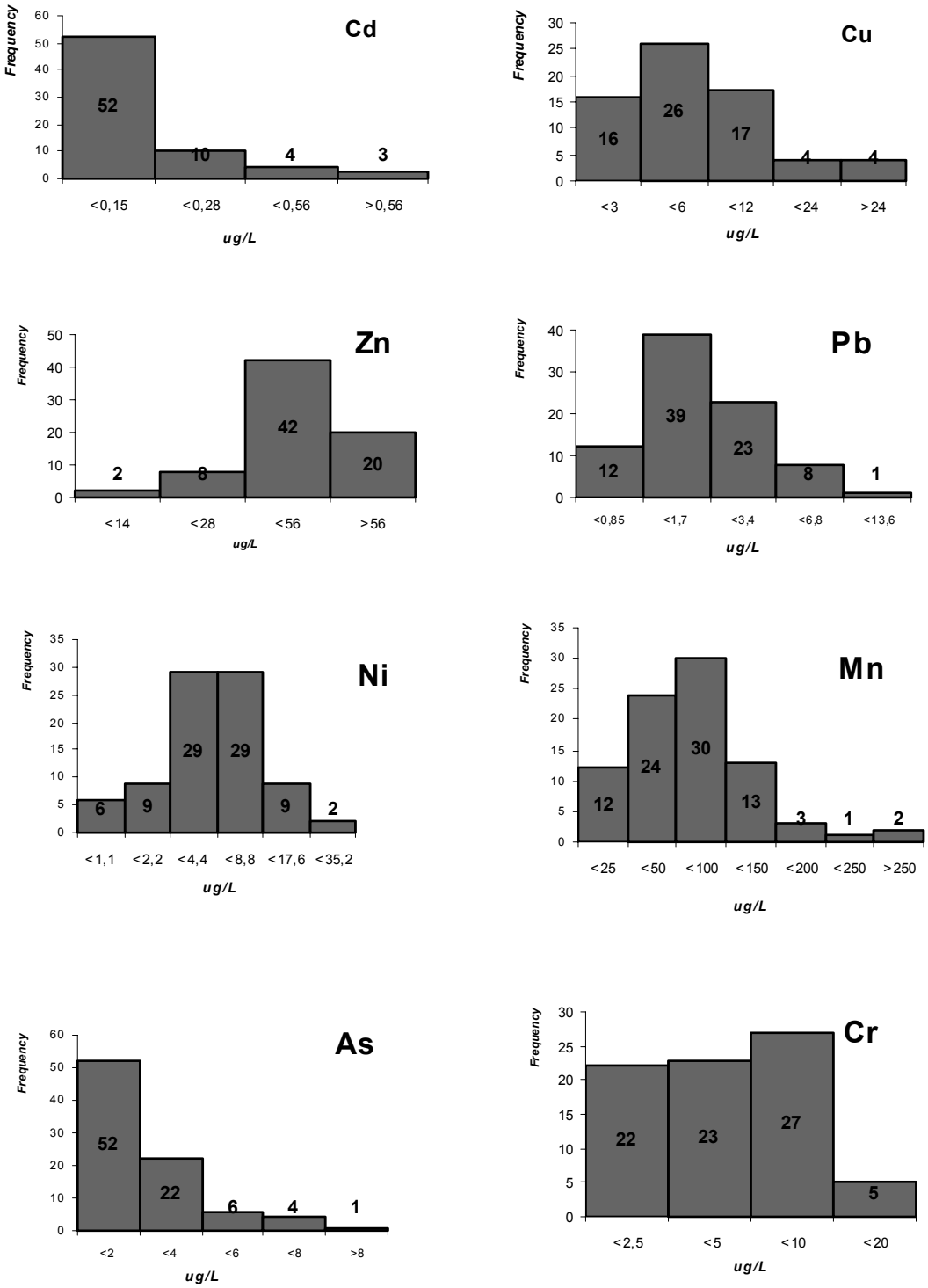

Figure 1: Occurrency of metals in water of the Odra River.

Table 2: Statistical parameters of heavy metals concentrations in the suspended particulate matter (SPM; *from Chałupki to Krosno Odrzańskie)* of the upper and middle Odra river; SPM concentrations.

		As	Cd	Cr	Cu	Ni	Pb	Zn	Mn	Fe
SPM n= 101	SPM Conc. mg/l	mg/kg								
min	1.2	8.0	1.8	42.4	6.2	22.1	24.4	351	1152	20806
max	116	302	39.8	351	493	1287	401	31369	11010	121316
arithm.mean	28.9	63.8	9.3	131	98.4	133	110	1867	4168	50679
geom.mean	23.0	50.5	8.0	120	77.9	88.9	98.0	1321	3637	47929
median	26.5	52.9	7.3	125	79.2	81.6	97.2	1221	4051	48822
SD	18.9	47.4	6.2	57.4	76.3	165	55.9	3430	2060	17309

5 Suspended particulate matter

Totally about 100 samples of suspended particulate matter (SPM) in the upper and middle Odra river, in five samplings: November ’97, May ’98, November ’98, June ‘99 and May 2000 were taken for analysis. Table 2 shows the statistical parameters of metal contents obtained for all of the SPM samples.

In the SPM samples taken in November ’97, the concentration of Cd, Cr, Cu and Pb was higher than in the samples from later sampling periods. The highest concentrations of Ni (1287), Zn (31369) and As (302) were stated in the samples from May ’98 (ADAMIEC & HELIOS–RYBICKA 2000; ADAMIEC & HELIOS–RYBICKA 2002b).

The results of metal concentrations determined in the suspended matter could be expressed in terms of LAWA classification (RAMSEY 1993). Figure 2 shows the LAWA classifying metals contamination of the SPM in the upper and middle Odra river, for the two samplings. The obtained results showed that the strong to very strong contamination (classes III/IV and IV) of the suspended matter for almost all samples along the Odra river over two sampling periods. Only sporadically the class III was stated, thus slight improvement of Cd contamination in the SPM from May 2000 could be observed.

With Pb, Zn and Cu the situation was at no time as critical as with Cd. Strong and moderate contamination for Pb and Cu (II-III, III classes) and very strong and strong for Zn (III-IV, III classes) was typical for ’97. However, after three years the situation has been improved, and in 2000, class II - moderate contamination with Cu, Zn, and in the upper river section with Pb, was dominated.

6 Conclusions

Results of the study carried out starting in May 98 showed that water samples have been strongly contaminated with cadmium, zinc and copper. The detected levels of the metal concentrations were found exceed the LAWA target values i.e., for Cd: 0.072 µg/L, Zn: 14 µg/L, Cu: 4 µg/L (ADAMIEC & HELIOS–RYBICKA 2002b). In case of Ni about 50% of the samples have concentration higher than target value 4,4 µg/L. Taking into considerations Cr – 93% and Pb – 85 % of the samples do not exceed target levels - 10 µg/L and 3.4 µg/L, respectively.

Highest Cd, Cu and Zn concentrations were observed particularly in the middle Odra River water and suspended matter, at the Lubin – Legnica Cu-mining and processing region. Generally the level of the metal contamination in the Odra river depends on the elements, sampling points for most of the metals and for Zn, As and Cr in water on sampling season.

The detected levels of metal contamination, mainly Zn, Cu, Pb and Cd, in the most of suspended matter of the Odra river were found to exceed the geochemical background or threshold values. The highest metal pollution of the Odra river system was found with cadmium, zinc, lead and arsenic. From the metals that were studied, Cd seems to be of particular concern because of high level and their high mobility in suspended matter, along river course. Particular in the suspended matter the carbonates play an important role in the accumulation processes of metals. The results showed that the dilution, re–suspension, and re–deposition processes at extreme high the Odra river water events in July 1997 have caused additional increase of metal

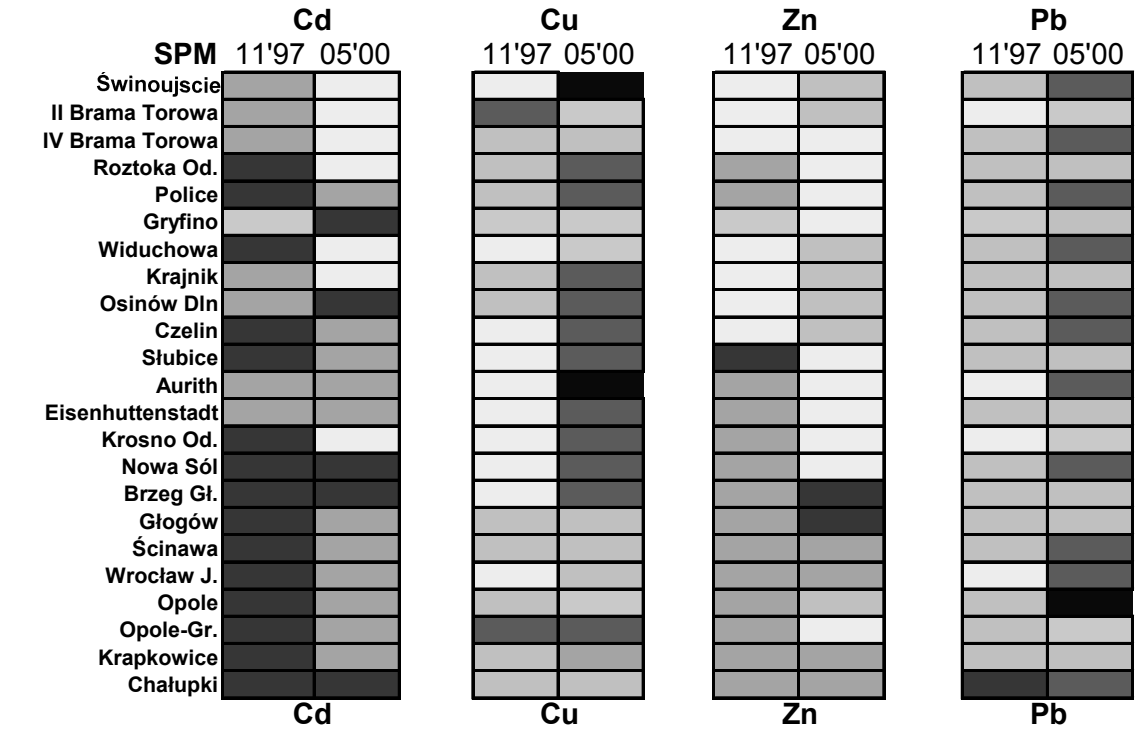

LAWA classes		[mg/kg]	Cu	Cd	Zn	Pb
IV	Very strongly contaminated		640	9.6	3200	800
III-IV	Strongly to very strongly contaminated		320-640	4.8-9.6	1600-3200	400-800
III	Strongly contaminated		160-320	2.4-4.8	800-1600	200-400
II-III	Moderately to strongly contaminated		80-160	2.4-1.2	400-800	100-200
II	Moderately contaminated		40-80	1.2-0.6	200-400	50-100
I-II	Unpolluted to moderately contaminated		20-40	0.6-0.3	100-200	25-50
I	Uncontaminated		<20	<0.3	<100	<25

Figure 2: The heavy metals situation in the Odra River suspended matter and bottom sediments from November 1997 and May 2000, expressed in LAWA classes.

concentrations in the suspended matter immediately after flood

References

ADAMIEC E., HELIOS–RYBICKA, E. & BEHRENS, K. (2000): Heavy metals in water and suspended matter in the Odra River after the flood in 1997. Intern Research Conference. Physicochemical problems of natural waters ecology. Szczecin, Poland, pp. 20.

HELIOS–RYBICKA, E. (1996): Environmental impact of mining and smelting industries in Poland. In: Environ. Geochem. Health. Geol. Soc. Sp. Publ. 113, pp 183 –193.

HELIOS–RYBICKA, E. & KNÖCHEL, A. (2000): Crucial load in the river Odra – impacts of floods on the situation of hazardous substances. IBMBF Symposium, Elbeforschung, Gewässer Landschaften, 21, pp 79–99.

KERSTEN, M. & FÖRSTNER, U. (1986): Chemical fractionation of heavy metals in anoxic estuarine and coastal sediments. Water Sci. Technol. 18, pp 121-130.

RAMSEY, M.H. (1993): Sampling and analytical quality control (SAX) for improved error estimation in the measurement of Pb in the environment using robust analysis of variance. App. Geochem. 2, pp 149-153.

IRMER, U. (2000): Requirements for the Implementation of the EC Water Framework Directive in Germany. Sediment Assessment in European River Basins. ISSN 1431–2409. BfG, 22 26-37.

ADAMIEC, E. & HELIOS–RYBICKA, E. (2000): Changes of heavy metals concentrations in suspended matter of the Odra river after the flood in 1997. Proc. of 5th Intern. Symp. Exhib. on Environmental Contamination in Central and Eastern Europe. Prague, Sept. 2000. pp 7.

ADAMIEC, E. & HELIOS–RYBICKA, E. (2002a): Heavy metals distribution in water of the upper and middle Odra river in period 1998 – 2000. Part IV International Odra Project. Polish Journal of Environmental Studies. Vol 11, No 6, 669-673.

ADAMIEC, E. & HELIOS–RYBICKA, E. (2002b): Assessment of total and mobile heavy metals content in the suspended matter and sediments of the Odra river system recommendations for river chemical monitoring. Part IV International Odra Project. Polish Journal of Environmental Studies. Vol 11, No 6, 675, 688.

Geochemistry and REE pattern of acidic pit lakes in Lower Lusatia (Germany)

Elke Bozau[1], Kurt Friese[1], Hans-Joachim Stärk[2]

UFZ – Umweltforschungszentrum Leipzig-Halle GmbH

[1] Sektion Gewässerforschung, Magdeburg, Brückstraße 3a, D-39114 Magdeburg

[2] Sektion Analytik, Leipzig, Permoserstraße 15, D-04318 Leipzig

Three acidic pit lakes of a former lignite mine were investigated for main components and rare earth elements (REE). The highest REE concentration and fractionation (enrichment of light rare earth elements) are correlated to the lowest pH-value and the highest mineralisation of the lake water.

1 Introduction

There are more than 100 acidic pit lakes in Lower Lusatia (Germany) caused by pyrite oxidation in the surrounding dump sediments (GELLER et al. 1998). A sequence of such pit lakes developed in the former lignite mine Plessa-Koyne (Figure 1). These lakes with pH-values of about 3 can not be used as drinking water reservoirs or for recreation activities.

The geochemistry and the rare earth element (REE) contents of three acidic pit lakes ("RL 107", "RL 111", "RL 117") were investigated. Mining periods and morphological data of the investigated lakes are given in Table 1.

2 Methods

Water samples of the lakes "RL 107" and "RL 117" were taken in 1997, water samples of the lake "RL 111" in 1997 and 2001. Temperature, pH, redox potential and O_2 in the water column were measured by a multi-parameter probe (Idronaut). Water samples were taken with a water sampler (Limnos). Chemical analyses were performed by ionic chromatography (SO_4, NO_3, Cl), photometry (NH_4), and ICP-OES (Ca, Mg, K, Na, Fe_{tot}, Al) on 0.45 µm filtered samples.

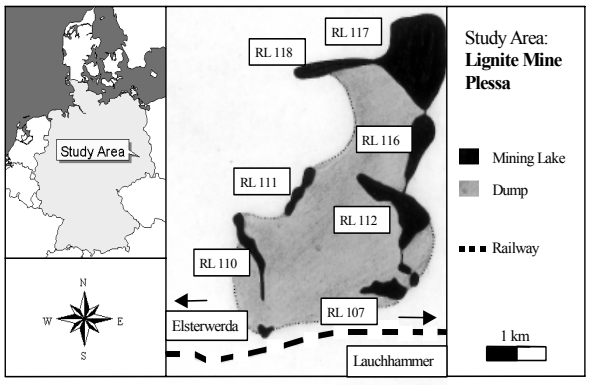

Figure 1: The former lignite mine Plessa-Koyne with the acidic pit lakes (BOZAU & STRAUCH 2002).

High REE contents in the lake water of all three lakes allowed a fast and relatively simple analysis by ICP-MS without pre-concentration. The chemical method is described in more detail by Bozau et al. (in review). In 1997, not all REE were analysed. The detection limits were improved in 2001.

A detailed geochemical investigation of the mining lake "RL 111" is still going on. Therefore, recent data of this lake are available. Since 1996, remarkable changes of the water chemistry of the mining lake "RL 111" did not occur (KNÖLLER 2000; BOZAU & STRAUCH 2002). In 2002, measurements by the multi-parameter probe indicated that the pH-values of the lakes "RL 107" and "RL 117" are still the same as measured in 1997.

3 Results

The lake water of all investigated lakes has low pH-values, as well as high iron and sulphate concentrations (Table 2, Figure 2). Lake "RL 107" has the lowest pH (2.4) and the highest iron and sulphate concentrations, whereas the lake "RL 117" with a pH-value of 3.0 shows lower iron and sulphate concentrations. K, Na, and Cl do not increase with lower pH-values. The lowest values are measured in pit lake "RL 107". Maybe the precipitation of minerals (e.g.

Table 1: Description of the investigated pit lakes (LENAB 1998).

	RL 107	**RL 111**	**RL 117**
Mining period	1897 – 1928	1929 – 1958	1956 -1966
Water level (m a.m.s.l.)	92.3	94.1	92.3
Area (m^2)	122,000	107,000	950,000
Volume (m^3)	230,000	500,000	10,450,000
Max. depth (m)	4.0	10.2	14.0
Average depth (m)	1.9	4.6	11.0

jarosite) from the lake water is responsible for the low K- and Na-values (GÖTTLICHER et al. 2001).

The chemical differences of the three lakes can be explained by the amount of inflowing acidified groundwater correlated to the extent of the bordering dump area. Erosion processes from the dump sediments on the lake shore also contribute to the lake acidification. If there is no thermal stratification in shallow lakes (e.g. lake "RL 107"), neutralisation processes by sulphate and iron reduction in the lake sediments are nearly impossible (PEINE 1998).

The REE concentrations show no significant change within the water profile of each lake and can be correlated with the pH-value and the mineralisation of the water (Figure 3). The North American Shale Composite (NASC, TAYLOR & MCLENNAN 1985) normalised REE pattern are characterised by an enrichment of the light rare earth elements (LREE). The enrichment of the light REE is also correlated with the pH-value. The lake "RL 107" with the lowest pH shows the highest enrichment of REE (La/Y 3.5), whereas the lake "RL 111" has a La/Y-ratio of 3.0. The REE fractionation probably increases with the acidification process. Speciation calculations indicate that the formation of sulphate complexes do not fractionate REE and can not be responsible for the light REE enriched pattern found in the acidic waters of the investigated mining lakes (BOZAU et al., in review; GIMENO SERRANO et al. 2000).

Compared to other acidic waters (caused by acid rain or pyrite oxidation) the enrichment of LREE seems to be untypical (BOZAU et al., in review). An enrichment of middle rare earth elements (MREE) is mostly found in acidic mine waters (ELBAZ-POULICHET & DUPUY 1999; WORRAL &

Table 2: Chemical characteristics of the investigated lakes (surface water, sampled in April 1997).

	RL 107	**RL 111**	**RL 117**
pH	2.4	2.6	3.0
Ca (mg/l)	327	229	102
Mg (mg/l)	45	29	15
K (mg/l)	3.3	3.6	4.3
Na (mg/l)	5.0	5.0	9.1
Fe (mg/l)	585	175	21
Al (mg/l)	47	38	1.7
SO_4 (mg/l)	2370	1320	429
Cl (mg/l)	4.4	8.5	17
NH_4-N (mg/l)	5.0	2.7	1.6
NO_3-N (mg/l)	0.9	0.3	0.1
La (µg/l)	182	75	2.6
Ce (µg/l)	390	169	6.7
Pr (µg/l)	34	15	0.6
Nd (µg/l)	118	52	2.3
Sm (µg/l)	18	8	0.42
Eu (µg/l)	4.5	2	<0.1
Dy (µg/l)	15	7	0.4
Ho (µg/l)	2.8	1.3	<0.1
Er (µg/l)	7.7	3.5	0.2
Tm (µg/l)	0.9	0.5	<0.1
Yb (µg/l)	5.0	2.5	<0.1
Lu (µg/l	0.7	0.3	<0.1

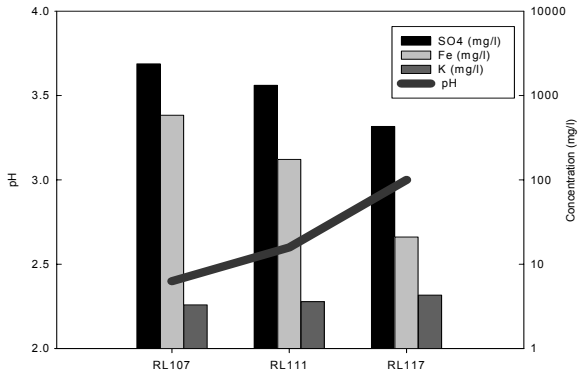

Figure 2: SO_4, Fe, K concentrations (mg/l) and pH-value of the investigated acidic pit lakes (measured in 1997).

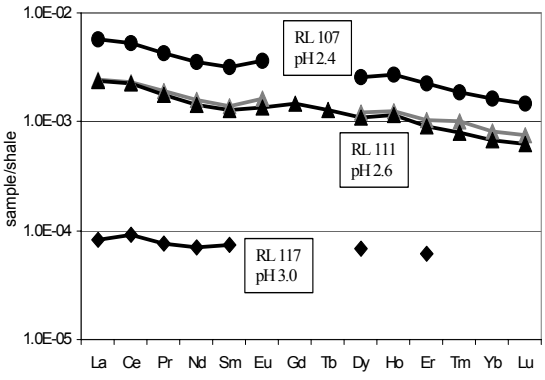

Figure 3: NASC normalised REE pattern of the investigated acidic pit lakes (Lakes "RL 107" and "RL 117" measured in 1997, lake "RL 111" measured in 1997 and 2001).

PEARSON 2001).

Lignite of the exploited seam has REE contents in the magnitude of the average shale and is also characterised by an enrichment of LREE. First REE investigations of lignite containing dump sediments (data not shown) lead to the conclusion that weathering processes combined with microbiological activity could be responsible for these uncommon REE pattern of the lake water.

4 Conclusions

The investigation of the three acidic lakes showed that the behaviour of REE depends on the acidification processes. The highest REE concentration and fractionation of the lake water are correlated to the lowest pH-value and the highest sulphate and iron concentrations. An enrichment of LREE in the NASC normalised pattern is typical for the investigated pit lakes.

Further investigations including other lakes of the former pit area, groundwater and dump sediments can be useful to understand the fractionation of REE during pyrite oxidation, as well as the geochemical development of the study area.

Acknowledgements

Special thanks are due to our colleagues from the Departments of Freshwater Research and Hydrogeology (UFZ), who assisted sampling and carried out chemical analyses.

References

BOZAU, E., LEBLANC, M., SEIDEL, J.L., STÄRK, H.-J.: Light rare earth elements enrichment in an acidic mining lake (Lusatia, Germany). Applied Geochemistry (in review).

BOZAU, E., STRAUCH, G. (2002): Hydrogeological aspects on biotechnological remediation of the acidic mining lake 111, Lusatia (Germany). Water, Air, and Soil Pollution: Focus, 2, 3, 15 – 25.

ELBAZ-POULICHET, F., DUPUY, C. (1999): Behaviour of rare earth elements at the freshwater-seawater interface of two acid mine rivers: the Tinto and Odiel (Andalucia, Spain). Appl. Geochem., 14, 1063 – 1072.

GELLER, W., KLAPPER, H., SALOMONS, W. (1998): Acidic Mining Lakes. Springer, Berlin – Heidelberg – New York.

GIMENO SERRANO, M.J., AQUÉ SANZ, L.F., NORDSTROM, D.K. (2000): REE speciation in low-temperature acidic waters and the competitive effects of aluminium. Chem. Geol., 165, 167 – 180.

GÖTTLICHER, J., POHLMANN, M., BOZAU, E., GASHAROVA, B. (2001): Mineralbildungen aus eisen- und sulfathaltigen Wässern. Beih. z. Eur. J. Mineral., 13, 1, 67.

KNÖLLER, K. (2000): Anwendung stabiler Umweltisotope zur Bewertung hydrochemischer Zustände und Prozesse in Folgelandschaften des Braunkohlebergbaus. Ph.D. Thesis, Department of Natural Sciences, University of Leipzig.

LENAB-ABSCHLUSSBERICHT (1998): Niederlausitzer Bergbaufolgelandschaft: Erarbeitung von Leitbildern und Handlungskonzepten für die verantwortliche Gestaltung nachhaltige Entwicklung ihrer naturnahen Bereiche. BMBF-Förderkennzeichen: 0339648.

PEINE, A. (1998): Saure Restseen des Braunkohletagebaus – Charakterisierung und Quantifizierung biogeochemischer Prozesse und Abschätzung ihrer Bedeutung für die seeinterne Neutralisierung. Bayreuther Forum Ökologie, Band 62.

TAYLOR, S.R., MCLENNAN, S.M. (1985): The continental crust: its composition and evolution. Blackwell, Oxford.

WORRAL, F., PEARSON, D.G. (2001): Water-rock interaction in an acidic mine discharge as indicated by rare earth element pattern. Geochim. Cosmochim. Acta, 65, 18, 3027 – 3040.

Formal Considerations on Argon-Argon Diagrams in $^{40}AR/^{39}AR$ Geochronometry

Sergei B. Brandt, Ivan S. Brandt, Sergei V. Rasskazov, Alexei V. Ivanov,

Institute of the Earth's crust SB RAS, Lermontov str., 128, 664033 Irkutsk, Russia

A formal analysis of argon isochrons in terms of diffusion and Arrhenius' laws shows that the $^{36}Ar/^{40}Ar$ versus $^{39}Ar/^{40}Ar$ diagram exhibits a linear graph as a true isochron and allows regressions and extrapolations, only when activation energies of diffusion for radiogenic argon-40 and nucleogenic argon-39 are equal and that for atmospheric (*contaminating*) argon is lower. In cases of distorted kinetic parameters of argon isotopes, when activation energies of diffusion for radiogenic argon 40 and nucleogenic argon 39 are different, excess argon with lower activation energy, curvilinear arrays and spreading of points occur, which may produce misleading interpretations of ages and $^{36}Ar/^{40}Ar$ value of *contaminating* argon.

1 Introduction

The need of a diagram with the $^{36}Ar/^{40}Ar$ versus $^{39}Ar/^{40}Ar$ coordinates had arisen with the development of a step heating procedure of argon releasing in ^{40}Ar-^{39}Ar technique. MERRIHUE & TURNER (1966) argued that, beside radiogenic ^{40}Ar and nucleogenic ^{39}Ar, a sample could contain *contaminating* argon, common for all fractions released during step heating. In the case of terrestrial samples, one had only to subtract from the total argon 40 released a part 295.5 times the measured atmospheric argon 36. In the case of meteoritic or planetary or incompletely degassed terrestrial samples, the problem was more complicated because the *contaminating* argon could differ by isotopic composition from the terrestrial atmospheric argon. The *contaminating* argon could be found by extrapolation to zero of an experimental point pattern due to the obviously linear relation

$$(^{40}Ar/^{36}Ar)_{tot} = (^{40}Ar/^{36}Ar)_{c} + (^{40}Ar/^{39}Ar)_{rad} \times (^{39}Ar/^{36}Ar) \qquad (1)$$

(subscripts are *tot* = total, *c* = contaminating, *rad* = radiogenic). For the perfection of the argon-argon diagram, it was suggested to use inverse coordinates: $x = {}^{39}Ar/^{40}Ar$; $y = {}^{36}Ar/^{40}Ar$. This was necessary to avoid infinities in samples extremely enriched with radiogenic argon when $^{36}Ar \rightarrow 0$ (TURNER, 1971; RODDICK & REX 1980).

The argon-argon diagram became a standard tool in routine $^{40}Ar/^{39}Ar$ age determinations. Linear regressions from scattered points were often used for determinations of *contaminating* argon (DICKIN 1995; MCDOUGALL & HARRISON 1999 and references therein). If temperature steps did not yield a plateau, a value at intercept of a regression line with abscissa was usually accepted as the most reliable approximation to the true age. There existed some verbal descriptions of the correlation diagram, but no strict mathematical deductions of its features combined with stepwise release of argon had been published yet.

In contrast to expression (1), the linearity of

$$(^{36}Ar_c/^{40}Ar_{tot}) = f(^{39}Ar/^{40}Ar_{tot}) \qquad (2)$$

is not obvious. It may exist in several cases and in others not. Are linear regressions and extrapolations justified if (2) is not a straight line, but a curve? Could it not yield artefacts and mislead to false deductions? These questions have impelled us to perform the present theoretic investigation.

A formal analysis of Ar-Ar isochrons combined with stepwise heating is performed. It is based on standard solutions of differential equations in partial derivatives (TIKHONOV & SAMARSKY 1953; WEBSTER & SZEGÖ 1930; FRANK & MISES 1937; MADELUNG 1957), taught at mathematical, physical and even chemical faculties.

2 Deduction of an Algebraic Expression for a $^{36}AR/^{40}AR$ versus $^{36}AR/^{40}AR$ Plot

Presuming contamination of a sample by atmospheric argon *(Ar_{atm})*, we aim to obtain an algebraic relation *y = f(x)*. Let be

$$y = \frac{^{36}Ar_{atm}}{^{40}Ar_{tot}}; \quad x = \frac{^{39}Ar}{^{40}Ar_{tot}}; \quad ^{40}Ar_{total} = ^{40}Ar_{atm} + ^{40}Ar_{rad} \tag{1abc}$$

Then we are compelled to assume, that

$$k = \frac{^{36}Ar_{atm}}{^{40}Ar_{atm}}; \quad l = \frac{^{39}Ar}{^{40}Ar_{rad}} \tag{2ab}$$

The expression (2a) means that the isotopic composition of *contaminating* argon should be constant for all steps of heating. According to the expression (2b), the nucleogenic argon 39 - radiogenic argon 40 ratio (or the ages of all thermal fractions) should be constant. Indeed, the latter rather severe condition presumes a straight line, parallel to the abscissa in the age-to-fraction-of-released-argon diagram. Thus, in the *xy* coordinates, this line means an isochron. The line becomes curvilinear, if conditions 2ab are not fulfilled.

From expressions (1ab) and (2ab) it follows that

$$y = \frac{k}{1 + \frac{^{40}Ar_{rad}}{^{40}Ar_{atm}}}; \quad x = \frac{l}{1 + \frac{^{40}Ar_{atm}}{^{40}Ar_{rad}}} \tag{3ab}$$

Express $^{40}Ar_{rad}$ from (3b) and substitute into (1a)

$$y = \frac{k}{1 + \frac{x}{l - x}} \text{ or finally } \frac{x}{l} + \frac{y}{k} = 1 \tag{4}$$

Equation (4) means a straight line with a negative slope *-k/l* intercepting at the point *k* with the ordinate and at the point *l* with the abscissa. Both points are to be determined as a goal of the whole procedure.

3 Kinetic Relations Describing Step Heating

In any mineral, radiogenic argon obeys the laws of diffusion and that of Arrhenius. The former shows the space-time dependence of argon concentration (*c*). Its solution for the mean concentration in the one-dimensional case is

$$c(t) = \frac{8}{\pi^2} \sum_{\nu=0}^{\infty} \frac{1}{(2\nu+1)^2} e^{-(2\nu+1)^2 \pi^2 Fo} \tag{5}$$

Concentration is a function of a dimensionless parameter, the Fourier's number

$$Fo = Dt / h^2$$

(*D* = the coefficient of diffusion, *t* = time, *h* = the size of the grain, from which diffusion occurs) the latter controls the temperature dependence of argon release

$$\frac{D}{h^2} = \frac{D_0}{h^2} e^{-\frac{E}{RT}} \tag{6}$$

(D_0 = the frequency factor, meaning *D* at $T \to \infty$; *E* = the activation energy of diffusion; *R* = the gas constant; *T* = temperature in *K*).

For the case of step heating, we can apply a stepwise-constant-diffusion relation deduced by (AMIRKHANOV et al. 1960; BRANDT et al. 1996)

$$\Delta c_i = \frac{8}{\pi^2} \sum_{\nu=0}^{\infty} \frac{1}{(2\nu+1)^2} e^{-(2\nu+1)^2 \pi^2 \sum_{i=1}^{n} \Delta Fo_i} (1 - e^{(2\nu+1)^2 \pi^2 \Delta Fo_n}) \tag{7}$$

(Δc_i are fractions of ^{36}Ar, $^{40}Ar_{atm}$, $^{40}Ar_{rad}$ or ^{39}Ar released at the *i*-th step of a sample heating; *Fo* = a dimensionless Fourier's number,

$$Fo = \frac{D\,t}{h^2} \tag{8}.$$

This formula is easily programmed and tabulated. The whole procedure was described more eplicit elsewhere (BRANDT et al. 2003).

4 Thermal Separation of Argon Components

We are dealing at least with three components of argon present in an irradiated sample: radiogenic, nucleogenic, and *contaminating* argon. Their behaviour during step heating is controlled by relations (5) and (6). Each of the argon components might have its own characteristic frequency factor D_0 and its activation energy of diffusion *E*. Differences in these parameters allow to separate them by thermal procedures.

For instance, a problem on the separation of radiogenic and contaminating argon of the atmospheric composition (further referred to as atmospheric argon) have been considered quantitatively by RASSKAZOV et al. (2000). To extract

only a *k*-th atmospheric fraction and retain a *l*-th radiogenic fraction of argon, the sample is to be preheated at a temperature

$$T = \frac{E-e}{R} \cdot \frac{1}{\ln\left(\frac{fo}{Fo} \cdot \frac{D_0/H^2}{d_0/h^2}\right)} \text{ during a}$$

$$\text{time } t = \frac{(D_0/H^2 Fo)^{\frac{e}{E-e}}}{(d_0/h^2 fo)^{\frac{E}{E-e}}} \qquad (9ab)$$

(capital letters *D, H, Fo* refer to radiogenic argon and small letters *d, e, fo* - to atmospheric argon;

$Fo = \frac{\pi k^2}{16}$; $fo = -\frac{1}{\pi^2}\ln\frac{\pi^2 l}{8}$).

We see that a *conditio sine qua non* for separating these two components is a difference between *E* and *e*. If *E-e=0, T* becomes zero and *t* becomes indefinite. Therefore, if two or more argon components of a sample have identical kinetic parameters, they are not separable by any thermal procedure and become indistinguishable being released congruently.

In a case of equal kinetic parameters of argon components, points of *i* thermal release steps will be represented in the *xy* coordinates ($x = {}^{39}Ar/{}^{40}Ar_{tot}$; $y = {}^{36}Ar/{}^{40}Ar_{tot}$) by a single point of a multiplicity of an order *i*. As fractions of argon components are inseparable, the point has no chronological meaning.

5 A Case of a True Isochron

During step heating, fractional release of an argon component with a lower activation energy occurs at lower temperature steps as compared to an argon component with an elevated activation energy (Fig. 1).

Taking into account expressions (9ab) suggest now that atmospheric argon is bound to the host structure looser (i.e. has a lower activation energy) than both radiogenic and nucleogenic. This is really plausible, as radiogenic and nucleogenic argon are produced within the crystalline structures themselves, whereas atmospheric argon is most likely impregnated into the structure under a huge pressure gradient.

For the sake of definiteness, we may consider a sample with a potassium content 2%, radiogenic ${}^{40}Ar = 1.0\times10^{-3}$ nmm^3/g and an age

$$t = 1.885\cdot10^9 \ln(J\frac{{}^{40}Ar_{rad}}{K}+1) = 12.5Ma$$

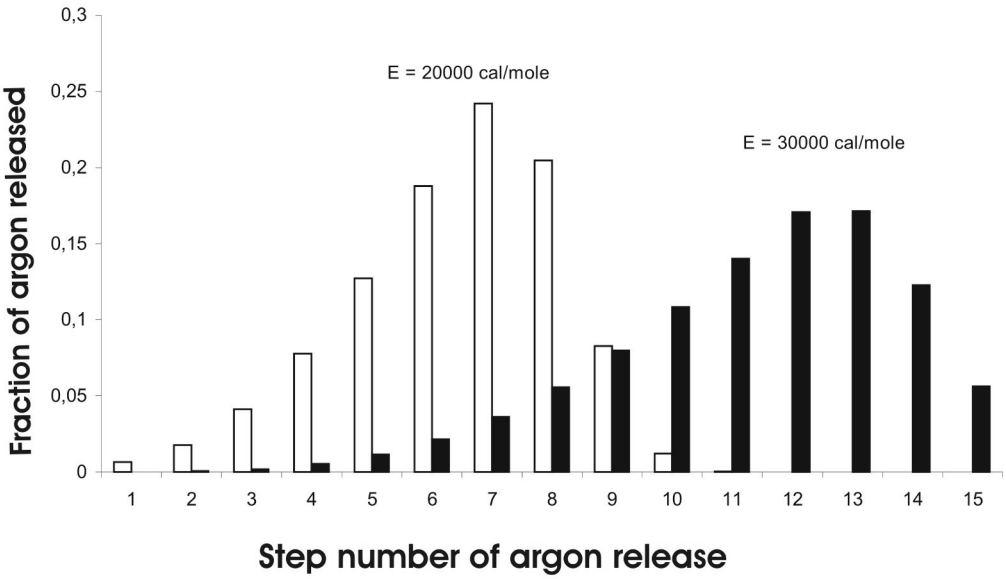

Figure 1: Comparison of argon release spectra at E = 20000 cal/mole and E = 30000 cal/mole as calculated by means of formula (7).

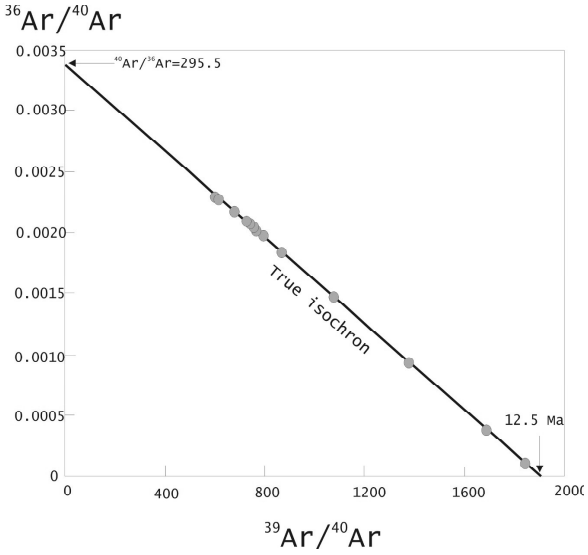

Figure 2: Argon-argon isotope plot for the case, when activation energies of diffusion for radiogenic and nucleogenic argon are equal and that for atmospheric is somewhat lower. An isochron in the form of an ideal straight line is obtained. Intercepts with the coordinate axes provide both the age of the sample and the isotopic composition of contaminating argon of atmospheric origin.

(for these units, the *J*-factor = *13.3* because argon is expressed in nmm^3/g and potassium in %).

For both the radiogenic and nucleogenic argon, assume a frequency factor $D_0/H^2 = 0.5\ s^{-1}$. $E_{rad} = E_{39} = 25000$ *cal/mole*. Finally, put the quantity of atmospheric argon remained in the sample at the instant of measurement as equal to the radiogenic argon. We ascribe to the atmospheric argon (composed of ^{40}Ar and a 1/295.5 part of ^{36}Ar) an activation energy (e_{atm}) of 23000 *cal/mole*. Results of calculations are plotted on Fig. 2.

The age of every fraction is 12.5 Ma. In the age-to-fraction-of-released-argon diagram, the age line is parallel to the abscissa (not shown). A shift of atmospheric argon towards lower activation energies stipulates an isochron with points corresponding to every thermal step ideally fitting the straight line in argon-argon diagram. Intercepts of the isochron with the coordinate axes determine compositions of the atmospheric argon and a single age of 12.5 Ma. And vice versa: if points fit a straight line intercepting with the coordinate axes at points mentioned, then it may be stated that the activation energies for radiogenic and nucleogenic argon are equal and that of atmospheric argon is somewhat lower.

In practice, most frequently, however, distorted age spectra are met. They are saddle shaped, stepwisely increasing or decreasing. Conditions (2b) for them are not fulfilled and argon-argon diagrams of the distorted patterns exhibit curvilinear arrays. Now, let us consider three examples of 'false isochrons' resulted from varying kinetic parameters of argon components.

6 A Case of a 'False Isochron' due to Unequal Activation Energies for Atmospheric, Nucleogenic, and Radiogenic Argon: $E_{atm} < E_{39} < E_{rad}$

It is worth considering this case, as cross sections for nuclear impact for all the lattice elements differ from zero, have final values. Neutron bombardment may loosen the lattice, induce radiation damages and cause a shift of argon release spectra.

Take $E_{rad} = 25000$; $E_{39} = 24500$ and $e_{atm} = 23000$ cal/mole. Calculations quite similar to the previous case exhibit results plotted on Fig. 3.

As compared to radiogenic argon, a lower activation energy of nucleogenic argon results in its elevated concentrations in fractions released at lower temperature steps. This is why an age-to-fraction-of-released-argon diagram shows a plateau somewhat lower than the reference line of the true age. Condition (2b) is violated in this case: the ^{39}Ar-^{40}Ar ratio is not constant

In argon-argon coordinates, points are not determining a straight line anymore, but are belonging to a curved array. Intercepts of the curve with the coordinate axes have another meaning than in the case of the true isochron. Attempts to "stratify" the curve by means of extrapolations and least square procedures are likely leading to artefacts. For regression calculations, an experimenter would be tempted to use the seemingly straight array of points shown by filled circles. The fictive regression equation is

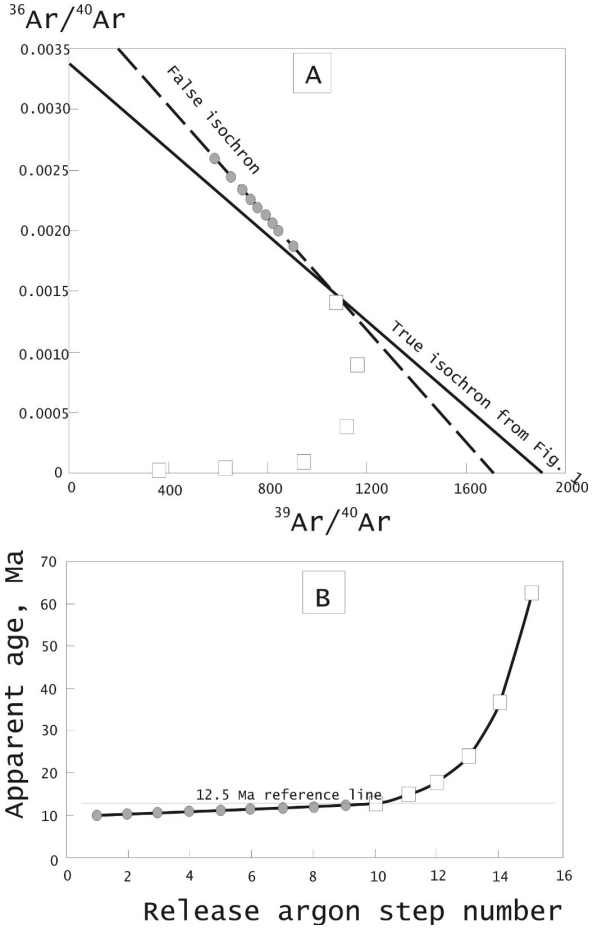

Figure 3: Argon-argon isotope plot (A) and age spectrum (B) for the case, when the activation energy of diffusion for nucleogenic argon 39 lies between those of radiogenic and atmospheric. Intercepts with coordinate axes give distorted results. A locus of points is not a straight line. In the array, filled circles mark a portion exhibited a 'false' isochron. Open squares are omitted from the isochron calculations.

$$\frac{^{36}Ar}{^{40}Ar} = -3 \cdot 10^{-4} \frac{^{39}Ar}{^{40}Ar} + 0.0040$$

This yields an intercept with the $^{36}Ar/^{40}Ar$ -axis at 0.0042 instead of 0.003384 - the input value of our calculation and an intercept with the $^{39}Ar/^{40}Ar$ - axis at 1700 instead of 1900.

So, in the case of unequal activation energies for atmospheric, nucleogenic, and radiogenic argon ($e_{atm}<E_{39}<E_{rad}$), the experimenter obtains a plateau younger than the true age, a 'false isochron' with an older age and a high ^{36}Ar-^{40}Ar ratio of *contaminating* argon. And vice versa: this pattern of age spectrum and high ^{36}Ar-^{40}Ar ratio of *contaminating* argon on an argon-argon diagram is likely a symptom of a shift in the activation energies of radiogenic and nucleogenic argon.

7 A Case of a 'False Isochron' due to Radiogenic Argon Losses in the Past

Underestimated ages due to radiogenic argon losses are met very often. According to kinetic theory, argon losses are negligible in young rocks and increase in the older ones. This is why experimenters are compelled to abandon the conventional potassium-argon method for rocks older than Late Cenozoic. When the distribution of argon inside an undisturbed mineral grain is homogeneous, the rate of argon release is higher, than in a case when the grain had lost some of its argon. Consider the equation (7), putting it *f (Fo)*.

$$f(Fo_0 + \Delta Fo) \neq f(\Delta Fo)$$

(Fo_0 = a Fourier's number characterizes argon losses, ΔFo is acquired during laboratory thermal treatment). This follows from an expansion into a Taylor series.

In a numeric example, suppose that the sample had recently lost one half of its argon. This loss corresponds to an initial Fourier's number $Fo_i = 0.049$. The calculation is performed quite similar, but to every value is added the Fourier's number 0.049. The results are shown on Fig. 4.

Apparent ages are relatively young. Radiogenic argon depletion results in a combination of increasing and then decreasing steps. On an argon-argon plot, the array has a double curvature. This pattern may be mistakably accepted as a result of usual 'spreading of experimental points' or 'damages in crystalline nuclei'. Some points may be omitted and a part of the array accounted for. The points shown by filled circles yield a regression line

$$\frac{^{36}Ar}{^{40}Ar} = -2.3 \cdot 10^{-4} \frac{^{39}Ar}{^{40}Ar} + 0.0035$$

An intersection of the line with the $^{39}Ar/^{40}Ar$ - axis indicates a distorted value 1550 without physical meaning and the one with the $^{36}Ar/^{40}Ar$ - axis gives the value 0.0035 accidentally close to atmospheric.

Samples with radiogenic argon losses in the past may be recognized through a quite specific age spectrum with ascending and descending steps

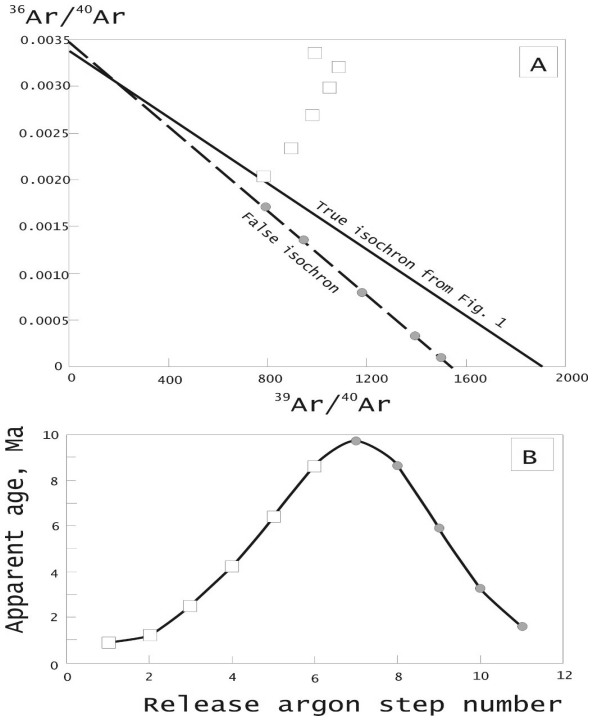

Figure 4: Argon-argon isotope plot (A) and age spectrum (B) for the case, when a sample had lost 50% of its radiogenic argon in the past. Symbols as in Fig. 3.

branches and large scattering points on the argon-argon plot.

8 A Case of a 'False Isochron' due to Excess Radiogenic Argon

Excess and inhereted argon are often present in intrusive rocks due to incomplete degassing and/or incomplete substitution of magmatic argon by the atmospheric. It has been identified in submarine lavas, in pyroxenes from intrusive rocks etc. Qualitatively an inclusion of excess ^{40}Ar could be thought as a capture of argon-gas bubbles at crystallization, and inhereted argon as a capture of individual argon particles by the main lattice during precipitation.

Consider first equal diffusion parameters for radiogenic, nucleogenic, and excess argon and lower activation energy for atmospheric argon. Quite similar to the section 5, we may see that at any thermal procedure, the three types of argon are released congruently. A shift of argon isotopic composition due to excess argon results in a 'false isochron'. Its intercepts yield abnormally low value of the ^{36}Ar-^{40}Ar ratio at the *y*-axis and an older age at the *x*-axis (not shown).

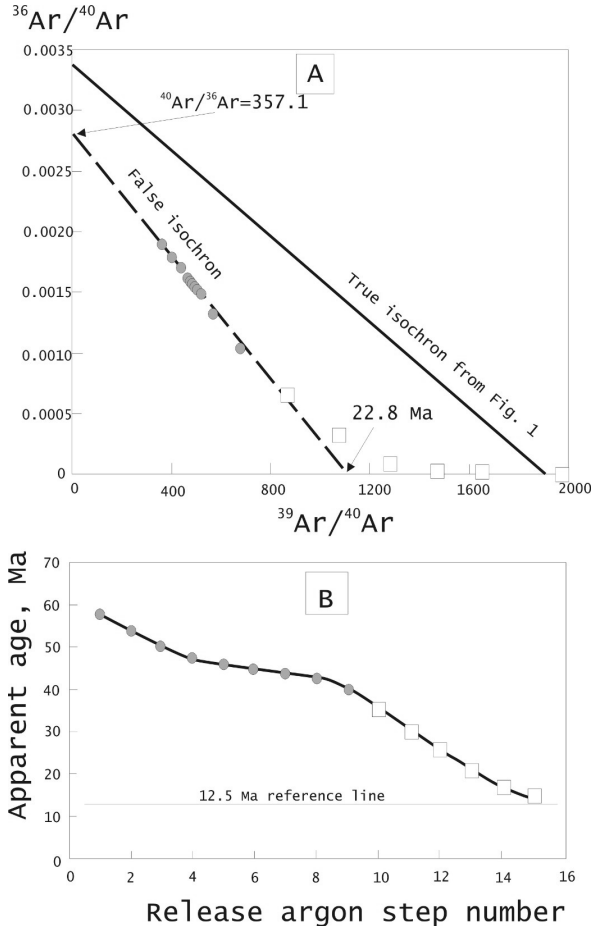

Figure 5: Argon-argon isotope plot (A) and age spectrum (B) for the case, when the activation energy of diffusion for excess argon lies between those of radiogenic (equal to nucleogenic) and atmospheric. Symbols as in Fig. 3.

Take the activation energy of excess argon (E_{exc}) slightly lower than those of radiogenic and nucleognic: $E_{rad}=E_{39}=25000;\ E_{exc}=24500,$ *and* $e_{atm}=23000$ *cal/mole;* $D_0= 0.5\ s^{-1}$. Take a sample with the age of 12.5 Ma having 2% potassium and 10^{-3} nmm^3/g radiogenic argon. Further let be the contents $^{40}Ar_{rad} = {}^{40}Ar_{exc} = {}^{40}Ar_{atm}$. Calculations for this case are quite similar to those of section 5.

On Fig 5B, we can see a descending succession of steps above the 12.5 reference line. On Fig. 5A, the points show curvilinear array. The part of the latter is interpreted as a 'false isochron' plotted lower then a 'true' one with no excess argon. The 'true isochron' is usually unknown to the experimenter and he has to draw a straight regression line through some points at the 'false isochron'. So, the experimenter should obtain an

intercept with the y-axis at 0.0028, corresponding to an ^{40}Ar-^{36}Ar ratio 357.1, instead of 295.5 and an intercept with the x-axis, corresponding to an age of 23.88 Ma, instead of 12.5 Ma. Interesting is that both the values are fictitious showing presence of excess argon.

9 Discussion

A formal analysis of the $^{36}Ar/^{40}Ar$ versus $^{39}Ar/^{40}Ar$ diagram shows that the true isochron is represented by a straight line allowing proper extrapolations and regressions only when activation energies of diffusion for radiogenic argon-40 and nucleogenic argon-39 are equal and the one for atmospheric argon is lower. It is the lower activation energy of atmospheric argon that makes possible using the argon-argon diagram. The latter allows a proper test for the plateau age. The true results are obtained if the plateau age is equal to the isochron value and intercept of the isochron with ordinate yields the atmospheric value of the $^{36}Ar/^{40}Ar$ at 0.003384.

In cases, when activation energies of diffusion for radiogenic argon-40 and nucleogenic argon-39 differ for some reasons, curvilinear arrays and spreading of points occur, which may produce misleading interpretations. If age spectrum do not yield a plateau, argon-argon diagram can not be used directly for determinations of the age and ^{36}Ar-^{40}Ar ratio of *contaminating* component. There arises the idea to approximate experimental curves by means of a proper choice of parameters of equation (7). In this study, we discuss some the most general features of argon-argon diagram for the cases considered.

An array rectilinear at the beginning and curvilinear at the end may be caused by the lower activation energy of nucleogenic argon than radiogenic as well as by presence of excess argon (Fig. 3, 5). A pattern of curvilinear array at the beginning and rectilinear at the end may be resulted from the argon losses in the past (Fig. 4).

More reliable information on kinetic relation of argon components is obtained from comparisons of age spectra and argon-argon diagrams. An ascending step pattern of age spectrum along with high $^{36}Ar/^{40}Ar$ value of the *contaminating* argon exhibits a case of lower activation energy for nucleogenic argon than radiogenic. If the plateau yields the age lower than the intercept of a correlation line with *x*-axis in argon-argon coordinates, the true age lies between the ages of the plateau and the 'false isochron'. It is noteworthy, that the lower activation energy of ^{39}Ar causes its losses (recoil) at a stage of irradiation. This effect makes confusing results during the step heating argon release.

A descending sequence of apparent ages along with lower $^{36}Ar/^{40}Ar$ indicates a 'false isochron' related to excess radiogenic argon with the lower energy of activation than radiogenic and nucleogenic. There exists no procedure to discriminate radiogenic and excess argon. The array on Fig. 5A has, however, a quite characteristic shape: rectilinear at the beginning and curved at the end. An age spectrum with ascending and descending steps and large scattering points on argon-argon plot is likely a result of argon losses in the past

10 Conclusions

A formal analysis of argon components in terms of diffusion and Arrhenius' laws shows that the $^{36}Ar/^{40}Ar$ versus $^{39}Ar/^{40}Ar$ diagram exhibits a linear graph as a true isochron and allows regressions and extrapolations only, when activation energies of diffusion for radiogenic argon 40 and nucleogenic argon 39 are equal and that for *contaminating* argon of atmospheric composition is lower.

The character of the point arrays on argon-argon diagram may provide indications on correlations of activation energies of its components: radiogenic, nucleogenic, and *contaminating*. Some portions of those curvilinear arrays (initial or final) may not correspond to the 'true isochrons' and their intersections with coordinate axes gain no physical sense. Strict rules for selection of these portions at present do not exist. Their formulation is an object for further investigations. There exists a possibility to determine kinetic parameters of the argon components in crystal structures through configurations of arrays of experimental points in argon-argon coordinates.

It is noteworthy that in terms of the present paper features of argon components can be characterized by higher or lower activation energies. It remains the question, whether these 'nuclei' or 'domains' or, in our terms, 'components of argon with a characteristic activation energy' are spatially separated or are distributed homogeneously over the whole host structure. In perthites, they are separated. On the other hand, it is plausible to suggest that particles of ^{39}Ar are surrounded by 'individual radiation damage zones' and distributed over the whole crystal structure. In our opinion, priority should be given to the advan-

tage of a quantitative estimation of array patterns. We have considered a few characteristic cases. Actually there exists an infinite lot of combinations of parameters. By a proper choice of the latter, every array could be approximated.

References

AMIRKHANOV, H.I., BRANDT, S.B. & BARTNITSKY, E.N. (1960): Radiogenic argon in minerals and rocks. Daghestan: USSR Academy of Sciences, Daghestan Branch, 202 p. (in Russian)

AMIRKHANOV H.I., BRANDT, S.B. & BARTNITSKY, E.N. (1961): Radiogenic argon in minerals and its migration. An. N.-Y. Academy Sci. 8, 235-275.

BRANDT S., RASSKASOW, S., BRANDT, I. & IWANOW, A. (1996): Betrachtungen zur Anspeicherung radiogenen argons in mineralen bei gleichzeitiger diffusion. Freiberger Isotopenkolloquium 1996 Proceedings, 35-46. (in German)

BRANDT, S.B., RASSKAZOV, S.V., BRANDT, I.S. & IVANOV, A.V. (2003): Formal consideration of isochrons in 40Ar/39Ar geochrometry, Geokhimiya (in Rusian, in press).

DICKIN, A.P. (1997): Radiogenic isotope geology. Cambridge: University Press. 490 p.

FRANK, PH. & MISES, R. (1937): Differential and integral equations of mathematical physics, P.2, Ed. GTTI, Moscow-Leningrad (Russian translation). 417 p.

MADELUNG, E. (1957): Die mathematischen Hilfsmittel des Physikers, 6, revidierte Auflage, Springer Verlag, Berlin, Göttingen, Heidelberg, 618 p.

MCDOUGALL, I. & HARRISON, T.M. (1999): Geochronology and thermochronology by the 40Ar/39Ar method, second edition, New York and Oxford, Oxford University Press, 269 p.

MERRIHUE, C.M. & TURNER, G. (1966): Potassium-argon dating by activation with fast neutrons. J. Geophys. Res. 71, 2852-2857.

RASSKAZOV, S.V., LOGATCHEV, N.A., BRANDT, I.S., BRANDT, S.B. & IVANOV, A.V. (2000): Geochronology and geodynamics in the Late Cenozoic (South Siberia - South and East Asia). Novosibirsk: Nauka Publishers, 288 p. (in Russian)

RODDICK, J.C., CLIFF, R.A. & REX, D.C. (1980): The evolution of excess argon in Alpine biotites. Earth Planet. Sci. Lett. 48, 185 - 208.

TURNER, G. (1971): 40Ar-39Ar ages from the lunar maria. Earth Planet. Sci. Lett. 11, 169-191.

TIKHONOV, A.N. & SAMARSKY, A.A. (1953): Equations of mathematical physics. 2-nd edition, Gostekhizdat, Moscow, 560 p. (in Russian).

WEBSTER, A. & SZEGÖ, G. (1930): Partielle Differentialgleichungen der mathematischen Physik, B.G. Teubner, Leipzig u. Berlin, v. 2. 530 p.

Forest Soil Development as investigated by Radioisotope Distributions

Detlef Degering[1], Sylke Schlenker[2], Sepp Unterricker[3]

[1] Saxon Academy of Sciences at Leipzig, Quaternary Geochronology Section, Bernhard-von-Cotta-Str. 4, D-09596 Freiberg/Sa.;
e-mail: degering@physik.tu-freiberg.de

[2] Geokompetenzzentrum Freiberg e.V., P.O. Box 1713, D-09587 Freiberg/Sa.

[3] TU Bergakademie Freiberg, Institute of Applied Physics, Bernhard-von-Cotta-Str. 4, D-09596 Freiberg/Sa.

1 Introduction

Soil can be considered as a set of layers which differ essentially in their physical and chemical properties. During the process of forest soil evolution, organic matter is supplied as litter and further decomposed by biologic activity. After structural destruction of plant remnants humic matter migrates via the soil solution into weathered mineralic subsoil. This results in a typical sequence of soil horizons: litter (L), fermented (Of) and humified (Oh) organic layers and mixed horizons (A) containing both mineralic and humic material. Occurrence and thickness of the organic horizons are governed by the decomposition rates and depend on environmental conditions like climate, availability of nutrients, litter composition etc., thus determining the appearing humus type. As a consequence of the occurring physicochemical conditions the upper part of the mineralic soil undergoes weathering processes leading to destruction of mineral structures and release of major and minor elements. Especially the lower organic and mixed horizons of forest soils are exposed to the impact of organic acids at low pH values down to pH 3.

Dynamic structures like forest soils can be advantageously studied by radiotracer methods. Experiments using the addition of artificial radionuclides are limited for obvious reasons to special investigation areas. Instead of this, the transuranic and fission nuclides distributed globally by the atmospheric nuclear weapons tests until 1963 and in Europe by the Chernobyl accident in 1986 may serve for the same purpose. The supply of those radionuclides took place in a limited time interval and for some of the nuclides data are available about the deposited activity per area (EUROPEAN COMMISSION 1998; HARDY et al. 1973; BUNDESAMT FÜR STRAHLENSCHUTZ, FACHBEREICH STRAHLENSCHUTZ 1992).

Nuclides from the natural decay series are able to provide additional information because of their differences in the chemical properties. Dynamic processes in varying chemical environments lead to accumulation and depletion of the individual nuclides. The resulting radioactive disequilibria are suited as fingerprints of the occurring differentiation processes.

In the present paper the investigations should be focused on the following topics:

(i) are the distributions of artificial radionuclides in forest soils stable enough to serve at present as markers of the time of their input?

(ii) is it possible to establish a quasicontinuous time scale by applying ^{210}Pb dating on soil horizons?

(iii) how do weathering processes influence the distribution of radionuclides in soil?

2 Sampling and Analytical Methods

All soil samples were taken *in situ* as slices of 1 - 2 cm thickness using a steel frame of 30 x 30 cm² area or a ring of 40 cm diameter to sample a defined area. This thin layer method allows the detection of small scale variations in the nuclide distributions within the profile. The material was dried at 40 °C for at least 48 h and after that it has been homogenised. Roots and stones larger than 5 mm were removed.

Table 1: Summary of the radionuclides detected and analysed by low level γ-spectrometry in soil samples from Saxony.

Radionuclide	Half life	Origin
^{238}U (via ^{234}Th, ^{234m}Pa)	$4.5 \cdot 10^9$ y	geogenic, ^{238}U-series
^{230}Th	$7.5 \cdot 10^4$ y	geogenic, ^{238}U-series
^{226}Ra (via ^{214}Pb, ^{214}Bi)	$1.6 \cdot 10^3$ y	geogenic, ^{238}U-series
^{210}Pb	22 y	geogenic, airborne input (^{222}Rn-daughter), ^{238}U-series
^{227}Ac (via ^{227}Th, ^{223}Ra, ^{219}Rn)	22 y	geogenic, ^{235}U-series
^{228}Ra (via ^{228}Ac)	5.8 y	geogenic, ^{232}Th-series
^{228}Th (via ^{212}Pb, ^{212}Bi, ^{208}Tl)	1.9 y	geogenic, ^{232}Th-series
^{40}K	$1.3 \cdot 10^9$ y	geogenic
^{7}Be	53 d	cosmogenic
^{125}Sb	2.8 y	artificial, Chernobyl fallout
^{134}Cs	2.1 y	artificial, Chernobyl fallout
^{137}Cs	30 y	artificial, Nuclear weapon tests and Chernobyl fallout
^{207}Bi	32 y	artificial, Nuclear weapon tests
(^{241}Pu=>) ^{241}Am	430 y	artificial, Nuclear weapon tests

For the radionuclide analysis two low-level-γ-spectrometry systems containing a 36 % p-type and a 38 % n-type HPGe detector were used, respectively. The sample material was filled into gas proof measuring containers of cylindrical shape or into Marinelli beakers. In most cases, long measuring times up to 48 h were necessary. The radionuclides detected in soil samples are given in Table 1 together with their origin. All radioisotopes could be determined simultaneously. Note that some members of the natural decay series were analysed via their γ-emitting daughter nuclides.

3 Sampling Sites

The radionuclide profiles in this paper were recorded at four sites in Saxony (Germany) intensively studied in the frame of the Level II European monitoring program (*Olbernhau 1*, *Laußnitz*, *Colditz* and *Bad Schandau*) (RABEN et al. 2000), at a site in the vicinity of a monitoring station of the Leipzig university (*Leipzig*) and in a larch forest near *Nassau* in the Erzgebirge mountains. Characteristics of the locations and of the investigated soils are summarised in Table 2. The chosen soils are typical for the Saxon area (SÄCHSISCHE LANDESANSTALT FÜR FORSTEN 2000) as well as the humus types which represent a broad field of degradation conditions ranging from fast decomposition of plant residues during one year (mull) to hindered disintegration in acidified soils (raw humus).

Because of the long measuring times for the γ-spectrometry only one soil section per sampling site could be taken. To get a widely representative profile of the sampled forest soil, preferably smooth and only little sloped sampling points at a minimum distance of 1.5 m from stems and centred between several trees were carefully selected.

4 Results and Discussion

4.1 General features of the investigated profiles

Fig. 1 illustrates typical activity distributions of radionuclides as found in similar shape in many of the observed soil sections. The great advantage of the thin layer sampling for the identification of accumulation and migration processes is clearly visible. Some features of the curves were generally found and can be summarised as follows:

4.1.1 naturally occurring nuclides:

- The radioactive equilibrium between ^{238}U and ^{226}Ra is disturbed in the upper layers, i.e. in the O- to B-horizons. Below that it is balanced and represents the activity level of the geological background
- ^{210}Pb supplied as Rn-daughter mostly from the atmosphere to the soil surface does reach its equilibrium to ^{226}Ra first in the mineralic layers. The excess in the organic and mixed layers is enormous and amounts to some hundreds of Bq per kg.

Table 2: Description of the locations and of the sampled forest soils in Saxony (Germany). The soil type is given according to the German classification (ARBEITSGEMEINSCHAFT BODENKUNDE 1994).

	Olbernhau 1	**Laußnitz**	**Colditz**	**Bad Schandau**	**Leipzig**	**Nassau**
geographic position	top of eastern Erzgebirge	30 km north from Dresden	40 km south-east from Leipzig	30 km south-east from Dresden	southern part of Leipzig	crest of eastern Erzgebirge
altitude above sea level	720 m	170 m	185 m	260 m	140 m	705 m
geological background	orthogneiss	aqueoglacial deposits	porphyr	basalt	sediment	Muscovite gneiss
vegetation	spruce trees, grass	pine trees, grass	oak trees, grass	beech trees	mixed flood plain forest, grass	larch trees, grass
soil type	silty loam-braunerde-podzol	sand-podzol	fine-sand-similigley	braunerde	vega-gley	Braunerde
humus type	raw humus - moder	raw humus	moder	moder	mull	raw humus
sampling date	July 26th, 1999	July 1st, 1999	September 20th, 1999	May 29th, 2001	June 13th, 2000	October 10th, 2000

- The nuclide ^{40}K is contained in natural potassium. Its distribution thus depicts the fraction of mineralic constituents in the soil matter. The sharp increase in the uppermost layers results from uptake by plants.

4.1.2 artificial nuclides:

- ^{137}Cs is detectable over the whole profile and represents the main activity of the artificial nuclides. The total activity contains contributions both from the weapons tests and from Chernobyl.
- The activity of the other caesium nuclide ^{134}Cs is about two orders of magnitude lower due to its shorter half life. Therefore, it falls at present below the detection limit in most of the samples. ^{134}Cs was only supplied by Chernobyl fallout. The ^{137}Cs/^{134}Cs ratio at the time of the Chernobyl accident amounted to 1.7 - 2.0 according to the literature (HÖTZL et al. 1987; WINKELMANN et al. 1986), own measurements on air filter samples gave a value of 1.9. This fact allows the separation of the total ^{137}Cs activity into the fractions from the weapons tests and from Chernobyl, respectively.
- In the soil sections the determination of ^{125}Sb now becomes difficult due to its short half life, comparable to that of ^{134}Cs.
- The fallout from atmospheric weapons tests before 1963 is represented by ^{241}Am and ^{207}Bi. The former is a daughter nuclide of the β-emitter ^{241}Pu (half life 14.4 y). Due to radioactive decay the activity of ^{241}Am grows continuously and will reach a maximum in the year 2037 (APPLEBY et al. 1991). ^{207}Bi is assumed to be produced by (d,xn)-reactions in the lead tamper or shield of thermonuclear weapons. Up to now, only little is known about the deposited ^{207}Bi activity in the environment.

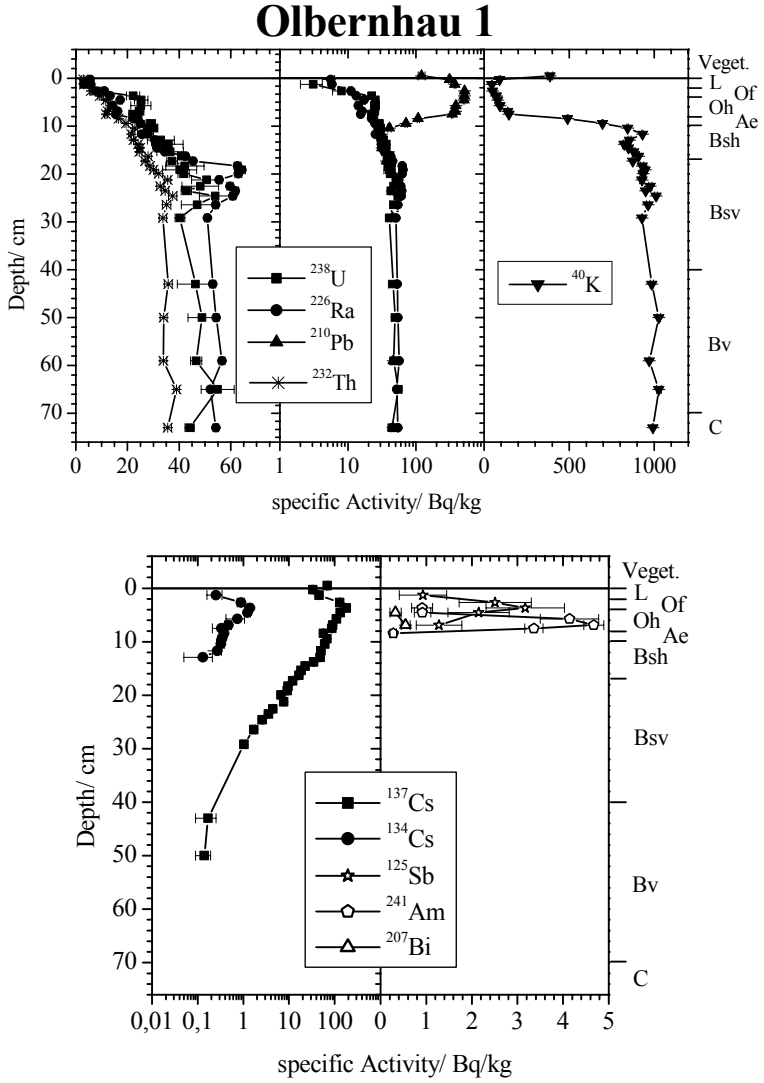

Figure 1: Distribution of natural (above) and artificial (below) radionuclides at sampling site Olbernhau 1. The soil horizons are classified at the right scale.

4.2 Distributions of artificial radionuclides and the time of deposition

Activity profiles of artificial nuclides at sites showing different humus and soil types are compared in Fig. 2.

Since the sampling method allowed the determination of the layer volumes, the results were given in terms of an activity concentration, i.e. in Bq per m² sampled area and cm layer thickness. This quantity illustrates more plastically the activity distribution in the sections as the mass-based specific activity in Bq/kg does.

The graphs of the ^{137}Cs activities are double peaked for the soils at *Olbernhau 1, Laußnitz* and *Colditz*. Whereas the first maximum appears in the organic Of/Oh horizons the second one is situated in mixed or mineralic layers (A(e,h)-Bsh). As calculated from the ^{134}Cs activities the upper peak contains mainly ^{137}Cs from Chernobyl accident, the lower one includes both contributions. Although the currently low ^{134}Cs activities cause large errors for the determination of the Chernobyl fraction, it is clearly visible that in layers containing the ^{241}Am peak, the Chernobyl ^{137}Cs concentration is low whereas a residue of ^{137}Cs from the weapons fallout is detected there. In the soil at *Leipzig* ^{137}Cs is broadly distributed in the Ah horizon with a large part of Chernobyl Cs at the maximum position.

Caesium as an alkali metal shows properties similar to potassium (SCHALLER et al. 1993) i.e. it is taken up by plants and fungi and strongly sorbed to clay minerals. Cs is not known to tend to complexation with organic matter. Therefore a two-stage-process is proposed for the interpretation of the ^{137}Cs profiles: during the first step Cs is incorporated into plants and remains in the dead material until it is decomposed. After this Cs moves via the soil solution downwards and is sorbed onto the surfaces of clay minerals. So the upper (Chernobyl-)^{137}Cs peak is assigned to 15 year old litter debris. The retention of ^{137}Cs from nuclear weapons tests in older organic horizons may be a consequence of direct transfer from the humus phase to the mineral content of this layer.

In general, in the forest soils except for the *Leipzig* site ^{125}Sb is detected in those layers which also contain the first maximum of Chernobyl ^{137}Cs. So we assume a migration behaviour similar to that of ^{137}Cs.

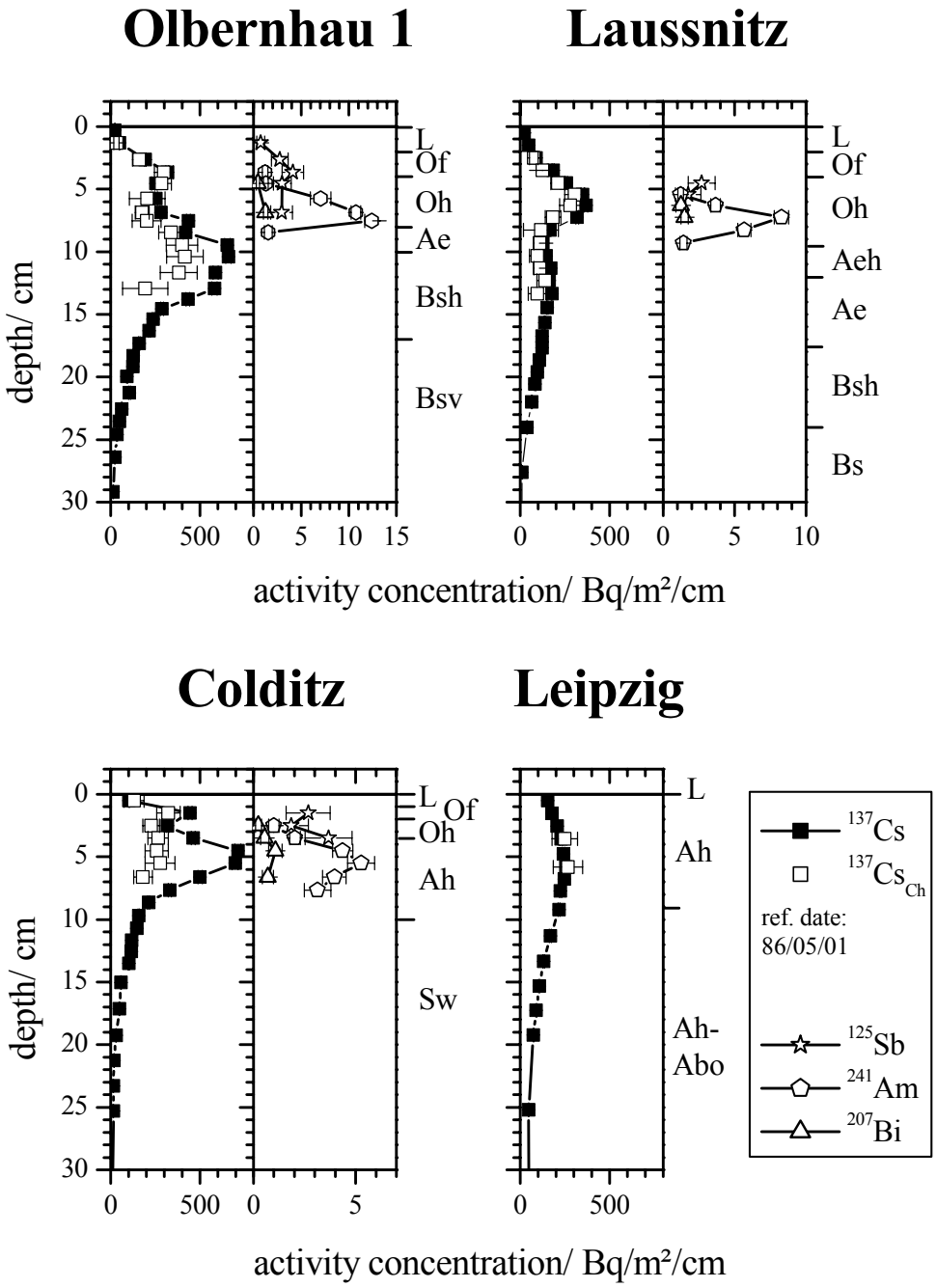

Figure 2: Distributions of artificial radionuclides at various sampling sites in Saxony. Values for ^{137}Cs are decay-corrected to May 1st, 1986. The Chernobyl fraction ($^{137}Cs_{Ch}$) of the total activity was calculated using a ^{137}Cs/^{134}Cs ratio of (1.9 $\pm$ 0.1) for fresh fallout. ^{241}Am and ^{207}Bi fell below detection limit at site *Leipzig*. The soil horizons are classified at the right scale.

The measured profiles and the above discussion specify the upper ^{137}Cs maximum as a rather transient time marker for the Chernobyl accident.

Completely different conclusions can be drawn for the bomb nuclides: The ^{241}Am distributions do not differ substantially between the sites *Laußnitz* and *Olbernhau 1*. The activity is concentrated at these similar sites in a single peak of 3 - 4 cm thickness located at the lower edge of the organic Oh horizon. At *Colditz* the Am-peak is found in the mixed Ah horizon with a rather blurred bottom side. In contrast to this, ^{241}Am disappears totally at site *Leipzig*, i.e. its activity falls down below the detection limit (about 1 Bq/m²/cm) in all layers.

Our measurements show ^{207}Bi distributions in the soils parallel to that of ^{241}Am. Its activity concentrations are unfortunately close to the detection limit so that detailed comparisons to the Am profile are not feasible. Nevertheless, ^{207}Bi is only included in layers also containing ^{241}Am. If an organic layer is missing (*Leipzig*) ^{207}Bi is again not detectable.

Americium exists in the environment in the oxidation state III and forms - just as its parent nuclide ^{241}Pu – stable complexes with organic ligands (KIM et al. 1989). It can be expected that the migration of the heavy metal nuclide ^{207}Bi is governed also by organic complexes as observed i.e. for lead and uranium. For this reason, it is reasonable to assume that, if ^{241}Am and ^{207}Bi were complexed in an initial state of litter decomposition, their plots reflect the distribution of organic material from the period of the nuclear weapons tests. Two facts support this hypothesis:

(i) From the data published in (HARDY et al. 1973; KREY et al. 1976) one can estimate ^{241}Am inventories between 16 and 40 Bq/m² at January, 1st, 2000 for central Europe. The total ^{241}Am inventories (Table 3) agree well with that data; i.e. at least a significant part of the primary input remained strongly fixed in the humus layer.

Table 3: Actual ^{241}Am inventories in the sampled forest soils.

	Total ^{241}Am inventory in Bq/m²
Laußnitz	20.0 ± 1.7
Olbernhau 1	29.4 ± 3.4
Colditz	21.0 ± 3.0

(ii) The nuclide distributions are narrow in Oh horizons but blurred in the Ah horizon of *Colditz* and disappear in the *Leipzig* profile. This conforms to the fate of plant residues – stacked as deposited in the O horizons but displaced as humate into the A horizons after further decomposition.

According to this discussion the $^{241}Am/^{207}Bi$ peaks are well suited i.e. stable time markers for the beginning of the 60´s. With their aid, the age of the lower part of the humus layer in the *Laußnitz* and *Olbernhau* sections can now be estimated to about forty years. At *Colditz* the humus turnover is accelerated and obviously finished after this period.

4.3 Dating of soil horizons by ^{210}Pb

The observed ^{210}Pb excess in the organic layers gives reason to the attempt of dating the organic horizons by means of the constant-rate-of-supply (CRS) model (APPLEBY & OLDFIELD 1978) which is successfully applied e.g. for lake sediments.

Lead as a heavy metal is well known for its ability to form stable organic complexes. So it is justifiable to presume as for $^{241}Am/^{207}Bi$ a complexation with organic material deposited at the same time like ^{210}Pb containing aerosols. In contrast to the fallout nuclides this supply is continuously with an at least approximately constant rate. Applying the CRS model to the soil system, its correctness can be controlled by comparison with the $^{241}Am/^{207}Bi$ peaks (≈ 40 y before sampling) and possibly with the upper (Chernobyl-) peak of the ^{137}Cs distributions (≈ 15 y before sampling).

The results in Fig. 3 for the sites *Olbernhau 1*, *Laußnitz* and *Colditz* show a good agreement between the age determination using ^{210}Pb and the time markers. Only the Cs-peak at site *Laußnitz* does not fit to the results which is probably related to the low clay content at this site. No ^{210}Pb excess was observed at site *Leipzig* where the organic layer is only a few millimetres thick.

Using these data, one can obtain conclusions about the turnover dynamics of the organic matter in the investigated soils. Tab. 4 summarises the ages at the base of the individual organic horizons. The lower decomposition rate of organic matter in Oh horizons of raw humus (Olbernhau 1, Laußnitz) compared to moder (Colditz) is clearly visible and emphasises the hampered microbial activity in acidified forest soils.

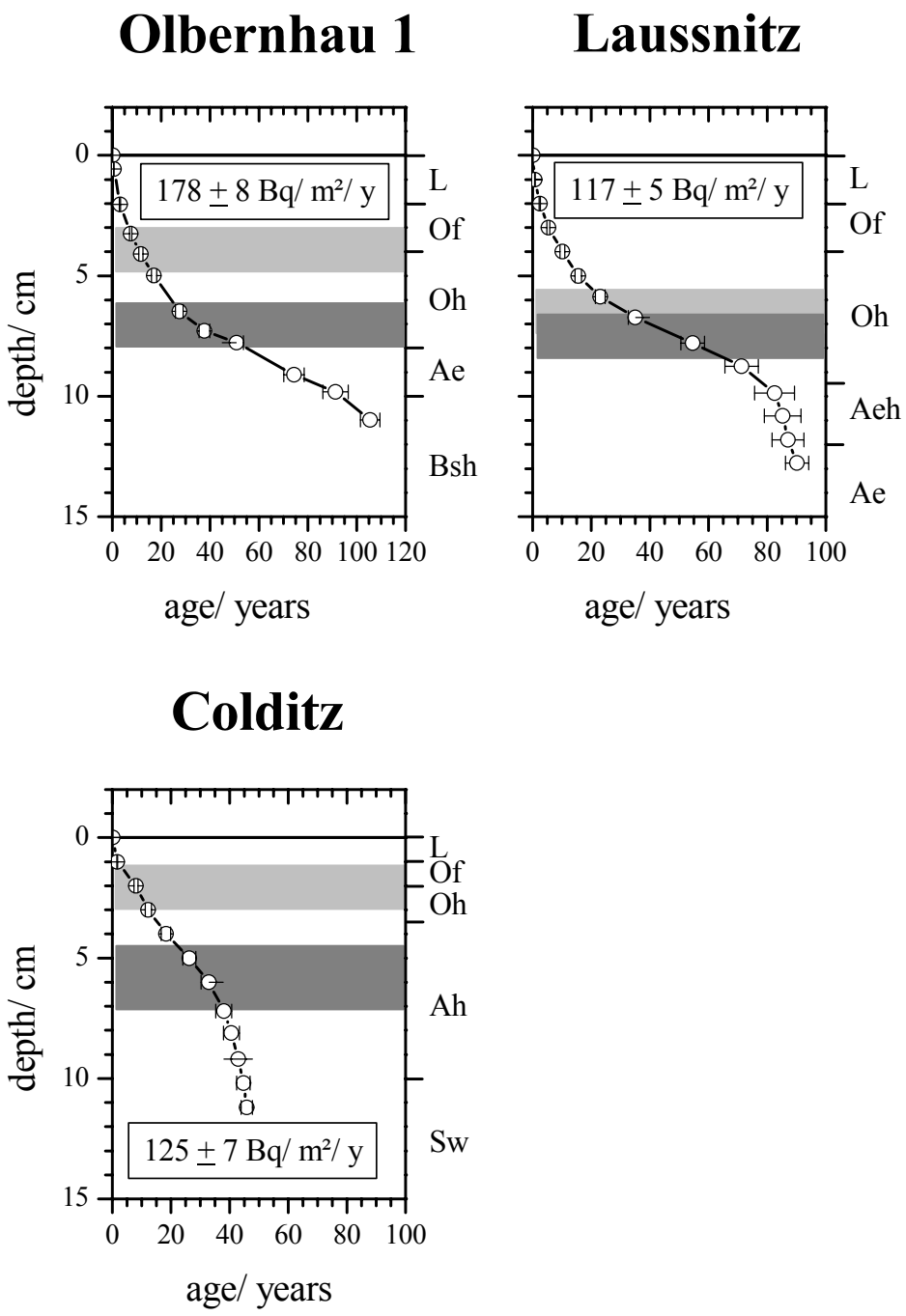

Figure 3: Results of ^{210}Pb age determination on soil layers using the CRS model. The mean activity supply per area and time as calculated from the total excess of unsupported ^{210}Pb is given in the boxes. Light and dark grey bars indicate the position of the upper (Chernobyl-) ^{137}Cs peak (≈ 15 y before sampling) and of the ^{241}Am/^{207}Bi peak (≈ 40 y before sampling), respectively.

Table 4: ^{210}Pb ages at the lower border of the organic horizons. The humus type at *Olbernhau 1*, *Laußnitz* and *Colditz* was raw-humus-moder, raw humus and moder, respectively. Dating failed at site *Leipzig* (humus type: mull) because of vanishing 210Pb excess.

Horizon	Olbernhau 1	Laußnitz	Colditz
L	3 y	2 y	2 y
Of	11 y	9 y	8 y
Oh	54 y	50 y	15 y
A(e,h)	94 y	80 y	46 a

4.4 Radioactive disequilibria and weathering

The compilation of ^{226}Ra/^{238}U ratios in a number of soils (Fig. 4.) shows in some cases remarkable disequilibria. Generally, three different behaviours can be distinguished:

- **Olbernhau 1 & Nassau:** obvious U-accumulation in Oh horizons; in mineralic horizons Ra-accumulation
- **Laußnitz & Colditz:** U-accumulation to a little extent in Oh horizons; in general no disequilibrium
- **Bad Schandau & Leipzig:** little overall Ra-accumulation

These effects are currently not completely understood. A possible explanation results from the presence of organic acids and low pH values (down to ≈ pH 3) in Oh layers of raw humus which may lead to enhanced weathering of mineralic particles. Traces of the discharged heavy metal Uranium are able to form organic complexes whereas Radium migrates to deeper layers and sorbs onto clay particles. Weathering should be less intensive in soils with higher quartz content as found in *Laußnitz* and in soils where an accelerated humus decomposition is connected with higher pH values (*Colditz*, *Bad Schandau*, *Leipzig*). This could explain the vanishing disequilibria in those sections. Further systematic work is necessary to clarify the effects leading to radioactive disequilibria in the upper soil layers.

5 Conclusions

The processes of soil evolution affect especially in the organic and mixed horizons the migration behaviour of natural and artificial radionuclides. Their distributions along a soil section can be successfully used for the determination of turnover rates of the soil organic matter. The degree of weathering processes is reflected by radioactive disequilibria in the ^{238}U decay series.Acknowledgement

The authors would like to express their gratitude to Dr. G. Raben and Dr. H. Andreae of the Saxon State Agency for Forestry, Graupa, for extensive support of soil sampling and helpful discussions.

One of us (S. Sch.) has been financially supported by the DFG Graduate School for Environmental Research in Geosciences and Geotechnics at the TU Bergakademie Freiberg/Sa.

.

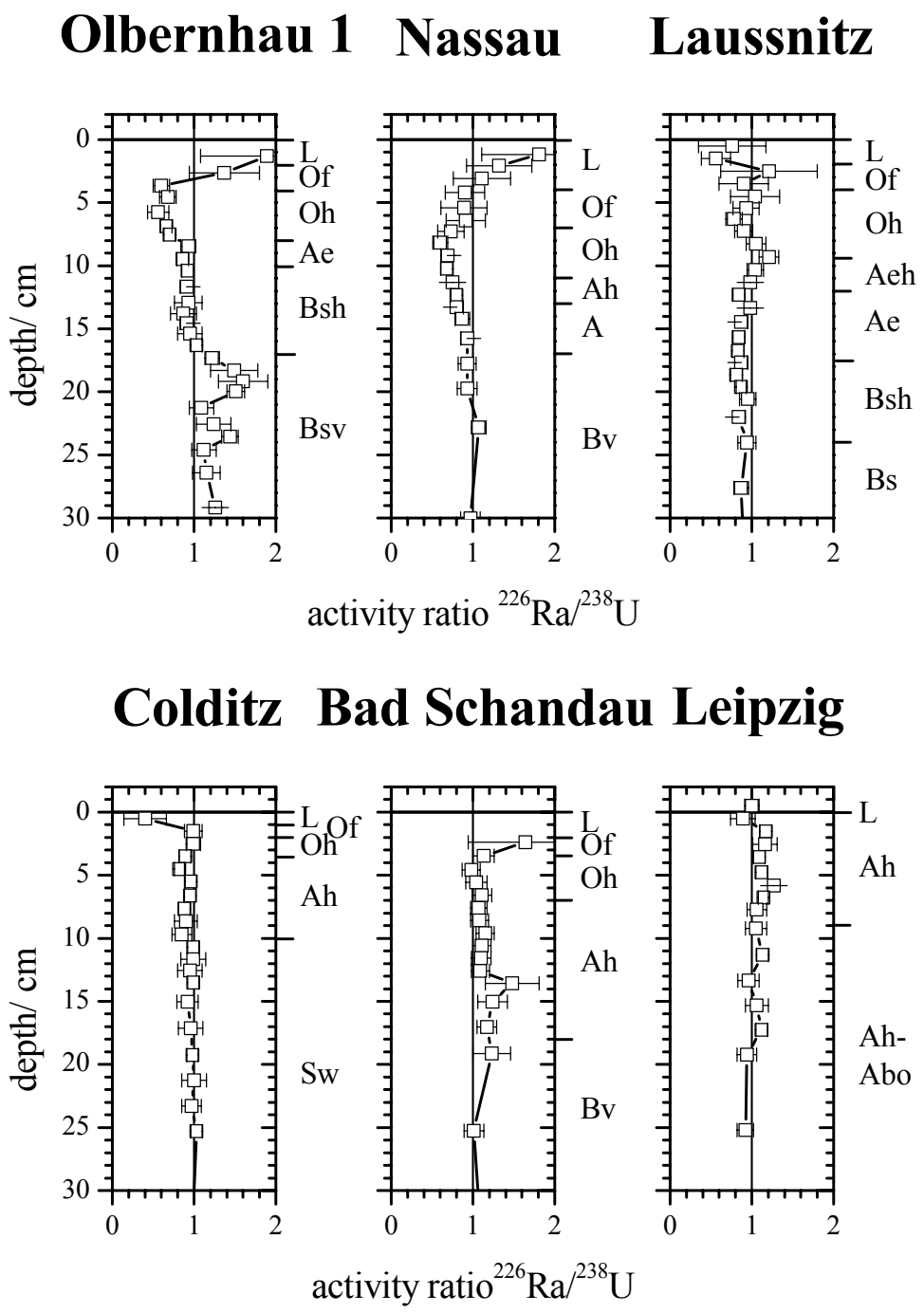

Figure 4: Distribution of the activity ratio $^{226}Ra/^{238}U$ in the investigated soils.

References

APPLEBY, P.G., OLDFIELD, F. (1978): The calculation of lead-210 dates assuming a constant rate of supply of unsupported ^{210}Pb to the sediment, Catena **5**, 1.

APPLEBY, P.G., RICHARDSON, N., NOLAN, P.J. (1991): ^{241}Am dating of lake sediments, Hydrobiologia, **214**, 35.

ARBEITSGEMEINSCHAFT BODENKUNDE (1994): *Bodenkundliche Kartieranleitung*, 4th ed., Hannover.

BUNDESAMT FÜR STRAHLENSCHUTZ, FACHBEREICH STRAHLENSCHUTZ (1992): *Die Auswirkungen des Unfalls im sowjetischen Kernkraftwerk Tschernobyl auf das Territorium der ehemaligen DDR im Jahre 1989*, ST-1/92, Bundesamt für Strahlenschutz, Berlin.

EUROPEAN COMMISSION, DG XII NUCLEAR FISSION SAFETY PROGRAMME (1998): *Atlas of Caesium Deposition on Europe after the Chernobyl Accident*, Office for Official Publications of the European Communities, Luxembourg.

HARDY, E.P., KREY, P.W., VOLCHOK, H.L. (1973): Global Inventory and Distribution of Fallout Plutonium, Nature **241**, 444.

HÖTZL, H., ROSNER, G., WINKLER, R. (1987): Ground Depositions and Air Concentrations of Chernobyl Fallout Radionuclides at Munich-Neuherberg, Radiochim. Acta, **41**, 181.

KIM, J.I., BUCKAU, G., BRYANT, E., KLENZE, R. (1989): Complexation of Am(III) with humic acid, Radiochim. Acta **48**, 135.

KREY, P.W., HARDY, E.P., PACHUKI, C., ROURKE, F., COLUZZA, J., BENSON, W.K. (1976): Mass Isotopic Composition of Global Fall-out Plutonium in Soil. In: *Transuranium Nuclides in the Environment*, Proc. of the Symp. on Transuranium Nuclides in the Environment, San Francisco 1975, IAEA-SM-199/39, p. 671;Vienna.,

RABEN, G., ANDRAE, H., MEYER, M. (2000): Long-term acid load and its consequences in forest ecosystems of Saxony (Germany), Water, earth and soil pollution **122**, 93. SÄCHSISCHE LANDESANSTALT FÜR FORSTEN (2000): *Bodenzustandserhebung (BZE) in den sächsischen Wäldern (1992 - 1997)*, Schriftenreihe der Sächsischen Landesanstalt für Forsten, Heft 20/2000, Graupa.

SCHALLER, G., LEISING, KRESTEL, R., WIRTH, E. (1993): *Vergleichende Betrachtung von Caesium und Kalium im Boden*, Schriftenreihe Reaktorsicherheit und Strahlenschutz, Bundesministerium für Umwelt, Naturschutz und Reaktorsicherheit, Bonn.

WINKELMANN, I., ENDRULAT, H.-J., FOUASNON, S., GESEWSKY, P., HAUBELT, R., KLOPFER, P., KÖHLER, H., KOHL, R., KUCHEIDA, D., MÜLLER, M.-K., SCHMIDT, H., VOGL, K., WEIMER, S., WILDERMUTH, H., WINKLER, S., WIRTH, E., WOLFF, S. (1986): Ergebnisse von Radioaktivitätsmessungen nach dem Reaktorunfall in Tschernobyl, ISH-99, Institut für Strahlenhygiene des Bundesgesundheitsamtes, Neuherberg.

Prospects of rare earth elements and other heavy metals as tracers in acid rock drainage (ARD) at the former uranium mining site of Ronneburg, Thuringia

Jörn Geletneky, Dirk Merten, Georg Büchel

Institute of Earth Science, Friedrich-Schiller-University, Burgweg 11, D-07749 Jena, Germany

Between 1950 and 1990 the Ronneburg mining district in the eastern part of Thuringia (Germany) was one of the largest uranium mining sites in the world. Since 1990 the remediation of the mining site is realized with the aim to reduce the concentrations of radionuclides and heavy metals in groundwater and surface waters. The remaining waste rocks mainly consists of black shales, metabasaltic rocks and carbonate of Ordovician to Devonian age, containing up to 7 wt% sulfides, 5–9 wt% organic carbon, 30-60 ppm uranium and a series of trace elements including rare earth elements (REE).

Aim of this study is to investigate the influence of acid rock drainage (ARD) of waste rock dumps on valley sediments, groundwater and adjacent creeks. High concentrations of SO_4^{2-}, Al, Ca, Cu, Fe, Mg, Mn, Ni, U, Zn, and REE were found in the seepage water. Utilizing REE concentrations (up to 3 mg/l total REE) normalized to shale, flow paths of seepage water in the surface water and in shallow groundwater of the valley sediments were detected.

1 Introduction

1.1 Background

The Ronneburg mining district (Fig. 1) in Eastern Thuringia (Germany) was one of the largest uranium mining sites in the world. Between 1950 and 1990 about 216000 t of uranium were produced in the eastern part of Germany. After the USA and Canada the former GDR was the third largest uranium producer in the world (BARTHEL 1993). About half of the production (113000 t) originated from the underground and the open pit operations near the city of Ronneburg. By the end of 1990 the mining legacy consisted of (i) a complex underground mine covering an area of 74 square kilometers with 40 shafts and about 3000 km of mine workings, (ii) the Lichtenberg open pit mine with an open volume of about 84 Mio. m³, (iii) 16 waste rock dumps with about 200 Mio m³ of partly acid generating waste rock, and (iv) about 1000 ha of contaminated areas.

Starting in 1990 the remediation projects are mainly aimed at reducing the radiological and chemical exposure of the public and the environment (GATZWEILER et al. 1997). One of the remediation topics is backfilling the former waste rock dumps into the open-pit mine of Lichtenberg. The passive flooding of the mine was initiated in 1998 and is expected to be completed between 2003 and 2005. The investigation area "Gessental" valley is expected to be the main discharge area for the flooding water in the future (GELETNEKY 2002; UNLAND et al. 2002).

1.2 Rare earth elements

REE (La-Lu) show smooth but continuous variations of their chemical behaviour as a function of their atomic number. After standardization to PAAS (Post Archean Australian Shale) (TAYLOR & MCLENNAN 1985) they can be used as tracers in ground water and surface water (JOHANNESSON 2000). Furthermore, they are suited to study processes such as dissolution, sorption, complexation (ASTROM 1993), (co)precipitation (BYRNE & KIM 1993) and especially water-rock interaction (WORRALL et al. 2001). The use of PAAS-normalized REE in flooded mines (WOLKERSDORFER 2002) and in acid rock drainage (MERTEN et al. 2002) show examples for their successful application as environmental tracers.

2 Geology

The uranium deposit of Ronneburg, Thuringia, Germany, is a strata-controlled, structure bound deposit. It consists of uranium concentrations in small scale brittle structures which form stockworks within or immediately adjacent to carbonaceous, pyritic black shales. The Paleozoic host rocks mainly consist of argillaceous and siliceous black shales with intercalations of dolomitic and phosporite nodule beds (Silurian "Graptolithenschiefer"). The main black-shale horizon lies below Ordovician carbonaceous sandy shales and overlies Silurian carbonate rocks ("Ockerkalk"). Some Devonian metabasaltic dikes and sills cut the metasedimentary rocks (DAHLKAMP 1993). The rocks contain up to 7 wt% sulfides, 5-9 wt% organic carbon, 40–60 ppm uranium and a series of trace elements.

The intensively folded and faulted, incompetent and competent rocks have high density small scale brittle structures (fissures, joints, faults). Permian and Tertiary supergene oxidation processes associated with mobilization and precipitation of trace elements created an oxidation and cementation zone. The irregular distribution and size of the ore bodies is controlled by major and minor faults. The uranium ore appeared near the surface in the southern part and down to 1000 m deep in the northern part of the Ronneburg mining district.

3 Investigation Area

The creek "Gessenbach" is the main drainage system in the Western part of the former uranium mining area. The Gessental valley is located between the cities of Ronneburg and Gera. Near the city of Ronneburg it is influenced by two former waste rock dumps called Gessenhalde and Nordhalde. The Gessenbach creek and its tributary Badergraben follow the valley in western direction (Fig. 1, Fig. 2).

The Gessental valley will be one of the main discharge areas of mine water in the post-flooding situation.

4 Hydrochemical Results

1.3 General Hydrochemistry

The hydrological situation of the Gessental valley is dominated by the existence of the former dumps and by the groundwater depression cone of the underground mine. The seepage waters in the western part of the Nordhalde (Q4, Q16 in Fig. 2) are highly mineralized (el. conductivity about 12 mS/cm), have a low pH (2-3.5) and high redox potentials (about 570 mV). This water has high concentrations of Fe, Ca, Mg, Al, Mn, SO_4, Si, Cu, Zn, Ni, Cd, Cr, U and REE. Discharge measurements in the Gessenbach creek showed that the amount of seepage water flow-

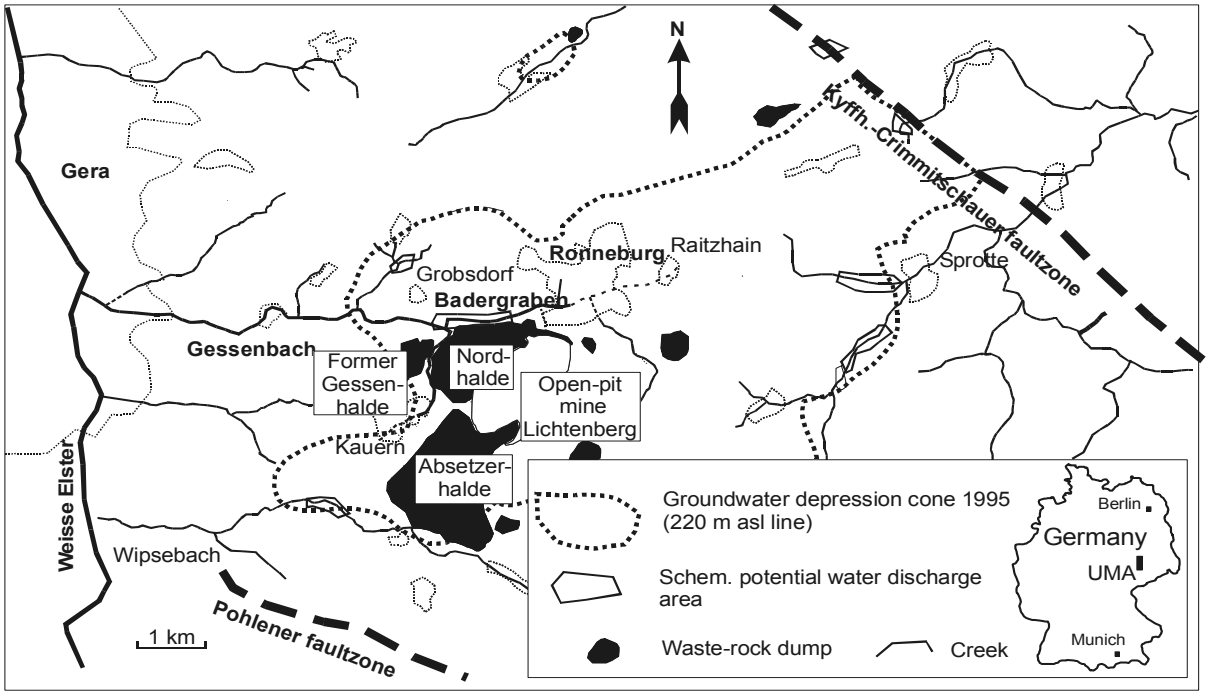

Figure 1: Gessental valley in the Western part of the former Uranium mining area of Ronneburg (GELETNEKY 2002). UMA: Uranium mining area of Ronneburg

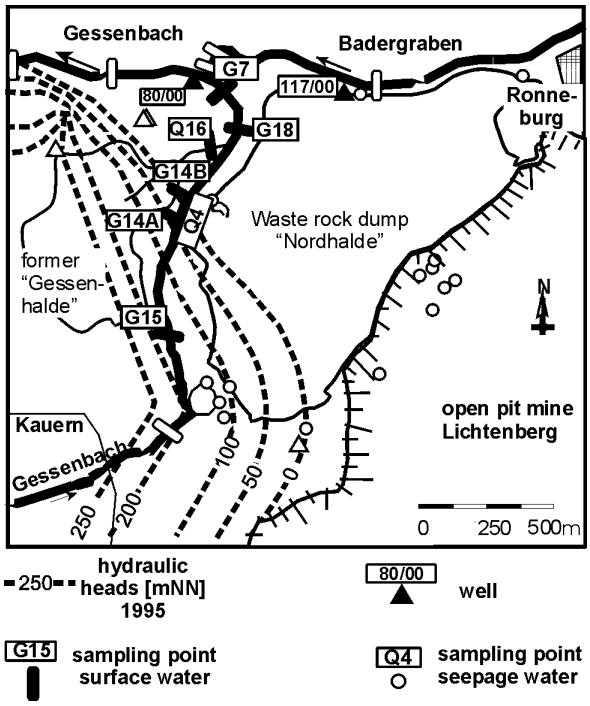

Figure 2: Sampling points of the surface water and groundwater around the waste rock dump "Nordhalde" and hydraulic head of the groundwater depression cone in 1995.

ing into the creek is low (less than 0.5 l/s).

To investigate the impact of the seepage water of the dumps on the Gessenbach creek and the grounddwater sampling was performed regularly at five sampling-locations (G15, G14A, G14B, G18, G7 in Fig. 2, Fig 3).

Before both creeks pass the dump the headwaters are strongly influenced by untreated municipal sewage from Ronneburg and Kauern (G15). The pH of the water is variable but mostly alkaline

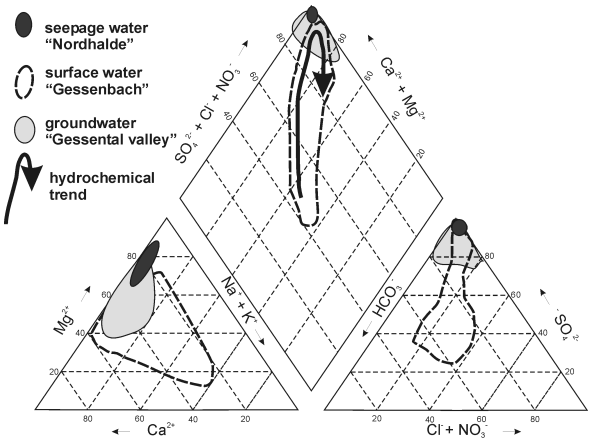

Figure 3: Piper-plot of the main hydrochemistry of the seepage and surface water and the groundwater of the Gessental valley.

(7.5-9). The electric conductivity (1.5-2 mS/cm) is low compared to the seepage water (12 mS/cm). When the Gessenbach creek passes the area of the Nord- and Gessenhalde the water becomes enriched in total dissolved solids (TDS), Fe, Ca, Mg, Al, Mn, SO_4, Si, Cu, Zn, Ni, Cd, Cr, U and REE. In Piper plots hydrochemical trends can be shown (Fig. 3). In the Gessenbach creek the chemical composition of the water changes from an alkaline Ca-Mg-SO_4-HCO_3-type to an acidic Mg-Ca-SO_4-type (Fig. 3).

Some of the components are transported as conservative tracers (Mg, Ca, Na, K, Cl, PO_4), others undergo reactive transport (Fe, Mn, Si, Cu, Ni, REE; GELETNEKY 2002).

The groundwater situation in the valley is strongly influenced by the groundwater depression cone. The alluvial sediments north of the waste rock dumps are only partly saturated with groundwater. However, groundwater in wells 117/00 and 80/00 could be sampled in summer 2000. The water can be classified as Mg–Ca-SO_4-type with a pH varying between 5.3 and 6.4, enriched in Fe, Zn, Ni, Co, Sr and a special REE-pattern (Fig. 3).

1.4 Using REE-patterns as tracers for ARD

Normalizing REE concentrations to Post Archaean Australian Shale (PAAS) enrichment of middle REE (Sm to Dy) and especially of heavy (Ho to Lu) REE as compared to the light ones (La-Nd) is observed in the investigated seepage waters.

For two investigated seepage waters (Q16, Q4, Fig. 2) significantly different REE patterns are obtained. Furthermore, the presence and absence of positive Ce anomalies could be observed. Nevertheless, for the seepage water of the Nordhalde (Q4) – sampled over a period of two years - the shale normalized REE pattern shows only minor variations, although the concentration differs. Thus, REE patterns are independent of REE concentrations and independent of discharge.

At the sampling points in the surface water (G14A, G14B, G18, G7) nearly the same REE pattern were observed (Fig. 4). This represent a diffuse inflow of REE-rich ARD of the dumps into the creek The absolute concentrations of REE in the creek are up to 100 times less than in seepage water due to mixing and (co)precipitation of REE. Lu/La and Sm/La rela-

tions show a significant decrease with increasing distance from the dump. This is caused by preferential (co)precipitation of heavy REE with amorphous Fe-hydroxides along the Gessenbach.

The general shape of the REE pattern of the dump Nordhalde can also be found in groundwater wells 117/00 and 80/00. However, the degree of enrichment of heavy REE is less pronounced. Again, the REE patterns of the groundwater samples as a function of time are very similar. The absolute concentrations of REE in groundwater are 1000 times lower than in seepage. A negative Ce anomaly is caused by precipitation of Cerianite due to the Eh-pH conditions in the groundwater (LEYBOURNE 2000).

In order to investigate whether the REE patterns in the seepage water resemble the REE concentrations in the Silurian source rocks LA-ICP-MS measurements were performed using glass beads of the most important lithologies "Ockerkalk" and fine grained alluvial sediments.

In contrast to the patterns of the seepage, the REE patterns of the Silurian rocks are featured by rather flat patterns with enrichment of middle REE (Sm – Dy). The concentrations of REE in the different lithologies differ only by a factor of 2.

Batch experiments using deionised water were performed. Results show that the REE concentrations eluted from the different lithologies differ by a factor of 1000. However, results show a preferentially leaching of heavy REE in all investigated source rocks. The highest absolute concentrations of REE appear in the eluates of the Silurian "Ockerkalk". This REE pattern closely reflects the pattern found in the seepage water. Therefore, it is assumed to be the most important source for the occurence of this special REE pattern.

5 Conclusions

It is shown that the identification of contaminant sources can be performed using shale normalized REE patterns. It is also possible to follow flow pathes of contamination in surface water and groundwater by using REE patterns.

Both the chemical composition and the REE pattern in the surface water show an influence of acid seepage water, which is originated from the dumps. The hydrochemical patterns of REE in the groundwater are comparable with signatures of the seepage. Both show enrichment in the

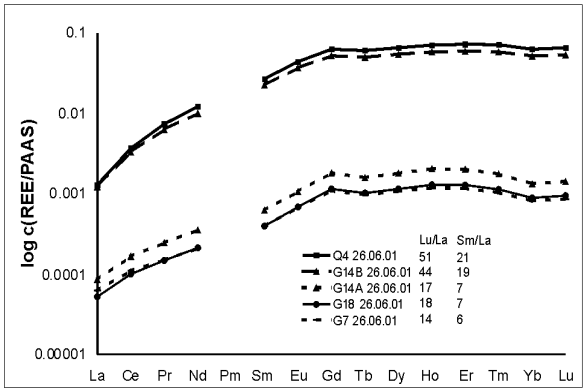

Figure 4: REE concentrations normalized to PAAS in June 2001 with enrichments in middle (expressed as Sm/La) and heavy REE (expressed as Sm/La) along a flowpath in the Gessenbach creek.

middle and in the heavy REE (MERTEN et al. 2002; GELETNEKY et al. 2001).

The REE patterns in the water samples do not reflect the source rock pattern as was demonstrated by laser ablation ICP-MS experiments. Percolation in batch experiments shows that the unique heavy REE enriched patterns are due to preferential leaching especially from Silurian "Ockerkalk".

References

ASTROM, M. (2001): Abundance and fractionation patterns of rare earth elements in streams affected by acid sulphate soils, Chem. Geol. 175: 249-258.

BARTHEL, F.H. (1993): Die Urangewinnung auf dem Gebiet der ehemaligen DDR von 1945 bis 1990. Geol. Jb. A142: 335-346.

BYRNE, R.H. & KIM, K.-H. (1993): Rare earth precipitation and coprecipitation behavior: The limiting role of PO43- on dissolved rare earth concentrations in seawater, Geochim. Cosmochim. Acta 57, 519-526.

DAHLKAMP, F.J. (1993): Uranium ore deposits. Berlin: Springer.

GATZWEILER, R., HÄHNE, R., ECKART, M., MEYER, J. & SNAGOVSKY, S. (1997): Prognosis of the flooding of uranium mining sites in east Germany with the help of the numerical box-modeling. In Veselic, M & Norton, J.P.J. (eds). Mine water and the environment, Proc. 6th IMWA congr., Bled, 8-12 September 1997.

GELETNEKY, J.W., MERTEN, D., & BÜCHEL, G. (2001): Seepage water from uranium mining

dumps in Eastern Thuringia, Germany: A hydrogeochemical study.- EUG 11, Strasbourg, J. Conf. Abs., 6: 44, Cambridge: Cambridge Publ.

GELETNEKY, J.W. (2002): Hydrogeologische/Hydrologische Untersuchungen einer Prä-Flutungssituation am Beispiel des Gessentals im ehemaligen ostthüringischen Uranbergbaugebiet.- Diss. Univ. Jena, 261 S; Jena.

JOHANNESSON, K.H. & LYONS, W. B. (2000). Rare earth elements in groundwater in: P. Cook and A. Herczeg (eds.) Environmental Tracers in Subsurface Hydrology: 85-492. Dordrecht: Kluwer.

LEYBOURNE, M.I., GOODFELLOW, W.D., BOYLE, D.R. & HALL, G.W. (2000): Rapid development of negative Ce anomalies in surface waters and contrasting patterns in groundwaters associated with Zn-Pb massive sulphide deposits. Appl. Geochem. 15: 695-723.

MERTEN, D., GELETNEKY, J., LAHL, K. & BÜCHEL, G. (2002): Delineation of contamination flows produced by acid mine drainage in a former uranium mining site (Ronneburg, Eastern Thuringia, Germany) by the use of rare earth elements. in Merkel, B., Planer-Friedrich, B., Wolkersdorfer, C (eds.) Uranium in the Aquatic Environment: 685-691.

TAYLOR, S.R. & MCLENNAN, S.M. (1985): The continental Crust: Its Composition and Evolution. Blackwell: Oxford.

UNLAND, W., ECKART, M., PAUL, M., KUHN, W. & OSTERMANN, R (2002): Groundwater rebound compatible with the aquatic environment – technical solutions at WISMUT`s Ronneburg mine. In: MERKEL, B., PLANER-FRIEDRICH, B., WOLKERSDORFER, C (eds.) Uranium in the Aquatic Environment: 667-676.

WOLKERSDORFER, C. (2002): Rare Earth Elements (REEs) as natural tracers in mine waters. In: MERKEL, B., PLANER-FRIEDRICH, B., WOLKERSDORFER, C (eds.) Uranium in the Aquatic Environment: 951-958.

WORRALL, F. & PEARSON, D.G. (2001): Water-rock interaction in an acidic mine discharge as indicated by rare earth element patterns. Geochim. Cosmochim. Acta 65: 3027-3040.


BERGAKADEMIE
TECHNISCHE
UNIVERSITÄT
FREIBERG

Dendrokorrektur und CO_2–Problem: Ein Beitrag zur ^{14}C–Datierungsmethode

Detlef Hebert

TU Bergakademie Freiberg, Institut für Angewandte Physik, Bernhard-von-Cotta-Str.4, 09599 Freiberg

E-Mail: hebert@tu-freiberg.de

^{14}C-Alter unterhalb von 10.000 Jahren können durch Anwendung von Dendrokorrekturkurven hinreichend genau in kalendarische Alter umgewandelt werden. Im Bereich höherer Alter zeigt sich eine zunehmend systematische Abweichung, die bei hohen ^{14}C–Altern etwa 3.000 Jahre betragen kann.

Ursache, sowie Zusammenhänge zwischen dem CO_2–Problem der Klimaforschung und Altersfehlern der ^{14}C–Methode werden erörtert.

1 Einführung in die ^{14}C–Methode

Die Radiokohlenstoff-Datierungsmethode wurde vor etwa 50 Jahren von LIBBY, ANDERSON, ARNOLD u.a. ausgearbeitet (BERGER & MARSHALL-LIBBY 1980).

W.F.Libby (Nobelpreis 1960) erkannte, dass das in der unteren Atmosphäre über die Reaktion ^{14}N (n, p) ^{14}C natürlich produzierte ^{14}C die mit dem CO_2 der Atmosphäre austauschenden Kohlenstoff-reservoire (Biosphäre, Hydrosphäre) radioaktiv markieren sollte und dass der ^{14}C–Gehalt organischer Materie infolge der radioaktiven Umwandlung von ^{14}C ($T_{1/2} = 5730$ a) altersabhängig sein muss:

$$a(\tau) = a_0 \cdot \exp\left(\frac{\ln 2}{T_{1/2}} \cdot \tau\right) \qquad (1)$$

Die wesentlichen Voraussetzungen für die Gültigkeit von Gleichung 1, nämlich:

- konstante Größe der globalen Kohlenstoffreservoire,
- zeitlich stabile Austauschverhältnisse zwischen diesen Reservoiren und
- zeitlich konstante ^{14}C–Produktion,

wurden damals als erfüllt angesehen.

DE VRIES stellte Ende der 50er Jahre fest, dass der ^{14}C–Gehalt des atmosphärischen CO_2 in der Vergangenheit Schwankungen unterlegen hatte (DE VRIES 1958), die zu Abweichungen der ^{14}C–Altervom kalendarischen Alter um einige Jahrhunderte führten. Als deren Ursache erkannte man später Schwankungen des magnetischen Dipolmomentes der Erde (BUCHA 1970), sowie periodische Änderungen des Sonnenaktivität (SONETT 1992).

Diese Unsicherheit der Radiokohlenstoff-Methode wurde für Alter bis zu 11.000 Jahren durch den Vergleich von ^{14}C–Altern mit dendrochronologisch bestimmten Altern (Dendro-

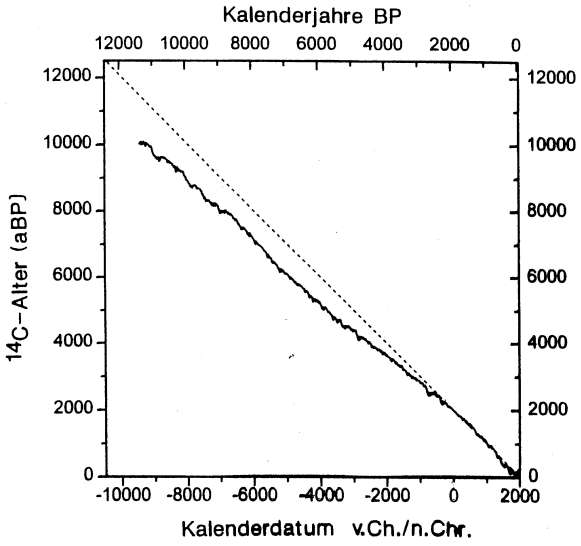

Abb. 1: Dendrokorrekturkurve (nach STUIVER 1982; PEARSON 1983; BECKER 1993).

korrekturkurve, Abb. 1) prinzipiell behoben (STUIVER 1982; PEARSON 1986; BECKER 1993).

Für den Altersbereich zwischen 12.000 und 44.000 Jahren sind, abgeleitet aus dem Vergleich von ^{14}C–Altern mit Uran-Thorium-Altern, Kalibrierkurven publiziert worden (BARD et al. 1990; BECK et al. 2001), die starke Abweichung der ^{14}C–Altervom kalendarischen Alter (ca. –5.000 Jahre) belegen. Als Ursache werden neben Magnetfeldschwankungen und Variationen der Sonnenaktivität „starke Veränderungen im globalen CO_2-Kreislauf" vermutet.

2 Das CO_2–Problem

Ein signifikantes Ereignis im CO_2–Austauschsystem ist aus der Klimaphysik bekannt: Es handelt sich um den raschen Anstieg des CO_2–Gehaltes der Atmosphäre am Eiszeitende, also zwischen 20.000 und 10.000 B.P.

Das haben CO_2–Bestimmungen an Luft aus Eisbohrkernen der Station Camp Century (Grönland) und Byrd (Antarktika) ergeben (DANSGAARD et al. 1971; JOHNSEN et al. 1972). Unterdessen ist die Variation des CO_2–Gehaltes der Luft zwischen 190 ppm im Hochglazial (zuletzt ca. 20.000 B.P.) und 280 ppm in der Warmzeit für vier Eiszeit-Warmzeit-Perioden (Abb.2).

Die deutliche Abnahme des CO_2–Gehaltes der Atmosphäre im Verlauf der Eiszeit hatte Anlass zu weitreichenden Befürchtungen hinsichtlich einer globalen Erwärmung infolge der anthropogenen CO_2–Freisetzung in jüngster Zeit gegeben

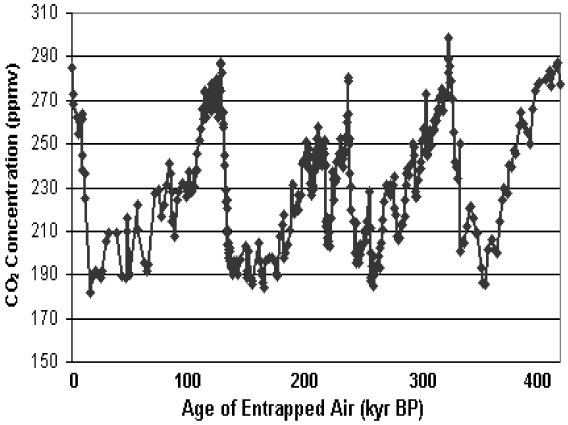

Abb. 2: CO_2-Gehalt in Luft eines Eisbohrkerns der Antarktisstation Vostok (BARNOLA et al. 2003).

(z.B. MANABE & WETHERALD 1975; FLOHN 1984; WIGLEY 1987; GRIESER, STAEGER & SCHÖNWIESE 2000). Ursache für die Einordnung des Kohlendioxides in die Gruppe der gefährlichsten Treibhausgase war einerseits eine zweifelhafte Extrapolation aus Untersuchungen zum natürlichen Treibhauseffekt (KONDRATYEV 1969) und andererseits der zunächst nicht bekannte Kausalzusammenhang zwischen CO_2-Absenkung in der Atmosphäre und globaler Temperaturabnahme bzw. der möglichen Umkehr beider Vorgänge.

Unterdessen gilt als erwiesen, dass die CO_2–Abnahme in atmosphärischer Luft der globalen Abkühlung innerhalb der Eiszeit folgte (Abb. 3).

Insbesondere ist aus Abb. 2 und Abb. 3 zu ersehen, dass das Klimasystem der Erde den Wechsel

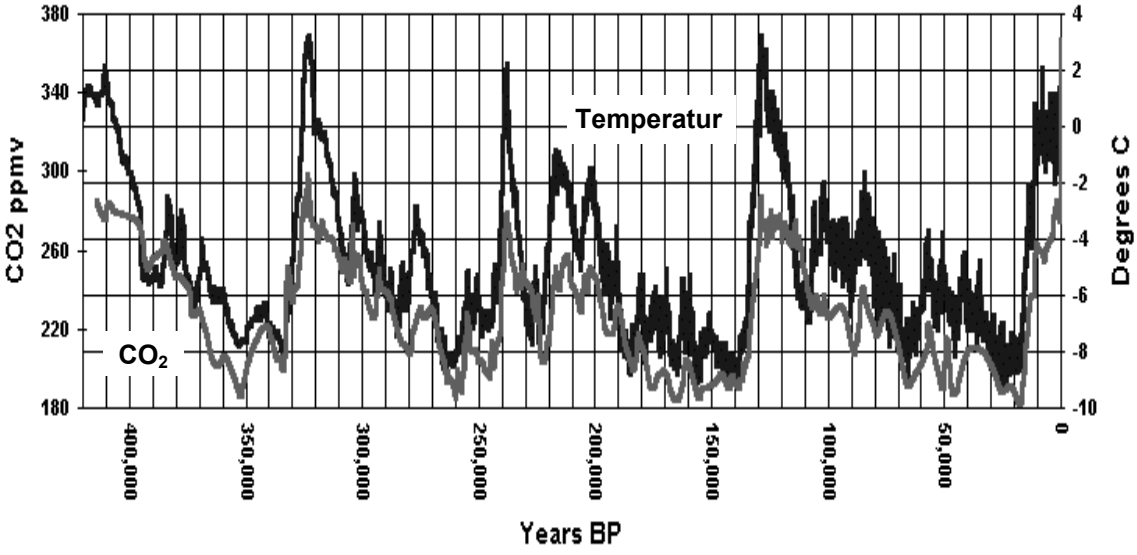

Abb. 3: Temperatur- und CO_2–Kurve eines Eisbohrkerns aus Vostok (Antarktika) für vier Eiszeit Warmzeit-Perioden (BARNOLA et al. 2003).

Eiszeit-Warmzeit viermal hintereinander mit jeweils etwa gleicher Amplitude der Temperatur sowie des CO_2–Gehaltes der atmosphärischen Luft vollzogen hat.

Die Tatsache, dass der CO_2–Inhalt der Atmosphäre sich gerade mitten im ^{14}C–Datierungszeitraum nahezu sprunghaft geändert hat, muss hinsichtlich möglicher Auswirkungen auf ^{14}C–Alter untersucht werden.

3 Der Pleistozäne CO_2–Speicher

Der Kohlendioxidgehalt der Luft ist im Verlauf einer Eiszeit innerhalb von ca. 100.000 Jahren von anfangs 290 ppm allmählich auf 190 ppm abgesunken und nach deren Ende wieder auf das ursprüngliche Niveau angestiegen (Abb. 2). Die der Atmosphäre jeweils entzogene CO_2–Masse beträgt knapp 260 Gt Kohlenstoff entsprechend 950 Gt CO_2 (Abb. 4).

Die Zeitkonstante für den Übergang von atmosphärischem CO_2 in den gesuchten Kohlenstoffspeicher muss in der Größenordnung von 100.000 Jahren liegen. Sie ist jedenfalls viel größer als alle im CO_2–Austauschsystem wirkenden Zeitkonstanten (z.B. Oberflächenwasser – Tiefsee ca. 1.000 Jahre (Abb. 4).

Als wahrscheinlichste Hypothese gilt, dass sich im Schelfbereich des pleistozänen Ozeans eine starke Entwicklung der ozeanischen Biosphäre (Foraminiferen) vollzog (BROECKER 1988; BROECKER 1996). Als Argument wird u.a. die Verschiebung des ^{13}C-Verhältnisses im Meeres-CO_2 zu positiven Werten hin genannt, was sich als Folge des bei der Assimilation auftretenden Isotopieeffektes (Bevorzugung des leichteren Kohlenstoffisotops ^{12}C) verstehen lässt. Wenn dieser Kohlenstoffspeicher am Eiszeitende abgebaut wird (warum), überträgt sich insbesondere auch sein ^{14}C–Gehalt auf das freigesetzte CO_2, das den Ozean wieder verlässt.

4 Auswirkungen auf ^{14}C–Alter

Der ^{14}C–Gehalt des aus dem Ozean in die Atmosphäre abgegebenen CO_2 muss etwa 80...90 pmC betragen haben; dies ist der für ozeanisches CO_2 typische Wertebereich (PENG & BROECKER 1992). Der ^{14}C–Gehalt des atmosphärischen CO_2 muss infolge dessen während des Übergangs von der Eiszeit zur Warmzeit abgenommen haben. Rechnerisch ergibt sich bei einer Mischung von 30% Ozean–CO_2 und 70% Luft–CO_2 (mit 100 pmC) ein ^{14}C-Anfangsgehalt von 95 pmC. Das Eiszeitende sollte folglich in Dendrokorrekturkurven oder beim Vergleich von U–Th–Altern mit ^{14}C–Altern temporär an zu hohen Radiokohlenstoffaltern sichtbar sein.

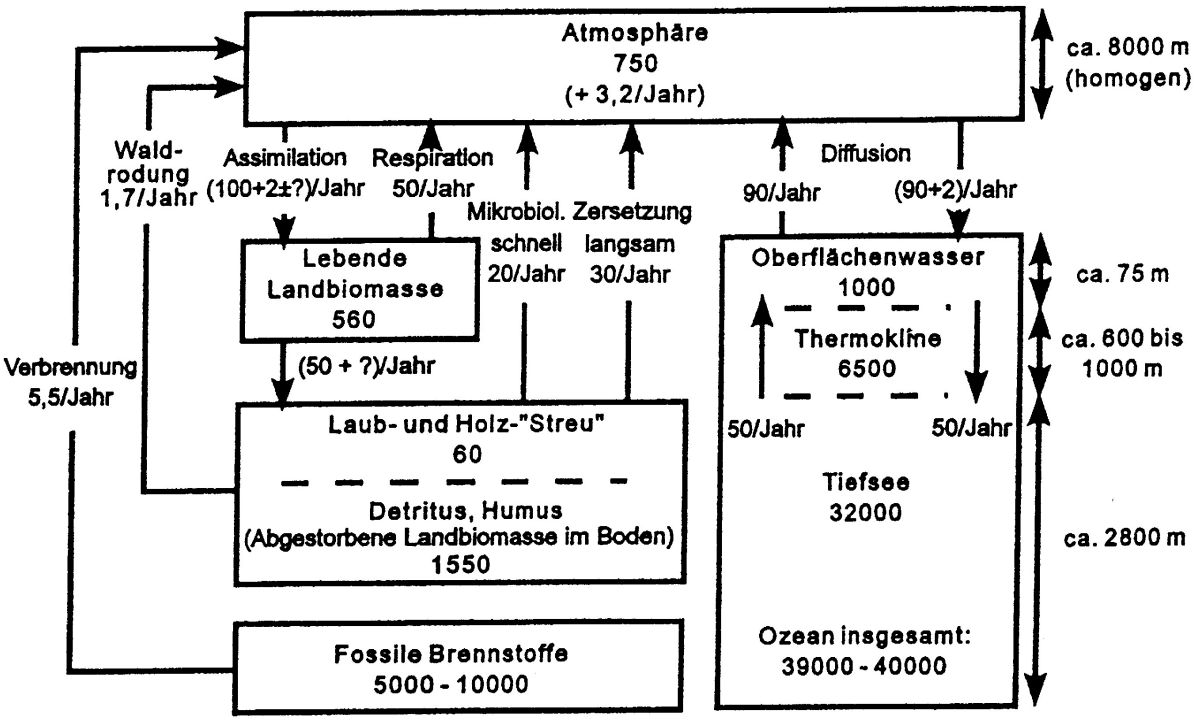

Abb. 4: CO_2–Austausch zwischen Atmosphäre, Biosphäre und Ozean – Inventar in Gt C, Flüsse in Gt C/a (ROEDEL 2000).

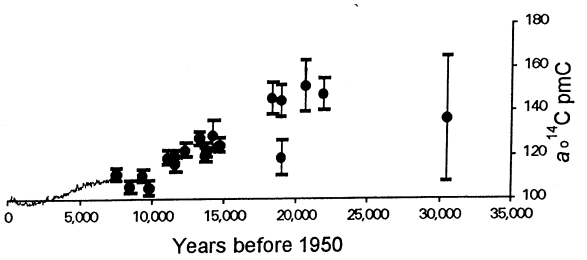

Abb. 5: Zeitliche Veränderung des C-14-Anfangsgehaltes aus (CLARK & FRITZ 1997) nach (BARD et al. 1993).

Wie Abb. 5 zeigt, ist dieser Effekt offenbar durch eine signifikant erhöhte ^{14}C–Produktion überdeckt, die als Folge eines kleineren Dipolmomentes des Magnetfeldes der Erde interpretiert wird (STERNBERG 1992).

Unterdessen wurde für den Zeitraum zwischen 10.000 a B.P. und 45.000 a B.P. eine ^{14}C–Kalibrierkurve angegeben, die eine hinreichend gute Übereinstimmung zwischen kalendarischen Alter und ^{14}C–Alter belegt (KITAGAWA & VAN DER PLICHT 1998; JÖRIS & WENINGER 2000).

Dank

Der Verfasser bedankt sich bei Herrn H. Fritz für die technische Anfertigung des Manuskriptes.

Literatur

BARD, E., ARNOLD, M., FAIRBANKS, R.G. & HAMELIN, B. (1993): Th-230, U-234 and C-14-Dates obtained by mass spectrometry on corals. – Radiocarbon 35 (1993) p.191—199.

BARD, E., HAMELIN, B., FAIRBANKS, R. & ZINDLER, A. (1990): Calibration of the ^{14}C Timescala over the past 30.000 years using Mass Spectrometric U-Th ages from Barbados Corals. – Nature, Vol.345 (1990) p.405—410.

BARNOLA, J., RAYNAUD, D., LORIUS, C. & BARKOV, N. I. (2003): Historical CO_2 Record from the Vostok Ice Core, in: Trends: A Compendium of data on Global Change. – Oak Ridge National Laboratory, Oak Ridge, Tenn., USA.

BECK, J. W. et al. (2001): Extremely Large variations of Atmospheric ^{14}C Concentration during the Last Glacial Period. – Science 292 (2001) p.2453—2458.

BECKER, B. (1993): A 11000-year German Oak and Pine dendrochronology for radiocarbon calibration. – Radiocarbon 35 (1993) p.201—213.

BERGER, R. & MARSHALL-LIBBY, L. (1980): Radiocarbon and Tritium – Publications of Willard Frank Libby. – Geo Science Analytical, Santa Monica, USA.

BROECKER, W.S. (1988): Der Ozean, S.144—155 in: Die Dynamik der Erde. – Spektrum der Wissenschaft, Heidelberg.

BROECKER, W.S. (1996): Plötzliche Klimawechsel, S.86—93. – Spektrum der Wissenschaft 1/1996, Heidelberg.

BUCHA, V. (1970): Influence of the Earth Magnetic Field on Radiocarbon dating, p.501—511. – Radiocarbon Variations and Absolute Chronology, Almquist & Wiksells, Uppsala.

CLARK, J. & FRITZ P. (1997): Environmental Isotopes in Hydrogeology. – Lewis Publishers, Boca Raton, New York.

DANSGAARD, W. et al. (1971): Climatic record Revealed by the Camp Century Ice Core. – The Late Cenozoic Glacial Ages, Yale University, 1971, p.37—56.

DEVRIES, H. (1958): Variation in Concentration of Radiocarbon with Time and Location on Earth. – Kon. Ned. Akad. Wet., Proc. Ser. B 61 p.94—102.

FLOHN, H. (1984): Das CO_2-Klima-Problem und die Rolle biologischer Vorgänge. – Biologie in unserer Zeit 14 (1984) S.42—47.

GRIESER, J., STAEGER, T. & SCHÖNWIESE, CH.-D. (2000): Statistische Analysen zur Früherkennung globaler und regionaler Klimaänderungen auf Grund des anthropogenen Treibhauseffektes. – Ber. Inst. Meteorol. Geophys. Uni Frankfurt/Main Nr.103.

HOUTERMANS, J., SUESS, H. E. & MUNK, W. (1967): The Effect of Industrial Fuel Combustion on the Carbon-14-Level of Atmospheric CO_2, p.57—68 – Radioactive Dating and Methods of Low-Level Counting, IAEA Vienna.

JOHNSEN, S. J. et al. (1972): Oxygen Isotope through the Antarctic and Greenland Ice Sheets. – Nature 235 (1972) p.429—434.

JÖRIS, O. & WENINGER, B.(2000): Towards an Absolute Chronology of the Last Glacial. – Journal of Quarternary Science, RAPID COMMUNICATION (2000) p.1—3.

KITAGAWA, H. & VAN DER PLICHT, J. (1998): Atmospheric Radiocarbon Calibration to 45.000 yr B.P. – Science 279 (1998) p.1187—1190.

KONDRATYEV, K. YA. (1969): Radiation in the Atmosphere. – Academic Press, New York, London.

MANABE, S. & WETHERALD, R. T. (1975): The Effects of Doubling the CO_2 Concentration on the Climate of a General Circulation Model. – Journal of the Atmosphere Sciencer 32 (1975) p.3—15.

PEARSON, G. W. et al. (1986): High-precision ^{14}C measurement of Irish oaks to show the natural ^{14}C variations from AD 1840 to 5210 B.C. – Radiocarbon 28 (1986) p.911—934.

PEARSON, G. W., BECKER, B. & QUA, F. (1993): High-precision ^{14}C measurement of German oaks to show the natural ^{14}C variations from 7980 to 5000 B.C. – Radiocarbon 35 (1993) p.93—104.

PENG, T.-H. & BROECKER, W.S. (1992): Reconstruction of Radiocarbon Distribution in the Glacial Ocean, p.75—92 in: TAYLOR, R. E. et al. (Eds.), Radiocarbon after Four Decades. – Springer, New York.

ROEDEL, W. (2000): Physik unserer Umwelt – Die Atmosphäre, 3.Auflag. – Springer, Berlin, Heidelberg.

SONETT, C. P. (1992): The Present Status of Understanding of the Long-Period spectrum of Radiocarbon, p.50—61 in: TAYLOR, R. E. et al. (Eds.), Radiocarbon after Four Decades – Springer, New York.

STERNBERG, R. S. (1992): Radiocarbon Fluctuations and the Geomagnetic Field, p.93—119 in: TAYLOR, R. E. et al. (Eds.), Radiocarbon after Four Decades. – Springer, New York.

STUIVER, M. (1982): A high-precision calibration of the AD radiocarbon timescale. – Radiocarbon 24 (1982) p.1—26.

WIGLEY, T. M. L. (1987): Relative Contributions of Different Trace Gases to the Greenhouse Effect. – Climate Monitor 16 (1987) p.14—28.


BERGAKADEMIE
TECHNISCHE
UNIVERSITÄT
FREIBERG

Hydrochemische und isotopengeochemische (S, O) Veränderungen von Grubenwasser auf einem vertikalen Fließweg

Manuela Junghans, Marion Tichomirowa

TU Bergakademie Freiberg, Institut für Mineralogie, Brennhausgasse 14, 09599 Freiberg, junghans@merkur.hrz.tu-freiberg.de, tichomir@mineral.tu-freiberg.de

The isotopic and chemical composition of water and dissolved sulfate of mine water from a mined and backfilled ore vein at the polymetallic sulfide deposit in Freiberg was used to study the mixing processes in mine water. It has been demonstrated that mine water with anomalous isotopic values is characterized by anomalous concentrations of anion, cations and metals, which is explained by a possible anthropogenic source. Using $\delta^{34}S_{SO4}$- and $\delta^{18}O_{SO4}$-values it has been calculated that 23 % to 62 % of sulfate in the mine water at the deepest level originate from sulfide oxidation. Isotope exchange as well as fixation processes may be the cause for larger variations of the $\delta^{34}S_{SO4}$- and $\delta^{18}O_{SO4}$-values at the deepest level investigated with higher residence times and lower flow rates of the mine water.

1 Einleitung und Untersuchungsziele

Stabile Isotope stellen natürliche Tracer dar, die Rückschlüsse auf Herkunft bzw. Mischungsverhältnisse von Wässern oder auf Prozesse, die die Wasserbeschaffenheit beeinflussen, erlauben. Die Isotopenverhältnisse des Schwefels und des Sauerstoffs können genutzt werden, um Aussagen über geochemische und biogeochemische Prozesse und Mischungsprozesse zu treffen, die in Bergwerken bzw. Grubenwässern ablaufen.

Fokus unserer Untersuchungen ist der abgebaute Erzgang „Schwarzer Hirsch Stehender“, auf dem untertage ein Grubenwasser auf drei Teufenniveaus beprobbar ist. Aufgrund seiner guten Zugänglichkeit war dieser Erzgang in den vergangenen Jahren Gegenstand geochemischer und isotopengeochemischer Untersuchungen (WINKLER 1998; WINKLER et al. 2000; BAACKE 2000; HAUBRICH et al. 2000; HAUBRICH 2001; HAUBRICH & TICHOMIROWA 2002). Die in diesem Artikel präsentierten weiterführenden Untersuchungen dienen einerseits der Erweiterung der Datenbasis für Isotopenwerte, anderseits der kombinierten Interpretation von geochemischen und isotopengeochemischen Daten, um zusätzlich Erkenntnisse über die zeitlichen Variationen von Mischungsprozessen und die Intensität der Sulfidoxidation zu gewinnen.

Die abgeleiteten zeit- und teufenabhängigen Zusammenhänge von geochemischen und isotopengeochemischen Parametern für den Erzgang „Schwarzer Hirsch Stehender“ sind notwendig für die Interpretation von unregelmäßigen Messdaten im weiteren Umfeld der Grube Himmelfahrt (des Freiberger Reviers), die wir in einem weiteren Artikel vorstellen werden.

2 Lage und Geologie/ Mineralogie

Der Erzgang „Schwarzer Hirsch Stehender“ war einer der bedeutendsten Erzgänge des Freiberger Reviers (zur Lage vgl. HAUBRICH & TICHOMIROWA 2002). Er wurde vor allem im Zeitraum 1850 bis 1896 abgebaut und verfüllt. Dieser Erzgang, der zur Quarz-Polymetall-Assoziation gehört (BAUMANN et al. 2000), führt hauptsächlich Galenit, Pyrit, Sphalerit und Arsenopyrit als Erzminerale und vorrangig Quarz als Gangart. Das Nebengestein bildet der Freiberger Graugneis.

3 Veränderung der Wassermenge und der chemischen Zusammensetzung des Grubenwassers mit der Tiefe

Das Grubenwasser, das drei Abbaue auf seinem ca. 400 m langen, zumeist vertikalen Fließweg durchströmt, wurde auf drei Sohlen beprobt (Abb. 1). Die hydraulische Verbindung zwischen den Beprobungspunkten konnte anhand eines Tracerversuchs nachgewiesen werden (HAUBRICH et al. 2000; HAUBRICH & TICHOMIROWA 2002). Die Fließzeit durch die Abbaue beträgt ca. eine halbe bis eine Stunde und deutet auf die Existenz größerer Wassertaschen hin (BAACKE 2000). HAUBRICH (2001) gibt auf allen drei Niveaus gleichbleibende Wassermengen an, wobei nur Messungen auf der 1.Sohle durchgeführt wurden. Im Gegensatz dazu wurde für die meisten Probenahmekampagnen in dieser Studie generell eine Abnahme der Wassermenge mit der Tiefe festgestellt. Unveränderte Wassermengen (von der Stollnsohle zur 1. Sohle sowie von der 1. zur ½ 3. Sohle) oder steigende Wassermengen (nur während der Probenahme am 1.7.2001) wurden seltener gemessen. Diese Beobachtungen werden auf eine Migration auf z.T. unterschiedlichen Fließwegen zurückgeführt. Wahrscheinlich werden in Zeiten mit erhöhtem Wasserangebot (Schmelzperiode, nach längeren Niederschlägen) zusätzliche Fließwege mobilisiert.

Die geochemische Zusammensetzung des Grubenwassers wird von verschiedenen Prozessen wie Freisetzung aus den Primärsulfiden, aus dem Nebengestein und Fällungs- bzw. Fixierungsprozessen bestimmt. Nach BAACKE (2000) und WINKLER et al. (2000) entspricht das Grubenwasser der Stollnsohle einem Mischwasser aus Bodensickerwasser und Grundwasser. Der Eintrag von Schwermetallen, Al, As und Sulfat aus der Sulfidoxidation wird von WINKLER et al. (2000) als gering eingeschätzt und von HAUBRICH (2001) anhand von $\delta^{34}S_{SO4}$-Werten des Grubenwassers auf der Stollnsohle bestätigt. Auf dem Migrationsweg von der Stollnsohle zur 1. Sohle bzw. ½ 3. Sohle erfolgt eine Zumischung von hochmineralisierten Porenwässern aus der Verwitterungsmatrix in den Abbauen, die zu einer Absenkung des pH-Wertes und einer steigenden Gesamtmineralisation führen (BAACKE 2000).

Die Schwermetalle Cu, Fe, Mn, Pb und Zn sowie As entstammen direkt der Oxidation der Sulfide (BAACKE 2000; HAUBRICH et al. 2000), was durch eine positive lineare Korrelation mit der Sulfatkonzentration für die 1. und ½ 3.Sohle bestätigt wird. Im Gegensatz zu Zn, Fe, Mn und Cd, deren Konzentrationen und Frachten mit der

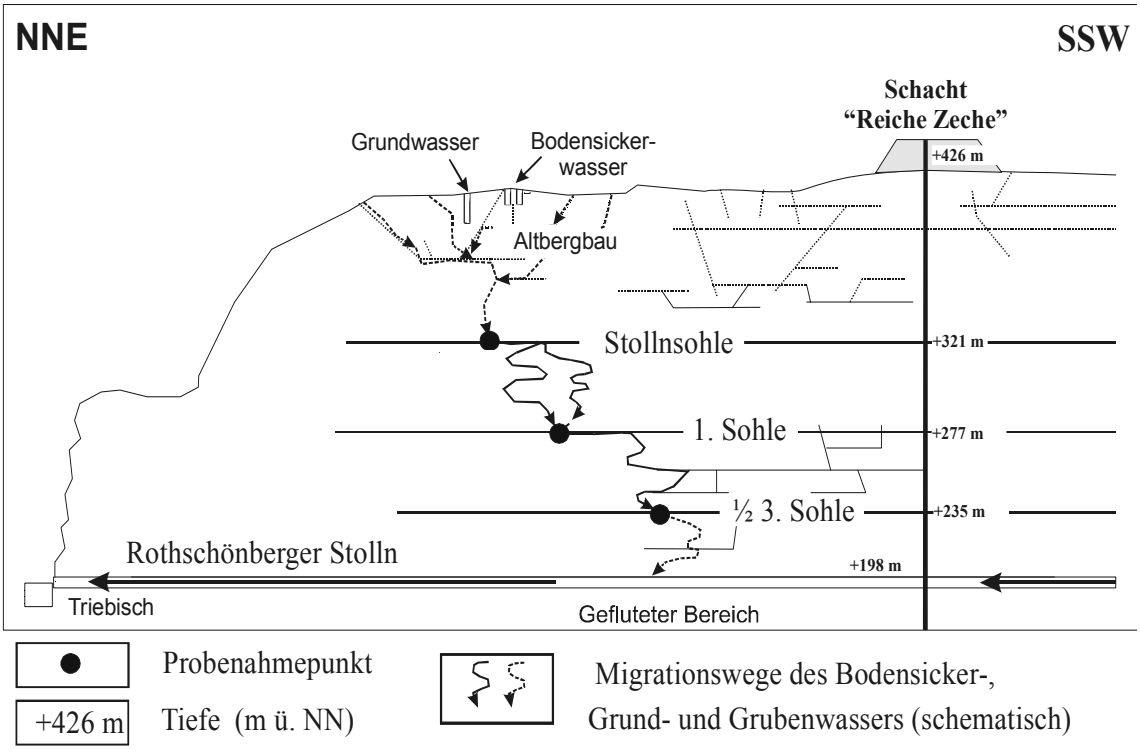

Abb. 1: Schematische Darstellung des untersuchten Migrationsweges auf dem Erzgang „Schwarzer Hirsch Stehender“ (verändert aus HAUBRICH & TICHOMIROWA 2002).

Tiefe steigen, werden As und Pb (teilweise) wieder fixiert. Als Senken kommen für Pb Anglesit [$PbSO_4$] und Jarosit [$(K, Pb)Fe_3(SO_4)_2(OH)_6$] in Betracht (HAUBRICH et al. 2000; TICHOMIROWA et al. 2003). As wird vermutlich an Eisenhydroxidpräzipitaten oder im Skorodit [$Fe(AsO_4)\cdot 2 H_2O$] fixiert (HAUBRICH et al. 2000; TICHOMIROWA et al. 2003).

Al, Mg und K werden vorrangig aus Biotit sowie aus K-Feldspat und Plagioklas aus dem Nebengestein und Versatzmaterial (Freiberger Gneis) freigesetzt, wobei dieser Prozess bei niedrigen pH-Werten verstärkt abläuft. Kalium kann bei der Bildung von Jarosit [$(K, Pb)Fe_3(SO_4)_2(OH)_6$] und Illit größtenteils wieder festgelegt werden (HAUBRICH et al. 2000; TICHOMIROWA et al. 2003).

Neben diesen für die meisten Probenahmekampagnen erkennbaren Trends der Freisetzung und Fixierung zeigen einige Elemente zu bestimmten Zeiten deutlich anomale Werte, die sich von der Stollnsohle bis zur ½ 3.Sohle verfolgen lassen; dies sind für Ca ungewöhnlich niedrige Konzentrationen (z.T. nur 50 % der sonst gemessenen Werte) für die Probenahmen am 24.05.00 sowie am 7.12.00. Cl zeigt erhöhte Konzentrationen auf allen drei Sohlen für die Probenahme am 29.04.02. Für die Probenahme am 11.04.00 können auf der Stollnsohle erhöhte Konzentrationen für Fe und As und niedrigere Konzentrationen für Na beobachtet werden. Zur Beprobung am 11.02.02 wurden ebenfalls niedrigere Na- und K-Konzentrationen gemessen. Wahrscheinlich können diese anomalen Werte auf eine andere Zusammensetzung des Grund- /Sickerwassers an diesen Messtagen zurückgeführt werden.

4 S- und O-Isotopenzusammensetzung des Grubenwassers

BAACKE (2000) und HAUBRICH & TICHOMIROWA (2002) interpretieren eine mit der Tiefe steigende Mineralisation des Grubenwassers auf dem Erzgang „Schwarzer Hirsch Stehender“ als Ergebnis der Mischung mit hochmineralisierten, sulfatreichen Lösungen. Diese Interpretation konnte durch eigene Ergebnisse bestätigt werden. HAUBRICH & TICHOMIROWA (2002) haben gezeigt, dass die $\delta^{34}S_{SO4}$- und $\delta^{18}O_{SO4}$–Werte mit der Tiefe sinken. Sie geben die Schwefelisotopenwerte als Maß für das aus der Sulfidoxidation resultierende Sulfat an. Steigende Sulfatkonzentrationen und sinkende $\delta^{34}S_{SO4}$-Werte der Grubenwässer wurden als Indiz für eine erhöhte Zumischung von hochmineralisierten Wässern durch Sulfidoxidation gedeutet. Demzufolge wurde eine Abhängigkeit beider Parameter voneinander für die drei Tiefenniveaus vermutet. Allerdings konnte nur für die 1. Sohle näherungsweise eine Abhängigkeit beobachtet werden (Abb. 2). Neben eigenen Messungen wurden in Abbildung 2 zum Vergleich Daten von Beprobungen im Jahr 1997 aus HAUBRICH & TICHOMIROWA (2002) ergänzt.

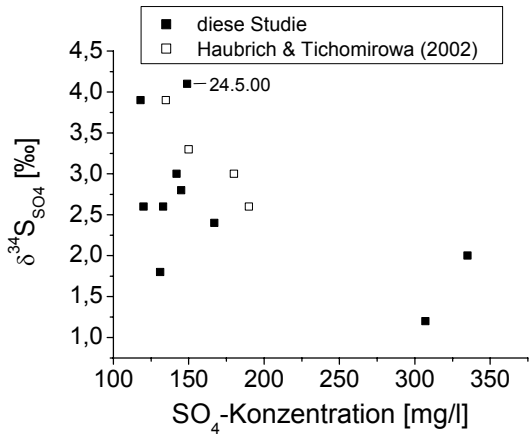

Abb. 2: Zusammenhang zwischen dem $\delta^{34}S_{SO4}$-Wert und der Sulfatkonzentration (1. Sohle).

Eine deutlich bessere Korrelation zeichnet sich zwischen $\delta^{18}O_{SO4}$ und der Sulfatfracht für die 1.Sohle ab (Abb. 3b), wobei zwei Probenahmen starke Abweichungen vom beobachteten Trend zeigen (11.4.00 und 24.5.00), die schon auf der Stollnsohle (mit Ausnahme des $\delta^{34}S_{SO4}$-Wertes am 11.4.00) erkennbar sind (Abb. 3a). Diese beiden Probenahmezeitpunkte sind ebenfalls durch anomale Konzentrationen einiger Elemente gekennzeichnet (11.4.00: Na, SO_4, K, Fe, As; 24.5.00: Ca). Die $\delta^{34}S_{SO4}$-Werte für die 1. Sohle zeigen neben abweichenden Werten, wie sie für $\delta^{18}O_{SO4}$ beobachtet wurden, stärkere Schwankungen. Wir vermuten eine zusätzliche anthropogene Sulfatquelle im Sicker- bzw. Grundwasser, die diese Abweichungen hervorruft. Es ist bemerkenswert, dass nicht alle anomalen Anionen- bzw. Kationenkonzentrationen ebenfalls anomale Isotopenwerte zur Folge haben. Es scheint jedoch, dass $\delta^{34}S_{SO4}$-Werte generell stärker auf eine Änderung des geochemischen Milieus (durch anthropogene Quellen bzw. Redoxreaktionen) reagieren als $\delta^{18}O_{SO4}$ -Werte.

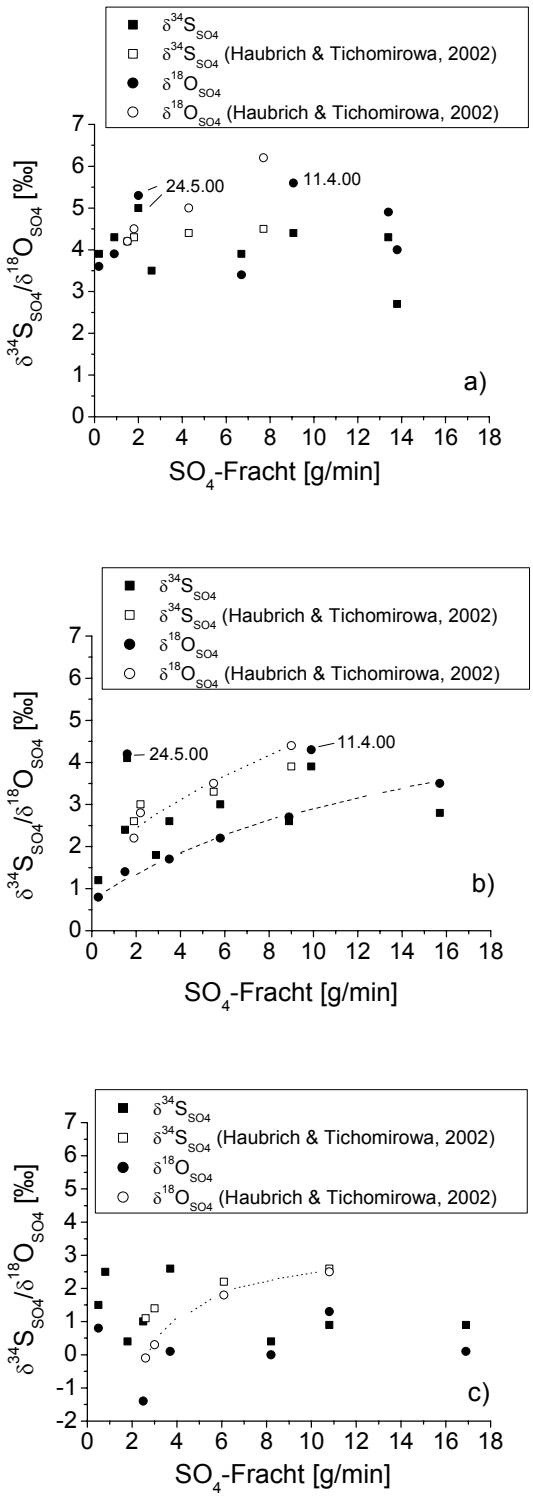

Abb. 3: Zusammenhang zwischen $\delta^{34}S_{SO4}$- und $\delta^{18}O_{SO4}$-Werten und der Sulfatfracht auf den drei Sohlen.

Für die ½ 3. Sohle weisen die $\delta^{34}S_{SO4}$- und $\delta^{18}O_{SO4}$-Werte von HAUBRICH & TICHOMIROWA (2002) für 1997 eine positive Abhängigkeit von der Sulfatfracht auf, die jedoch durch zusätzliche Daten nicht bestätigt werden konnte (Abb. 3c). Generell höhere Sulfatkonzentrationen und niedrigere $\delta^{34}S_{SO4}$ und $\delta^{18}O_{SO4}$-Werte sowie niedrigere pH-Werte weisen auf einen höheren Anteil an Porenwässern mit einer höheren Verweilzeit der Grubenwässer für unsere Probenahmekampagne 2000—2002 hin. Wahrscheinlich führen Austausch-, Fixierungs- und Verdunstungsprozesse sowie zeitweiliges Austrocknen der Verwitterungsmatrix zu stärkeren Streuungen der $\delta^{34}S_{SO4}$- und $\delta^{18}O_{SO4}$- Werte

Den Zusammenhang zwischen $\delta^{34}S_{SO4}$- bzw. $\delta^{18}O_{SO4}$- Werten und der Wassermenge auf der 1. Sohle zeigt Abbildung 4. Mit steigender Wasserdurchflussmenge steigen $\delta^{34}S_{SO4}$- und $\delta^{18}O_{SO4}$ – Wert an, was auf eine verstärkte Zumischung von Grund- bzw. Bodensickerwasser bei höherem Wasserangebot (Schneeschmelze, Starkniederschlagsereignisse) zurückzuführen ist. Der Anteil der hochmineralisierten Porenlösungen nimmt somit bei hohem Durchfluss immer mehr ab.

Ein Vergleich mit den Daten aus HAUBRICH & TICHOMIROWA (2002) zeigt, dass 1997 sowohl höhere $\delta^{34}S_{SO4}$- als auch höhere $\delta^{18}O_{SO4}$-Werte gemessen wurden, wobei die größeren Differenzen mit bis zu 1,7 ‰ für $\delta^{18}O_{SO4}$ beobachtet werden (Abb. 3b, Abb. 4a und b). Die arithmetischen Mittelwerte der $\delta^{34}S_{SO4}$- und $\delta^{18}O_{SO4}$-Werte auf der Stollnsohle von HAUBRICH & TICHOMIROWA (2002) ergeben 4,4 ‰ bzw. 5,0 ‰. Im Vergleich dazu liegen die Mittelwerte der nachfolgenden Beprobungen (4/2000—7/2002) bei 4,0 ‰ bzw. 4,1 ‰. Es ist somit schon auf der Stollnsohle ein deutliches Absinken des $\delta^{18}O_{SO4}$-Wertes zu verzeichnen. Dies kann möglicherweise auf eine Infiltration von Niederschlagswasser mit niedrigeren $\delta^{34}S_{SO4}$- und $\delta^{18}O_{SO4}$-Werten zurückzuführen sein. Neuere Isotopenmessungen (10/2000—1/2002) an Niederschlägen in Freiberg deuten ein leichtes Absinken des $\delta^{34}S_{SO4}$-Wertes im Vergleich zu 1997 an. Zur zeitlichen Veränderung der $\delta^{18}O_{SO4}$-Werte im Niederschlag kann keine Aussage getroffen werden, da keine aktuellen Messdaten für $\delta^{18}O_{SO4}$ vorliegen.

Es wurde versucht, anhand der $\delta^{34}S_{SO4}$- und $\delta^{18}O_{SO4}$-Werte der Grubenwässer den Anteil des Sulfates abzuschätzen, der aus der Sulfidoxidation abzuleiten ist. $\delta^{34}S_{SO4}$- und $\delta^{18}O_{SO4}$-Werte auf der Stollnsohle zeigen keine Abhängigkeit von der Wassermenge und der Sulfatfracht, was die Annahme bestätigt, dass es sich hierbei um ein von Sulfidoxidationsprozessen relativ unbeein-

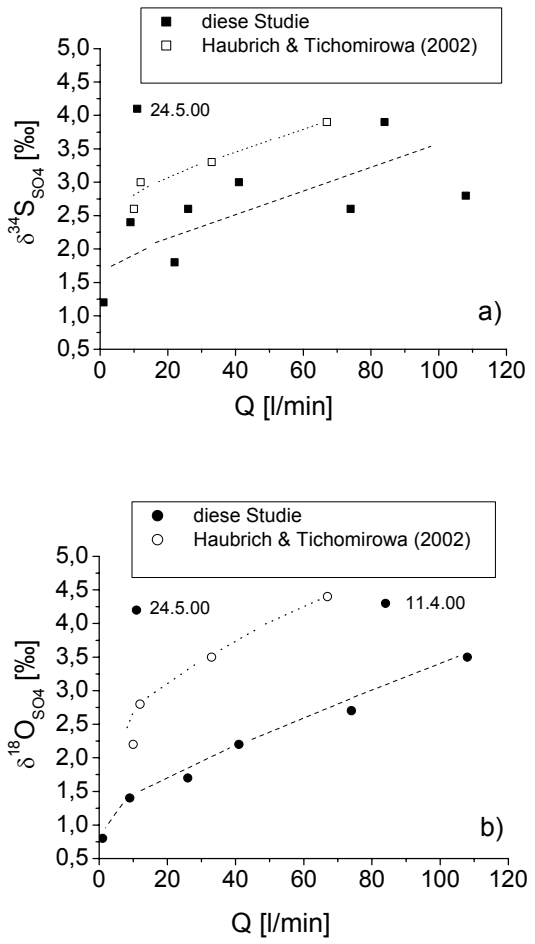

Abb. 4: Zusammenhang zwischen $\delta^{34}S_{SO4}$- und $\delta^{18}O_{SO4}$-Werten und der Wassermenge auf der 1. Sohle.

flusstes Wasser handelt. Demzufolge können die mittleren $\delta^{34}S_{SO4}$- (3,9 ‰) und $\delta^{18}O_{SO4}$- Werte (3,8 ‰) dieser Wässer (mit Ausnahme der Beprobungen vom 11.4.00 und vom 24.5.00) zur Charakterisierung des Grund- und Bodensickerwassers verwendet werden, welches noch keinen Einfluss von Sulfidoxidationsprozessen aufweist. Die zweite Sulfatquelle stellen die hochmineralisierten Porenlösungen der Verwitterungsmatrix in den Abbauen dar. Diese können z.T. stark variierende $\delta^{34}S_{SO4}$ (-2,8 bis –0,3 ‰) und $\delta^{18}O_{SO4}$-Werte (-10,0 bis –2,0 ‰) aufweisen (HAUBRICH & TICHOMIROWA 2002; TICHOMIROWA et al. 2003). Für weitere Berechnungen wurde deshalb der Mittelwert aller Werte für hochmineralisierte Porenlösungen aus HAUBRICH & TICHOMIROWA (2002) und TICHOMIROWA et al. (2003) verwendet. Demzufolge ist das Endglied „hochmineralisierte Porenlösung“ durch einen $\delta^{34}S_{SO4}$-Wert von –1,6 ‰ und einen $\delta^{18}O_{SO4}$ von –5,7 ‰ charakterisiert.

Mittels der Isotopenwerte der beiden Endglieder (Grund- und Bodensickerwasser, hochmineralisierte Porenlösung) wurde der Anteil des Porenwassersulfats im Grubenwasser auf der 1. und ½ 3. Sohle abgeschätzt.

Der Anteil des Porenwassersulfats liegt für die 1.Sohle zwischen 16 % und 48 % (Mittelwert 29 %) nach einer Abschätzung mittels $\delta^{34}S_{SO4}$ und zwischen 3 % und 50 % (Mittelwert 23 %) mittels $\delta^{18}O_{SO4}$. Für die ½ 3. Sohle wurden 23 % bis 62 % mit einem Mittelwert von 50 % nach $\delta^{34}S_{SO4}$-Werten und 27 % bis 54 % (Mittelwert 41 %) nach $\delta^{18}O_{SO4}$-Werten berechnet.

Die Berechnungen ergeben z.T. recht gute Übereinstimmungen auf der 1. Sohle für Sulfatanteile, die aus hochmineralisierten Porenlösungen stammen. Die größten Differenzen ergeben sich für die Probenahmen am 15.3.01 und 11.2.02, für die die höchsten Wassermengen im gesamten Beprobungszeitraum gemessen wurden. Die berechneten Anteile auf der ½ 3. Sohle zeigen eine weniger gute Überstimmung im Vergleich zur 1.Sohle, was die stärkere Streuung der $\delta^{34}S_{SO4}$- und $\delta^{18}O_{SO4}$-Werte widerspiegelt. Die aus den Daten von 1997 (HAUBRICH & TICHOMIROWA 2002) ermittelten Anteile sind für ähnliche Wasserdurchflussmengen mit denen neuerer Beprobungen vergleichbar.

Im Vergleich zu den hier berechneten Anteilen des Sulfats aus den Porenlösungen am Grubenwasser werden bei BAACKE (2000) Durchschnittswerte der Elementmobilisation durch Sulfidverwitterung für das Jahr 1997 für den gesamten durchflossenen Abbau (Stollnsohle bis ½ 3. Sohle) von ca. 85 bis 95 % für Cd, Cu, Fe, Mn, Pb und Zn angegeben. Dagegen tragen die Abbaue lediglich mit 23 % zur As und Ni-Fracht bei.

Zur Abschätzung der Intensität der Sulfidoxidation können als geochemische Tracer die Sulfatgehalte zur Anwendung kommen. Nachteilig für Sulfat als Indikator wirkt sich die Bildung von sulfathaltigen Sekundärmineralen und somit eine teilweise Fixierung von Sulfat aus. Zn, das aufgrund seiner hohen Mobilität als ein weiterer Indikator dienen kann, wird jedoch lediglich bei der Sphaleritoxidation freigesetzt und berücksichtigt nicht die Anteile aus Galenit, Pyrit und Arsenopyrit. Wir glauben, dass mittels $\delta^{34}S_{SO4}$- und $\delta^{18}O_{SO4}$-Werten eine realistischere Einschätzung des zeitlichen Verlaufs der Sulfidverwitterung vorgenommen werden kann, da Fixierungsprozesse zu keinen oder nur unwesentlichen Fraktionierungen führen und Zumischungen

Tab. 1: Prozentualer Anteil des Porenwassersulfats am Grubenwassersulfat auf der 1. und ½ 3. Sohle.

Probenahmedatum	Anteil des Sulfats des hochmineralisierten Porenwassers aus der Sulfidoxidation am Grubenwassersulfat [%]			
	1. Sohle		½ 3. Sohle	
	Berechnung mittels $\delta^{34}S_{SO4}$	Berechnung mittels $\delta^{18}O_{SO4}$	Berechnung mittels $\delta^{34}S_{SO4}$	Berechnung mittels $\delta^{18}O_{SO4}$
23.4.97*	8	6	30	24
31.7.97*	18	14	37	30
19.9.97*	23	21	50	45
13.10.97*	30	26	54	48
07.12.00	48	32	43	32
16.01.01	34	50	50	53
15.03.01	20	3	53	39
24.07.01	27	26	52	56
22.11.01	16	17	62	40
15.01.02	23	22	23	39
11.02.02	23	12	53	27
29.04.02	38	n.b.	62	n.b.
Mittelwert (ohne *)	29	23	50	41

* Daten aus HAUBRICH & TICHOMIROWA (2002)

weiterer Quellen deutlich anhand abweichender Isotopensignaturen erkannt werden können.

5 Zusammenfassung

Im Rahmen der Untersuchungen an dem abgebauten Erzgang „Schwarzer Hirsch Stehender“ konnte festgestellt werden, dass Wässer, die anomale Isotopenwerte zeigen, ebenfalls anomale Elementkonzentrationen aufweisen. Diese könnten durch eine zusätzliche (anthropogene) Sulfatquelle verursacht worden sein.

$\delta^{34}S_{SO4}$- und $\delta^{18}O_{SO4}$ -Isotopenverhältnisse auf der 1. Sohle zeigen an, dass der Anteil der hochmineralisierten Porenlösungen auch bei hohem Durchfluss immer mehr abnimmt. Im Vergleich zu 1997 gewonnenen Isotopendaten ist ein Absinken der $\delta^{34}S_{SO4}$- und $\delta^{18}O_{SO4}$-Werte zu beobachten, was möglicherweise auf eine Infiltration von isotopisch leichteren Niederschlagswässern zurückzuführen sein kann.

Anhand von $\delta^{34}S_{SO4}$ und $\delta^{18}O_{SO4}$ wurde der Anteil des Porenwassersulfats am Grubenwasser berechnet. Dieser liegt zwischen 3 und 50 % auf der 1. Sohle und 23 % und 62 % auf der ½ 3. Sohle.

In den Abbauen der ½ 3. Sohle spielen bei deutlich geringeren Wassermengen möglicherweise Austausch-, Fixierungs- und Verdunstungsprozesse sowie möglicherweise zeitweises Austrocknen der Verwitterungsmatrix ein Rolle, die zu stärkeren Streuungen der $\delta^{34}S_{SO4}$- und $\delta^{18}O_{SO4}$-Werte führen.

Literatur

BAACKE, D. (2000): Geochemisches Verhalten umweltrelevanter Elemente in stillgelegten Polysulfiderzgruben am Beispiel der Grube ”Himmelfahrt” in Freiberg/Sachsen. Dissertation. TU Bergakademie Freiberg. 139 S.

BAUMANN, L., KUSCHKA, E., SEIFERT, T. (2000): Die Lagerstätten des Erzgebirges. Enke Verlag. 300 S.

HAUBRICH, F. & TICHOMIROWA, M. (2002): Sulfur and oxygen isotope geochemistry of acid mine drainage – the polymetallic sulfide deposit "Himmelfahrt Fundgrube" in Freiberg (Germany). – Isotopes in Environmental and Health Studies, vol. 38 (2). S.121—138.

HAUBRICH, F., BAACKE, D., KLUGE, A.; KINDERMANN, A. & WINKLER, C. (2000): Sulfidverwitterung in aufgefahrenen Erzgängen – ein Feld komplexer geochemischer, mineralogischer und mikrobiologischer Forschung. In: WIPPERMANN, T. (Hrsg.): Bergbau und Umwelt – langfristige geochemische Einflüsse. GUG-Schriftenreihe Geowissenschaften und Umwelt Bd. 5. Springer-Verlag, Hannover. S. 57—66.

TICHOMIROWA, M., PELKNER, S., JUNGHANS, M. & HAUBRICH, F. (2003): Sulfide oxidation in acid mine drainage: relationship between precipitated and dissolved sulfates at the polymetallic sulfide deposit Freiberg (Germany) and consequences for mobilisation of heavy metals. Wiley (angenommen)

WINKLER, C. (1998): Verfolgung des vertikalen Migrationsweges und Bilanzierung ausgewählter Elemente entlang der mineralisierten Gangzone des „Schwarzen Hirsch Stehenden Nord“. Unveröffentl. Diplomarbeit. TU Bergakademie Freiberg. 127 S.

WINKLER, C., BAACKE, D., KLUGE, A. & BEUGE, P. (2000): Geochemische und hydrogeologische Untersuchungen im Ausbißbereich eines Erzganges im Hinblick auf die Elementmigration – eine interdisziplinäre Aufgabenstellung. In: WIPPERMANN, T. (Hrsg.): Bergbau und Umwelt – langfristige geochemische Einflüsse. GUG-Schriftenreihe Geowissenschaften und Umwelt Bd. 5. Springer-Verlag, Hannover. S. 151—161.


BERGAKADEMIE
TECHNISCHE
UNIVERSITÄT
FREIBERG

Neutronenaktivierungsanalyse zur Herkunftsbestimmung archäologischer Obsidianartefakte

Kirstin Kasper, Ernst Pernicka

Institut für Archäometrie, TU Bergakademie Freiberg

Obsidian entsteht als metabstabiles Erstarrungsprodukt rasch abgekühlter, sehr SiO_2-reicher, hochviskoser Laven und ist in vielen stein- und bronzezeitlichen Kulturkreisen zur Herstellung von Gebrauchsgegenständen, Werkzeugen und Waffen verwendet worden. Durch Werkstoff-Eigenschaften wie Härte und scharfkantigen Bruch ist er ein besonders geeignetes Material. Die Vorkommen sind, im Gegensatz zu anderen steinzeitlichen Werkzeugmaterialien (z.B. Knochen, Silex), auf känozoische Vulkangebiete beschränkt.

Obsidianartefakte werden aber auch in vorzeitlichen Fundstellen angetroffen, welche weit entfernt von natürlichen Vorkommen sind. Eine Herkunftsbestimmung dieser Objekte kann somit Handelsbeziehungen im Neolithikum aufzeigen.

Zur Korrelation von Lagerstätten und Artefakten wird ein geochemischer *„Fingerabdruck"* des Gesteins erstellt, welcher eine signifikante Unterscheidung zulässt. Obsidian eignet sich aufgrund seiner Entstehung und der daraus resultierenden sehr homogenen Verteilung der Spurenelemente besonders gut für diese Provenienzanalyse.

Die Pionierarbeiten auf diesem Gebiet wurden im östlichen Mittelmeer durchgeführt und haben zu einer weitgehend vollständigen Erfassung und geochemischen Charakterisierung der geologischen Vorkommen in der Ägäis und in Zentralanatolien geführt. Diese Datenbasis hat bereits wichtige Erkenntnisse über die Verbreitung des Obsidians aus diesen Lagerstätten erbracht, wie etwa den indirekten Nachweis der Schifffahrt in der Ägäis im 6. Jahrtausend oder die konsistente Verbreitung des mittelanatolischen Obsidians bis in die südliche Levante bereits im Neolithikum (RENFREW et al. 1965, 1966, 1968; CANN & RENFREW 1964). Im Gegensatz dazu sind die ostanatolischen und transkaukasischen Lagerstätten nur wenig untersucht. Infolge dieser Wissenslücke folgerte RENFREW (1968), daß nur begrenzte Handelsbeziehungen zwischen kaukasischen Völkern und Bewohnern südlicher Regionen existierten. Nachfolgende Forschungen (BLACKMAN 1984; KELLER & SEIFRIED 1990; KELLER et al. 1996) widerlegten diesen Aussage. Der erste Nachweis der prähistorischen Nutzung armenischer Obsidianlagerstätten erfolgte durch eine Studie von BLACKMAN (1984); anhand eines Obsidian-Artefakts aus Tal-e Malyan, datiert in die Kafteri-Periode (2100—1800 vor Ch.), aus dem Hochland von Iran.

Durch umfassenden Analysen von KELLER et. al. (1996), mittels RFA und INAA, an 13 ostanatolischen und armenischen Lagerstätten konnten bereits 17 Gruppen bzw. Subgruppen klassifiziert werden. Dennoch sind die bisher gewonnen geochemischen Daten nicht ausreichend für eine detaillierte, statistisch fundierte Aussage über die Handelsverbindungen zwischen den Fundstellen und den derzeit bekannten und analysierten Quellen. Der bisherige Forschungsstand erschwert daher die Korrelation von Obsidianvorkommen mit Artefakten aus prähistorischen Siedlungen im Transkaukasus bzw. des Nahen und Mittleren Ostens.

Diese Wissenslücke soll durch ein europäisches Gemeinschaftsprojekt geschlossen werden. In einer multilateralen Studie im Rahmen des ESF Programmes „European Collaborative Research Projects in the Social Sciences (2001—2003)" (Partner: TU Bergakademie Freiberg, Universität Pisa, Maison de L'Orient Méditerranéen, Lyon) werden die Obsidianlagerstätten und Artefakte aus Ostanatolien, Georgien, Armenien, Aserbaidschan und Nachitschevan im Gelände untersucht und im Labor geochemisch analysiert und geologisch datiert.

Die Analyse erfolgt an der TU Bergakademie Freiberg, Institut für Archäometrie, mittels INAA, einem hochempfindlichen Verfahren

der analytischen Chemie zur qualitativen und quantitativen Spurenanalyse. Es ermöglicht die zerstörungsfreie Bestimmung von Spurenelementgehalten in geringen Probenmengen. Die Konzentrationen von bis zu 50 Spurenelementen können simultan in den Proben gemessen werden. Die Nachweisgrenzen liegen im ppm bis ppb Bereich. Ein weiterer Vorteil der Methode ist, dass die Proben nicht aufbereitet werden müssen (z.B. ist die Untersuchung von Einzelkristallen möglich), und nach der Messung noch für weitere Untersuchungen (z.B. Mikrosonde) zur Verfügung stehen. Das Prinzip der Methode beruht darauf, dass die Proben (zusammen mit geeigneten Standards) in einem Reaktor mit Neutronen bestrahlt werden, wobei in der Probe radioaktive Isotope gebildet werden, die unter Aussendung von charakteristischer Gammastrahlung (die das analytische Signal darstellt), zerfallen. Die Energie und Intensität der Gammastrahlung wird mit einem Reinstgermaniumdetektor gemessen, mit Standardwerten verglichen, und erlaubt so die Berechnung der Elementgehalte. Bisher wurden vor allem Obsidianartefakte aus den frühbronzezeitlichen Fundstellen Minberek, Camay und Padar (NW-Aserbaidschan) analysiert.

Ihre Herkunft konnte eindeutig der einzigen georgischen Lagerstätte in Chikiani zugeordnet werden. Sie befindet sich im Südosten des Landes am Paravan-See und erstreckt sich über mehrere hundert Meter entlang des nordöstlichen Hanges des Chikiani-Vulkans. Der Obsidian ist vergesellschaftet mit Bimsstein, rhyolitischen Tuffen, Perliten und Ignimbriten (KELLER et al. 1996). Das K/Ar-Alter wird mit 2,6—2,8 Mio. a (BIGAZZI et al. 2001) angegeben. Die von BLACKMAN et al. (1998) und KELLER et al. (1996) untersuchten Gesteinsproben bildeten eine homogene Gruppe, welche durch ihren hohen Ba-Gehalt charakterisiert wird. Vermutlich wurde dieses Vorkommen schon im Neolithium entdeckt und als Rohstoffquelle zur Werkzeugproduktion genutzt (BLACKMAN et al.1998).

Literatur

BADALIAN, R., BIGAZZI, G., CAUVIN, M.-C., CHATAIGNER, C., JRBASHYAN, R., KARAPETYAN, S.G., ODDONE, M.. & POIDEVIN J.-L. (2001): An international research project on Armenian archaeological sites: fission-track dating of obsidians. Radiat. Meas., 34, 373—378.

BLACKMAN, M.J. (1984): Provenance studies of middle eastern obsidian from sites in highland Iran. Archaeol. Chem. III.Adv. in Chem. Ser. 205: 19—50

BLACKMAN, M.J., BADALIAN, R., KIKODZE Z. & KOHL P. (1998): Chemical characterisation of Caucasian obsidian geological sources. In: CAUVIN, M.-C., GOURGAUD, A., GRATZUE, B., ARNAUD, N., POUPEAU, G., POIDEVIN, J.-L. & CHATAIGNER, C.: L'obsidienne au proche et Moyen Orient. Du volcan à l'util. BAR International Series 738.Archaeopress, Oxford, England, 205—226.

CANN, J.R. & RENFREW. C. (1964): Characterization of obsidian and its application to the Mediterranean region. Proc. Prehist. Soc. 30: 111—132.

KELLER, J., DJERBASHIAN, R., PERNICKA, E., KARAPETIAN, S.G., NASEDKIN, V. (1996): Armenian and Caucasian obsidian occurrences as sources for the neolithic trade: Volcanological setting and chemical characteristics. In:. DEMIRCI, S., ÖZER, A.M. & SUMMERS, G.D. (eds.): Archaeometry 94. Proc. of the 29th Int. Symp. on Archaeometry, Ankara 9-14 May 1994, Tübitak, Ankara, pp. 69-86.

KELLER, J. & SEIFRIED, C. (1990): The present status of obsidian source characterization in Anatolia and the Near East. PACT 25, 57—87.

RENFREW. C., DIXON, J.E. & CANN, J.R. (1965): Obsidian in the Aegean. Ann. B.S.A. Athens, 60, 225.

RENFREW. C., DIXON, J.E. & CANN, J.R. (1966): Obsidian and early cultural contact in the Near East. Proc. Prehist. Soc. 32: 30—72.

RENFREW, C., DIXON, J.E. & CANN, J.R. (1968): Further analysis of Near Eastern obsidians. Proc. Prehist. Soc. 34: 319—331.

REE enrichment in groundwaters of the polysulphide ore deposit Freiberg

Anreicherung von Selten Erden Elementen in Grubenwässern der Polysulfidlagerstätte Freiberg

Werner Klemm, Ulrich Knittel, Sebastian Sachse, Miriam Händel

TU Bergakademie Freiberg, Institut für Mineralogie

The rare earth elements (REE) are considered to be relatively immobile during weathering and alteration of rocks (e.g., MCLENNAN 1989), though more recent studies have shown, that at least the light REE (LREE) are not that immobile (e.g., PRICE et al. 1991; POLAT et al. 2003). The assumed immobility was in part based on the low concentration of REE in river and ocean waters (typically in the range x – xx µg/l; e.g. ELDERFIELD et al. 1990). Likewise, the high ionic potential suggests that the REE are expected to be rather immobile in aqueous environments, as they should tend to form hydroxides.

The advent of analytical procedures with higher sensitivity, in particular ICP-MS techniques, have stimulated renewed interest in the aqueous geochemistry of the REE (e.g., ELDERFIELD et al. 1990). MÖLLER (2000) and WORRAL & PERSON (2001) for example, used REE patterns of groundwaters as fingerprints for the identification of the host rocks of groundwaters.

Preliminary work by BAAKE et al. (1989) has shown, that acid mine waters and sinter deposits in the polysulfide ore deposit Freiberg are in part highly enriched in REE. This study extends this work in order to adress the following questions:

1. what is the source of the REE concentrated in acid mine waters, the host rocks of the deposit (i.e. the Freiberg Gray Gneiss) or gangue (i.e. calcite, fluorite)?
2. what controls the REE patterns in acid mine waters, the composition of the REE source or interaction of the waters and deposits (sinters)?

The present contribution is largely a status report on ongoing research and is mainly focussed on the chemistry of the mine waters.

1 Procedures

Water samples (100 ml), taken in the underground workings of the Freiberg Mine and the Mulde River, were filtered using 0,45 µm cellulose acetate filters. Unfiltered water samples were collected for comparison. Both sample types were acidified immediately after collection with HNO_3. Acidified solutions (about 5% HNO_3) were analyzed using a Perkin-Elmer E-LAN 5000A quadrupole inductively coupled plasma mass spectrometer. For cabonates, 0.5 g samples were dissolved at 50 °C in 2 ml conc. HCl and solutions were diluted 1:10 before measurement. As internal standard 10 µg/l Rh were added. In order to minimize isobaric interferences, the following isotopes were measure: ^{89}Y, ^{139}La, ^{140}Ce, ^{141}Pr, ^{147}Nd, ^{147}Sm, ^{151}Eu, ^{160}Gd, ^{159}Tb, ^{163}Dy, ^{165}Ho, ^{166}Er, ^{169}Tm, ^{171}Yb, ^{175}Lu. Detection Limits are 0.05µg/l for Y, La, Ce, Pr, Nd, and Er, and 0.005 µg/l for Sm, Eu, Gd, Tb, Dy, Ho, Tm, Yb, and Lu.

2 Results

Water samples are subdivided into waters from veins with sulfide mineralization, waters from veins filled with barite and fluorite, waters from barren fractures and mixed waters. Overall, the REE concentrations vary by five orders of magnitude, the highest concentrations being found in

waters percolating in mineralized veins. The lowest concentrations, which are in the same range as the river waters of the Mulde River, were found in unmineralized fractures and veins carrying fluorite-barite mineralization.

As already indicated by leaching experiments (e.g. PRICE et al. 1991) and Eh-pH-diagrams (e.g. BROOKINS 1989) and known from data for geothermal (e.g., MÖLLER 2000) and mine waters (e.g., LEYBOURNE et al. 2000; WORRAL & PERSON 2001), the REE concentration in the water increases with decreasing pH. In water with pH = ca. 2.5 total REE contents are 11-13 [mg/l. Even higher REE contents of up to 690 [mg/l total REE contents have been reported for mine waters from the Bathurst Mining Camp, Canada (LEYBOURNE et al. 2000). In a plot pH vs. log[ΣREE] a linear relationship between total dissolved REE's and pH is indicated (Fig. 1).

REE concentrations in filtered water samples and unfiltered water samples are almost identical in waters with high total REE contents and low pH (Fig. 2, 3; see also analyses Sa5f and Sa5u in Table 1), suggesting that the REE may be truly in solution. It should be noted, however, that ELDERFIELD et al. (1990) found that waters passed through filters with pore size 0.2 µm sometimes had lower total REE contents than when passed though 0.4 µm pore size. In samples with higher pH and lower total REE, filtered waters contain in part significantly lower total REE concentrations compared to unfiltered waters (Fig. 3, 4; see for example analyses Sa9f and Sa9u in Table 1). This is perhaps related to the stability of Fe-hydroxides in waters with higher pH, to which the REE are absorbed.

All waters show moderate enrichment in light rare earth elements (LREE) in chondrite normalized plots (Fig. 5). Highly mineralized waters exhibit a significant Eu-anomaly, which is not obvious in the waters with low concentrations of REE. On the other hand, waters with low REE concentrations exhibit positive Y-anomalies.

A potential source of the REE concentrated in the mine waters is the Freiberg Gneiss which forms the host rock of the vein mineralization. Within this study, a sample of this rock was analyzed and used for normalization in Fig. 6. REE-rich waters normalized to the gneiss exhibit negative Eu-anomalies, which, however, might be due to the sample selected for normalization (SACHSE 2002), which does not exhibit an Eu-anomaly. TICHOMIROVA et al. (2001) reported

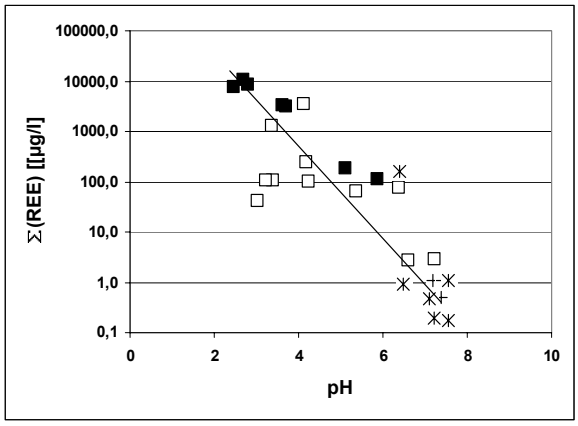

Figure 1: Total REE contents of water samples [µg/l] plotted vs. pH (filled symbols represent samples from veins with sulphide mineralization, open squares are mixed waters, crosses represent samples from veins with fluorite-barite mineralization, and stars samples from non-mineralized fractures).

virtually identical REE patterns for Freiberg Gneiss except that their samples do exhibit Eu-anomalies. In addition, we note that with decreasing total REE contents, an increasing Y-anomaly develops.

In contrast, calcite from the veins appears not to be a potential source of the REE in mine waters (work in progress) because most calcite samples studied so far show less LREE enrichment than the groundwaters or are even LREE depleted (Fig. 7), which would require some fractionation process during dissolution. In addition, several samples (not plotted in Fig. 7) exhibit significant *positive* Eu-anomalies.

Several authors (e.g., MÖLLER 2000) have pointed out that Y because of its trivalent oxidation state and of its ionic size, which is similar to that of Ho, should behave in a similar way as the REE during igneous processes, whereas during dissolution and precipitation processes Y may behave differently. Hence Y-anomalies probably do not reflect host rock compositions but rather processes related to dissolution and transport. The increasing Y-anomaly observed in Freiberg Grey Gneiss normalized patterns hence may reflect incomplete dissolution whereas the lack of a notable Y-anomaly in acidic waters with high REE contents indicates unfractionated transfer of REE and Y from the host rock to the waters.

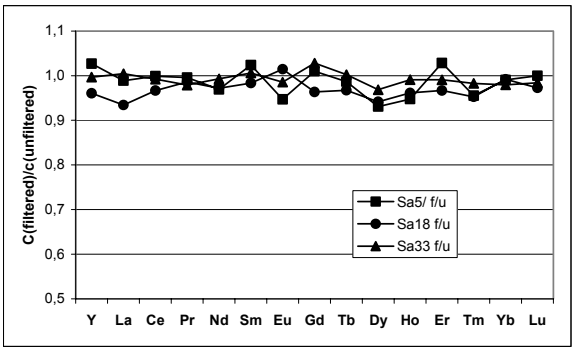

Figure 2: REE concentration in filtered water samples from veins with sulphide mineralization relative to concentrations in unfiltered samples.

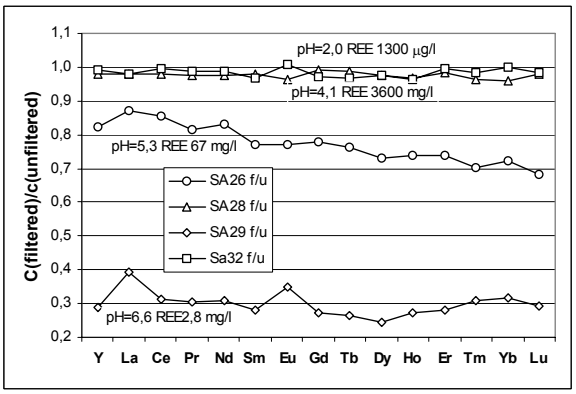

Figure 3: REE concentration in filtered mixed samples relative to concentrations in unfiltered samples, pH values and REE concentrations are provided at the patterns.

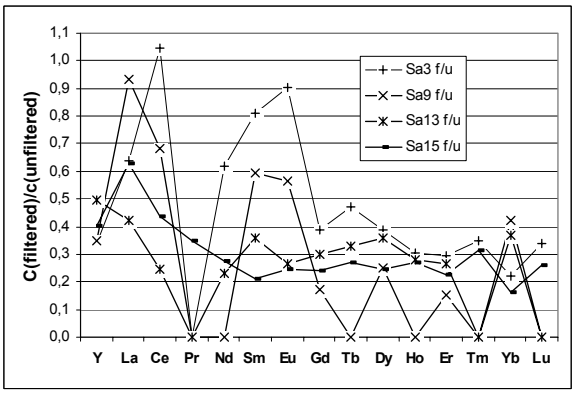

Figure 4: REE concentration in filtered samples relative to concentrations in unfiltered samples for waters from barite-fluorite veins and from unmineralized veins (note that values of 0 indicate that concentrations in the filtered sample were below detection limits).

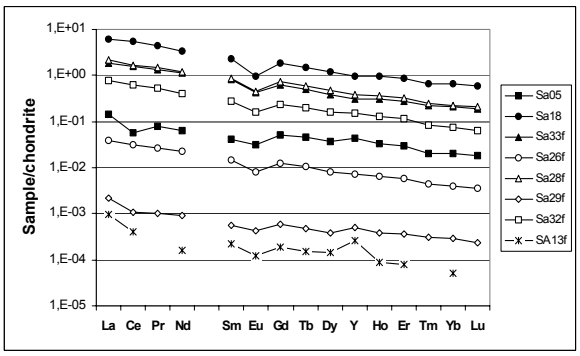

Figure 5: Waters from vein with sulphide mineralization (filled symbols, symbols as in Fig. 1) and mixed waters (open symbols, symbols as in Fig. 2) normalized to chondritic values (BOYNTON 1984).

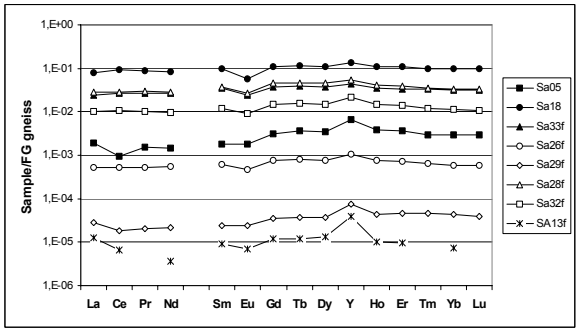

Figure 6: Waters from vein with sulphide mineralization (filled symbols, symbols as in Fig. 1) and mixed waters (open symbols, symbols as in Fig. 2) normalized to the Freiberg Grey Gneiss (SACHSE 2002).

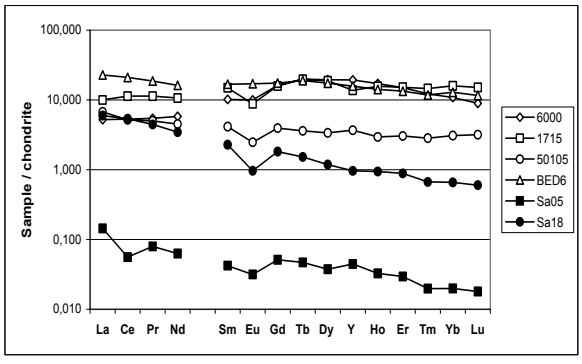

Figure 7: REE patterns of gangue calcite (open symbols) compared to REE patterns of highly mineralized waters (closed symbols). Chondritic values from BOYNTON (1984).

.

Table 1: REE concentrations in mine waters [µg/l]: Samples Sa5, Sa18, and Sa33 come from veins mineralized with sulphides, whereas samples Sa3 and Sa9 come from fluorite-barite veins (letters 'f' and 'u' indicate filtered and unfiltered samples, respectively). Samples Sa26, Sa28, Sa29and Sa32 are mixed waters, samples Sa13 and Sa15 come from unmineralized fractures (letters 'f' and 'u' indicate filtered and unfiltered samples, respectively).

Sample	Sa5f	Sa5u	Sa18f	Sa33f	Sa3f	Sa3u	Sa9f	Sa9u
Y	78.57	76.52	1700	544	1.06	3.11	0.25	0.71
La	44.65	45.16	1850	568	0.35	0.55	0.25	0.27
Ce	45.0	45.1	4330	1280	0.27	0.26	0.16	0.23
Pr	9.69	9.73	543	166	bdl	0.08	bdl	bdl
Nd	37.7	38.9	2070	683	0.23	0.37	bdl	0.10
Sm	8.21	8.02	445	161	0.030	0.037	0.021	0.035
Eu	2.32	2.45	70.9	30.5	0.014	0.016	0.006	0.010
Gd	13.3	13.1	471	161	0.043	0.11	0.012	0.068
Tb	2.22	2.25	72.2	23.8	0.010	0.020	bdl	0.008
Dy	12.06	12.96	382	126	0.052	0.13	0.019	0.074
Ho	2.35	2.48	67.6	22.4	0.013	0.043	bdl	0.015
Er	6.19	6.02	185	58.9	0.040	0.14	0.008	0.054
Tm	0.64	0.67	21.6	7.08	0.006	0.018	bdl	0.008
Yb	4.15	4.19	137	44.4	0.025	0.11	0.023	0.054
Lu	0.58	0.58	19.3	6.10	0.006	0.018	bdl	0.009
pH	5.10	5.10	2.68	3.61	7.40	7.40	7.34	7.37

bdl = below detection limit

	Sa26f	Sa26u	Sa28f	Sa29f	Sa29u	Sa32f	SA13f	SA13u	SA15f	SA15u
Y	12.7	15.5	677	0.90	3.11	262	0.47	0.94	67.0	167
La	12.4	14.2	678	0.68	1.72	242	0.30	0.71	51.1	81.3
Ce	24.9	29.0	1330	0.86	2.74	499	0.32	1.30	64.9	149
Pr	3.27	4.02	183	0.13	0.42	63.5	nn	0.12	5.72	16.4
Nd	13.8	16.7	735	0.55	1.77	249	0.09	0.41	17.6	63.5
Sm	2.89	3.75	169	0.11	0.39	54.7	0.043	0.12	2.73	13.1
Eu	0.60	0.77	33.2	0.031	0.090	11.5	0.009	0.034	0.83	3.33
Gd	3.23	4.15	194	0.15	0.55	62.2	0.050	0.17	5.58	23.4
Tb	0.49	0.64	28.5	0.023	0.085	9.54	0.007	0.023	0.97	3.60
Dy	2.59	3.55	154	0.12	0.51	52.2	0.045	0.13	5.11	21.0
Ho	0.46	0.63	26.4	0.027	0.10	9.14	0.006	0.023	1.12	4.13
Er	1.23	1.66	68.5	0.078	0.28	23.7	0.017	0.062	2.30	10.3
Tm	0.14	0.20	7.85	0.010	0.033	2.64	nn	0.007	0.34	1.09
Yb	0.83	1.16	47.1	0.060	0.19	15.6	0.010	0.028	0.96	5.89
Lu	0.12	0.17	6.61	0.008	0.026	2.03	nn	0.006	0.20	0.75
pH	5.34	5.34	4.10	6.58	6.58	3.34	6.48	6.48	6.40	6.40

bdl = below detection limit

Table 2: REE concentrations [µg/g] in calcites (samples 6000, 1715, 50105, BED6) and Freiberg Gray Gneiss (samples FGGn01-1, FGGn01-2).

Sample	6000	1715	50105	BED6	FGGn01-1	FGGn01-2
Y	34.1	24.3	6.5	27.8	10.5	13.9
La	1.62	3.09	2.08	7.06	20.7	26.2
Ce	4.28	9.15	4.19	17.0	40.3	54.2
Pr	0.66	1.38	0.61	2.28	5.30	7.07
Nd	3.48	6.37	2.70	9.69	21.7	28.9
Sm	1.99	2.90	0.81	3.27	3.97	5.27
Eu	0.73	0.65	0.18	1.25	1.22	1.31
Gd	4.18	4.09	1.02	4.51	3.65	4.78
Tb	0.94	0.93	0.17	0.90	0.531	0.698
Dy	6.25	6.04	1.08	5.59	2.99	3.86
Ho	1.23	1.12	0.21	1.02	0.5	0.7
Er	3.15	3.19	0.64	2.80	1.49	1.95
Tm	0.40	0.47	0.092	0.38	0.2	0.2
Yb	2.26	3.33	0.64	2.69	1.23	1.57
Yb	2.26	3.33	0.64	2.69	1.23	1.57

References

BAACKE, D., MARTIN, M., KLUGE A., SCHLÖSSER, D. & HEINRICH, E. (1998): Migration von Seltenerdelementen und Präzipitation in Sintern schwermetallreicher Grubenwässer. Wissenschaftliche Mitteilungen, TU Bergakademie Freiberg, Institut für Geologie, S. 149-156.

BOYNTON, W.V. (1984): Cosmochemistry of the rare earth elements; meteorite studies. In: Rare earth element geochemistry, Henderson, P (ed) Elsevier Sci. Publ. Co., 63-114

BROOKINS, D.G. (1989): Aqueous geochemistry of rare earth elements. In: Geochemistry and mineralogy of rare earth elements, (eds.) Lipin, B. R; McKay, G A, Reviews in Mineralogy, vol.21, 201-225.

ELDERFIELD, H., UPSTILL-GODDARD, R. & SHOLKOVITZ, E.R. (1990): The rare earth elements in rivers, estuaries, and coastal seas and their significance to the composition of ocean waters. Geochimica et Cosmochimica Acta, 54, 971-991.

LEYBOURNE, M.I., GOODFELLOW, W.D., BOYLE, D.R., & HALL, G.M. (2000): Rapid development of negative Ce anomalies in surface waters and contrasting REE patterns in groundwaters associated with Zn-Pb massive sulphide deposits. Applied Geochemistry, 15, 695-723.

MCLENNAN, S.M. (1989): Rare earth elements in sedimentary rocks; influence of provenance and sedimentary processes. In: Geochemistry and mineralogy of rare earth elements, (eds.) Lipin, B. R; McKay, G A, Reviews in Mineralogy, vol.21, 169-200.

MÖLLER, P. (2000): Rare earth elements and yttrium as geochemical indicators of the source of mineral and thermal waters. In: Hydrogeology of crystalline rocks (eds.) Stober, I; Bucher, K, Water Science and Technology Library, 34, 227-246.

POLAT, A. HOFMANN, A.W., MUENKER, C., REGELOUS, M. & APPEL, P.W.U. (2003): Contrasting geochemical patterns in the 3.7-3.8 Ga pillow basalt cores and rims, Isua greenstone belt, Southwest Greenland; implications for postmagmatic alteration processes. Geochimica Cosmochimica Acta, 67, 441-457.

PRICE, R.C., GRAY, C.M., WILSON, R.E., FREY, F.A. & TAYLOR, S.R. (1991): The effects of weathering on rare-earth element, Y and Ba abundances in Tertiary basalts from southeastern Australia. Chemical Geology, 93, 245-265.

SACHSE, S. (2002): Die Geochemie der seltenen Erden in der plometallischen Sulfidlagerstätte Freiberg/Sachsen. Unpublished Diploma thesis, TU Bergakademie Freiberg.

TICHOMIROWA, M., BERGER, H.J., KOCH, E.A., BELYATSKI, B.V., GOETZE, J., KEMPE, U., NASDALA, L. & SCHALTEGGER, U. (2001): Zircon ages of high-grade gneisses in the eastern Erzgebirge (Central European Variscides); constraints on origin of the rocks and Precambrian to Ordovician magmatic events in the Variscan foldbelt. Lithos, 56, 303-332.

WORRALL, F. & PEARSON, D.G. (2001): The development of acidic groundwaters in coal-bearing strata; Part I, Rare earth element fingerprinting. Applied Geochemistry, 16, 1465-1480.


BERGAKADEMIE
TECHNISCHE
UNIVERSITÄT
FREIBERG

Metrological View of Probabilistic Modelling of Trace Elements Behaviour in Aqueous Environments

Günther Meinrath

RER Consultants, Schiessstattweg 3a, D-94032 Passau

Technische Universität Bergakademie Freiberg, Institut für Geologie, D-09596 Freiberg

Technische Universität Bergakademie Freiberg, Institut für Anorganische Chemie, D-09596 Freiberg

Numerical modeling of trace component in waters is discussed under a metrological point of view. Some basic metrological concepts are presented and justified. The current problems of analytical chemistry in adopting metrological concepts are illustrated and the consequences for thermodynamic data collections outlined. The importance of meaningful measurement uncertainties for thermodynamic quantities are demonstrated by applying the LJUNGSKILE code for investigation of uncertainties in chemical speciation to some aspects of acid mine drainage.

1 Introduction

The investigation of trace element behaviour in natural aqueous systems is an important sector of environmental study. The distribution and fluxes of minor elements may serve as indicators for physicochemical and biological processes in nature. The enormous complexity of most natural aqueous systems requires sensitive and selective analytical techniques for qualitative and quantitative determination of the constituent(s) of interest. Modern instrumental analysis has a broad range of techniques at hand from single atom detection to coupled speciation techniques for inorganic and organic materials analysis including biosubstances. The versatility of the instruments is enhanced by powerful chemometric data analysis techniques. Bioanalytical methods, i.e. immunoassays and biosensors, further extent the toolbox of analytical chemistry. The enormous progress in computing power is one of the major driving forces behind these developments. Impressive as the progress is, there are considerable caveats and warnings that, however, have their difficulties to reach the attention of those involved in the application of analytical methods and techniques.

The quantitative description of trace element behaviour is intimately connected with analytical chemistry. Either the site specific chemical input data of a model have been obtained by chemical analysis or the geochemical database has been obtained from chemical thermodynamic studies which deeply rely on analytical techniques. It should be reminded that the thermodynamic constants describing ion interaction in aqueous solutions result from the quantitative determination of often very sensitive solution equilibria.

For the applicant of chemical information, e.g. thermodynamic or site-specific data in reactive transport modeling, follows that the reliability of chemical data is much less than anticipated. Since quality control measures for chemical data came under discussion only recently no straightforward recommendation how to use these chemical data can be given.

2 Some Metrology Basics

Metrology is the science of measurement. A measurement is a comparison. Since there are no comparisons without imperfectly known errors, the significance which one can give to the measurement must take account of this uncertainty. Two independent measurements can be comparable only if they are both related to the same reference. Because measurements play an important role in daily life, the importance of such fundamental references has been recognised early. Today a system of seven fundamental units (metre, kilogram, second, ampere, kelvin, mole and candela) form the basis of sytème international d'unités (SI). The SI is backed by international treaties (convention du mètre) and subsequent international agreements, e.g. the reconnaissance mutuelle (Mutual Recognition Agree-

ment; MRA). Ideally, all comparisons should be made to these basic units, thus warranting traceability. Traceability is the property of the result of a measurement or the value of a standard whereby it can be related to stated references, usually national or international standards, through an unbroken chain of comparisons all having stated uncertainties (VIM 1994). Practically, there exists a hierarchy of standards running from the basic units as realized by the national metrological institutions (NMI) down to the working standard materials applied in the laboratories of research institutes and industry. The bureau international des poids and mèsures (BIPM) near Paris/France warrants the comparability of the realisations in different NMI. Thus the very basic uncertainty present in each laboratory measurement results from the comparisons of the different references with the higher standard (national standard, calibration standard, working standard; WIELGOSZ 2002).

The SI is strongly directed to the physical world. Chemical measurements have become a subject of metrology only in 1972 with the adoption of the mol as a SI unit. The quantity of which the mol is the bisic unit is 'amount of substance'. Most chemists will never have heard about this quantity neither use this term during their professional lifetime. The quantity of which mol is the unit is still under considerable discussion. To take an example, the term 'psammity' was proposed (KELL 1977) but not adopted. Another suggestion is 'Dalton'. One of the major problems is the fact that it is not possible to state the mass of an atom in terms of the number that appears on the periodic table and in SI units. There is no feasible method to determine the mass of a single atom with sufficient precision to define 1 u = m(^{12}C)/12 = 1.xyz.... · 10—2^{7} kg. One is forced to use 'a non-SI unit accepted for use with SI, the 'unified atomic mass unit' (u) defined as 1 u = m(^{12}C)/12 or to resort to the 'relative atomic mass' nomenclature. In addition, chemists measure concentration in units of mole per liter. Liter is a derived unit. In terms of SI 'the word liter may be employed as a special name for the cubic decimeter...(but that) liter should not be employed (to describe) high accuracy volume measurements'. Thus the status of the liter is ambiguous and, perhaps, even confusing. Worse, some textbooks use M to represent the unit mol/L. Sometimes M is termed molarity, sometimes molar concentration. IUPAC (International Union of Pure and Applied Chemistry) holds position that the adjective molar, when applied to extensive quantities, signifies division of that quantity by chemical amount (n) expressed in moles. The quantity expressed in mol/L is to be called 'amount of substance concentration'. However, the Clinical Chemistry Division of IUPAC suggests 'substance concentration'. Instead of M, the IUPAC recommends the use of 'c' to designate mol/L.

3 Accuracy in Analytical Chemistry

In an editorial (DE BIÈVRE 1999), Prof. de Bièvre described the presentation of an ICP-mass spectrometer. The device came with a software transforming the commonly single line in the mass spectrum into a three-dimensional graphics. The three-dimensional graphics made it possible for the analyst to vary the measurement parameters during a measurement and to monitor the consequences of his changes real-time in the graphics display. The manufacturer made considerable efforts to communicate how to optimize by this way the repeatability by using the relative standard deviation of the three-dimensional signal als a criterion. The manufacturer demonstrated this procedure using several lines as examples selling to the audience that the best value for the emasured quantity would be the value with the best repeatability. To reach this goal there was no hesitation to modify the the measurement parameters while going from one isotope to the next. As a consequence, different isotopes in the same sample were measured under different measurement conditions. The results, however, were finally combined. The optimisation of signal heights on basis of repeatabilities is irritating. De Bièvre however described that most potential clients felt thrilled by the idea to operate such a machine in the way demonstrated by the manufacturer.

It would be short-sighted to blame the manufacturer for this style of presentation of a complicated measurement instrument. Manufacturers are rarely scientists but merchands. They want to sell – to do so they are oriented to the requests and desires of their clients. The clients have to make clear to the manufacturers that they are only willing to buy equipmet that is easy to handle, transparent in its construnction, aiming at repeatable measurement results under comparable conditions of measurement – instead of transfering the experience to the manufacturers that black boxes including complicated data treatment gadgets sell nicely.

The dilemma described by de Bièvre isn't a recent one (CHALMERS 1993). In the early times of analytical chemistry the need to differentiate between precision, accuracy and repeatability has been emphasised eagerly. "Das Ziel eines Analytikers darf nicht sein, Resultate zu erzielen die absolut genau sind – welche meiner Überzeugung nach nur durch Zufall erreicht werden können – sondern dem genauen Werte so nahe zu kommen wie es chemische Analytik möglich machen kann" (Berzelius 1779 – 1848) and "Ein Chemiker, der nicht einen Eid darauf ablegen legen würde, dass seine Arbeit sorgfältig und genau ist sollte seine Ergebnisse niemals an die Öffentlichkeit geben, denn in dem Falle wären diese Ergebnisse von zerstörender Wirkung, nicht nur für ihn selbst, sondern für die gesamte Wissenschaft" (Fresenius 1818 – 1897). The australian metrologiest G. Price calls the procedure described above 'a warranty for the absence of accuracy' (PRICE 2000). There is obviously a problem in analytical chemistry that has gone unnoticed for a considerable time. The enthusiasm with reference to the new possibilities resulting from the instrumental revolution in analytical chemistry has left out of sight the necessity to understand the importance of the accuracy of a value from analytical measurement.

4 Quality of Thermodynamic Data Collections

There is no need for analytical chemistry to feel shame for its past achievements during the past decades. The limits have been pushed enormously. However, the strength of analytical chemistry is not necesarily the quantification of amounts of substances but the proof of identity of molecules. It is almost routine nowadays to analyse the stereochemical structure of a natural compound inambiguously, to synthesise this compound and to proof that natural and synthetic material are identical. There is no need to question analytical chemistry in general. The user of thermodynamic information must keep in mind that determination of thermodynamic data is a complicated and extremely time-consuming process. Before the advent of high-speed desktop computers,thermodynamic data has never been determined with such far-reaching applications in mind as reactive geochemical transport modeling.

The fundamental reason for the collection of thermodynamic databases is the relationship

$$\Delta G^\circ_R = - RT \ln K^\circ. \quad (1)$$

ΔG°_R is the Gibbs free energy available in a reaction under standard conditions (commonly 298.15 K and 1013 hPa), while K° is the equilibrium constant of the reaction under the same conditions. R is the fundamental gas constant and T the absolute temperature in kelvin. Eq. (1) relates the measurable quantity K° to the fundamental laws of thermodynamics. Hence, a constant K° determined under one condition is valid independently from time and space. In other words, K° is a fundamental law of nature itself. Hence, it is possible to measure a constant K° under convenient conditions in a laboratory and apply the result in a geochemical calculation, e.g. at much lower concentrations and meda of vastly different chemical composition. For other processes with potential relevance in natural aqueous systems, e.g. sorption and kinetically controlled processes, no equivalent to eq. (1) exists that would warrant a comparable justification for data transferability. On the contrary, both processes are known to depend sensitively on physico-chemical conditions.

For a long time, eq. (1) has been considered as a justification for the collation of thermodynamical data into so-called 'databases' (better: data collections). Such databases are abundant and may differ considerably. Especially, they do not provide any indication of the reliability of a numerical value, e.g. by stating an uncertainty. In most but the most important cases (e.g. dissociation constants of CO_2 in aqueous solutions, solubility of $CaCO_3$ or the autoprotolysis constant of H_2O) the amount of data is too small for a proper statistical treatment. In addition, evaluation process of thermodynamic data have been much too complicated even for an approximate statistical analysis of the measurement process. Hence, the main justification of a collection of a thermodynamic data is the deep belief of the compilators to recognise 'good' data if seeing it... (MEINRATH & LIS 2002).

Nowadays the situation has improved fundamentally. ISO has issued the Guide to the Expression of Uncertainty in Measurement (GUM 1993). This guide responds to the urgent demand of general rules for the assessment of data reliability valid in all fields of technology and science. The major NMI have established departments for 'Metrology in Chemistry'. EURACHEM, the organisation of European analytical laboratories, has issued a guideline for applying the GUM rules to analytical chemistry (EURACHEM 2000). Modern statistical tools, e.g. computer-intensive methods of statistical analysis like the bootstrap

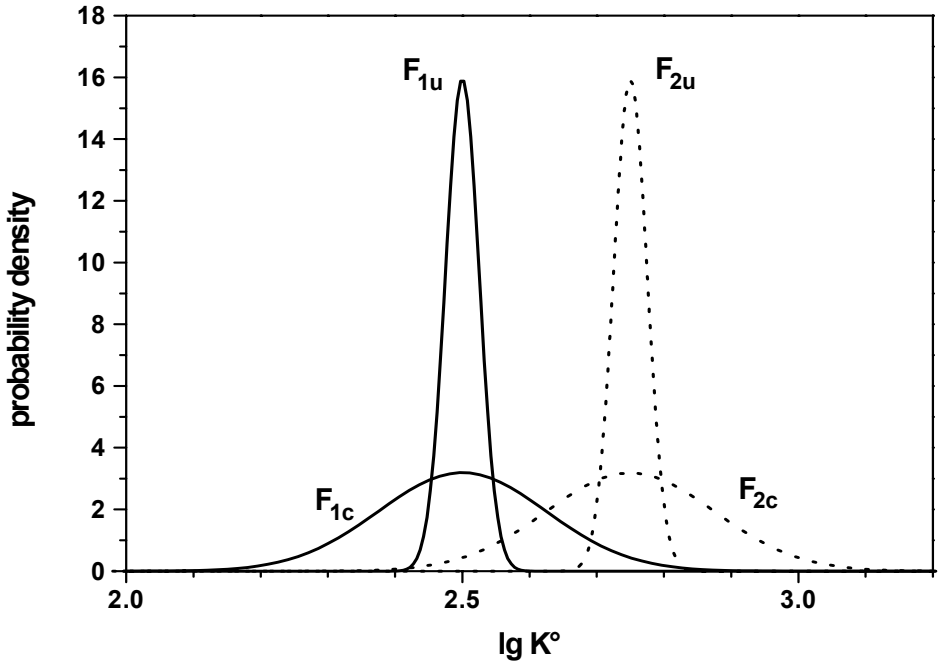

Figure 1: Two researchers (F_1 and F_2) study the same chemical system and report thermodynamic constant lg K°. Both assume a measurement uncertainty of ±0.05 (.68 percentile) (researcher 1: F_{1u}; researcher 2: F_{2u}). The probability distributions F_{1u} and F_{2u} do not overlap and

(EFRON & TIBSHIRANI 1997) allow a statistical analysis of the analytical processes from which thermodynamic data are derived (MEINRATH 2001; MEINRATH & LIS 2002; MEINRATH, EKBERG & STRÖMBERG 2003). The procedure to establish a complete measurement uncertainty budget of a thermodynamic value are rather complicated. A completely satisfactory uncertainty budget also needs to include measurement uncertainty of auxiliary data, notably the pH in case of pH-dependent reactions. Assessing the measurement uncertainty of pH is still work in progress (SPITZER & WERNER 2002; MEINRATH & SPITZER 2000). There is still some way to walk.

4.1 Both overinterpretation and underestimation of data reliablity invite problems

There is no safe side to walk when it comes to assessment of data quality of thermodynamic data. There are few systems where conditions can be found to obtain information on one species uncorrelated with the other components of the system. Hence, chemical systems are prone to correlation at different levels (MEINRATH 2000). A fundamental property of each chemical system is the number of species involved in the equilibrium under study. This question must be answered mostly from a limited number of data points more often than not correlated and nonlinear. Overinterpretation of accuracy and precision leaves unexplained variance and causes the introduction of non-existent species. Underestimation risks to ignore relevant but less dominant species. A similar situation exists for the values of the thermodynamic constants themselves. Figures 1/2 represent the both situations schematically. Two researchers are assumed to have determined a formation constant in the same system under comparable conditions. For sake of simplicity it is assumed that the results are free from bias and the uncertainty follows normal distributions. In figure 1, the total uncertainty budget is underestimated constants. The both distribution curves do not overlap – the discrepancy is significant. Tedious redeterminations will be necessary. In figure 2, the situation is reversed; the researchers underestimate the total uncertainty budget. Their distributions overlap significantly indicating agreement in the results.

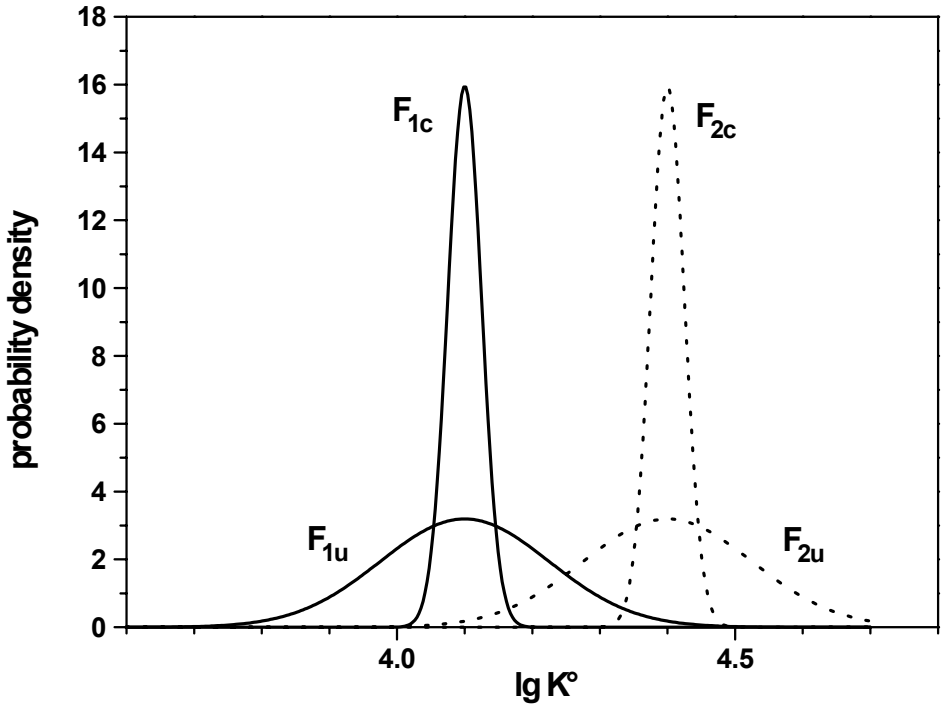

Figure 2: The reverse situation to figure 1 is illustrated. Both researchers overestimate the complete uncertainty budget of their measurements. They conclude reasonable agreement. If, however, the curves F_{1c} and F_{2c} represent the realistic total uncertainty budget, the system is likely to be incorrectly interpreted.

However, in such a situation experimental variance is incorrectly attributed to the species with the formation constant lg K° that should be attributed to another, probably unnoticed, species.

As a matter of fact there isn't any data collection where these questions have been addressed or even answered. The assessment of uncertainties in chemical measurement is a recent activity. Since progress mostly is understood in doing things better and better, a field of research where the limitations of chemical data (not seldom highly acclaimed) are investigated does not expect to receive much focus. Its competences require such unpleasant fields as statistics (seen from most chemists as a 'cure' (THOMPSON 1993) and scientific computing. Considering that most chemists never have attended a statistical course beyond the most rudimentary introduction of t-tests and, perhaps, ANOVA, enthusiasm for metrology in chemistry should be expected to be moderate.

Table 1: Selected hydrolysis constants of Fe(III) from different compilations.

$Fe(OH)^{2+}$	$Fe(OH)_2^{+}$	$Fe(OH)_3°$	$Fe_2(OH)_2^{4+}$	$Fe_3(OH)_4^{5+}$	$Fe(OH)_4^{-}$	$Fe(OH)_{3(s)}$	source
61[a)]	9[a)]	2[a)]	20[a)]	5[a)]	3[a)]		JESS
-2.19	-5.67	-12.0	-	-	-21.6		B/M
-2.5	-6.5	-12.0	-3.0	-6.1	-21.6		CIV
-2.19	-5.67	-12.56	-2.95	-6.3	-		PQC
-2.19	-4.59	-	-2.85	-6.3	-		NIST
-2.05	-6.35	-13.45	-2.90	-6.04	-21.43	3.20	JESS[b)]

[a)] number of literature references in the JESS database for a particular species; b) the weights given in JESS database indicate that only $FeOH^{2+}$ can be considered to be well characterised. B/M: BAES & MESMER 1976; JESS: Joint Expert Speciation System: MAY & MURRAY 1991; 2000; NIST: MARTELL et al. 1993; PQC: PHREEQC Default Database (PARKHURST 1995); CIV: CHEMVAL (1992)

Table 2: Uncertainties applied in calculation of the speciation diagram Fig. 4.

	uncertainty level I	uncertainty level II
$FeOH^{2+}$	± 0.28	± 1.0
$Fe(OH)_2^+$	± 0.22	± 0.5
$Fe(OH)_3^\circ$	± 0.23	± 0.5
$Fe(OH)_4^-$	± 0.23	± 0.5
$Fe_2(OH)_2^{2+}$	± 0.2	± 0.5
$Fe_3(OH)_4^{2+}$	± 0.2	± 0.5
$Fe(OH)_{3(s)}$	± 0.23	± 0.5

5 Making uncertainties visible: the Ljungskile code

The total uncertainty budget of a complicated quantity like a thermodynamic constant is a somewhat abstract concept. Does it really matter whether a constant is given as, say, lg K° = 4.3 or, say lg K° = 4.3 ± 0.15? As a matter of fact, there are only very few examples available in literature where the importance of uncertainty in thermodynamic constants has been discussed. Because geochemical modeling involves usually a large number of species, to take uncertainty in each species into account may become a task difficult to be tackled. As an illustrating example of uncertainty propagation, the probabilistic speciation code Ljungskile will be applied using Fe(III) at trace concentration levels as an example (ÖDEGAARD-JENSEN, MEINRATH & EKBERG 2003).

Iron is an important element in the environment. The Fe(II)/Fe(III) redox equilibrium in combination with the considerable differences in chemical behaviour of the both states causes mineral formation, alteration and dissolution. Iron is a limiting element for biochemical processes (MARTIN & FITZWATER 1988). Iron affects the

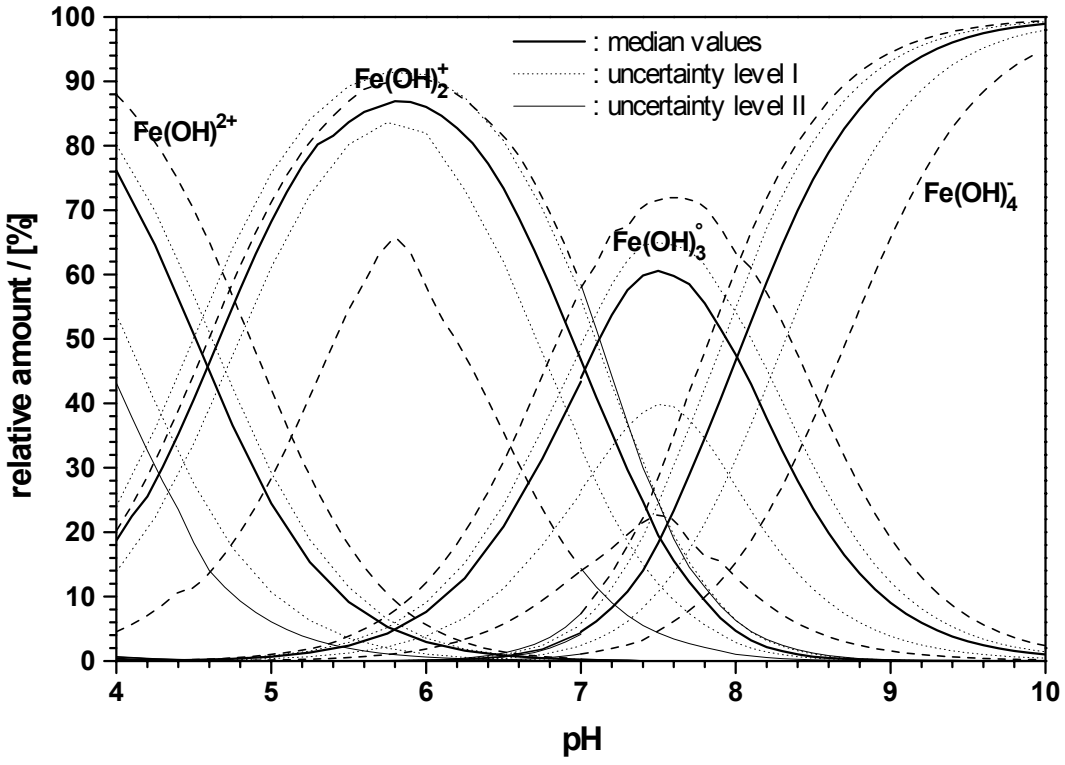

Figure 3: Probable composition of an aqueous solution in equilibrium with $Fe(OH)_3$(s) and very low ionic strength (I < 10—3 mol L^{-1}) (LJUNGSKILE simulation). The Fe(III) hydrolysis species are taken into account with formation constants given in last row of Table 1 and two uncertainty levels given in Table 2.

rates of redox processes and the redox state of natural waters (MILLERO, YAO & AICHER 1995). In acid mine drainage (AMD) iron plays an important role as a source of hydronium ions, e.g. from acid producing sulfide minerals. The study of AMD is an important field of research, however, it is often not sufficiently appreciated that the thermodynamic data basis for a modeling of the complex processes in AMD is rather poor. After compilation of the vast majority of reports on the thermodynamics of Fe(III) hydrolysis publicly available, MAY AND MURRAY (1991) conclude that only the formation constant for $FeOH^{2+}$ is well characterised. It is also apparent from Table 1 that the elicitations in the compilations are not independent of each other.

When using mean values of a thermodynamic constant for each species, speciation codes to solve the respective systems of equations are available. But propagating probability density curves through a speciation code is a task running on a different level of complexity. However, in combining non-parametric statistics, efficient algorithms and high-speed computers feasible ways to solve the problem can be found. Such an approach has been implemented in the code LJUNGSKILE 1.0, where stratified sampling strategies are combined with the speciation code PHREEQC to evaluate estimates for speciation variability as a result of uncertainties in the formation constatns. In the present implementation, the species and the uncertainties must be explicitely specified by the user. A solid phase can be selected but an uncertainty for the solubility product cannot yet be specified. Due to the absence of meaningful uncertainties in literature, the uncertainties must be estimated. A calculation for the Fe(III)-H_2O system at $(Fe)_{total}$ = 10—8 mol L^{-1} is shown in fig. 3 using two uncertainty levels (.68 percentiles).

It is obvious that the polynuclear species are absent. Provided, the formation constants are not grossly underestimated, they do not play a role in solid-aqueous phase equilibria of Fe(III) at very low ionic strengths. It is alos obvious that reporting relative species amounts to the percent level is inadequate. The uncertainties are in the order of ten percent. Both methods advice care in the statement which species is dominating in the region pH 6.5 to pH 8.5. This pH region is typical for natural aqueous systems. Independent whether uncertainty ranges are symmetric or asymmetric, the uncertainties in the relative composition of the solution are in the order 10^1 %. Considering the abundance of mean value-based speciation calculations and diagrams in the literature with figures given to the tenth of a promille and even beyond, it is obvious that in the future diagrams and calculations without stated uncertainty should not be acceptable because the risk of over- and misinterpretation is high.

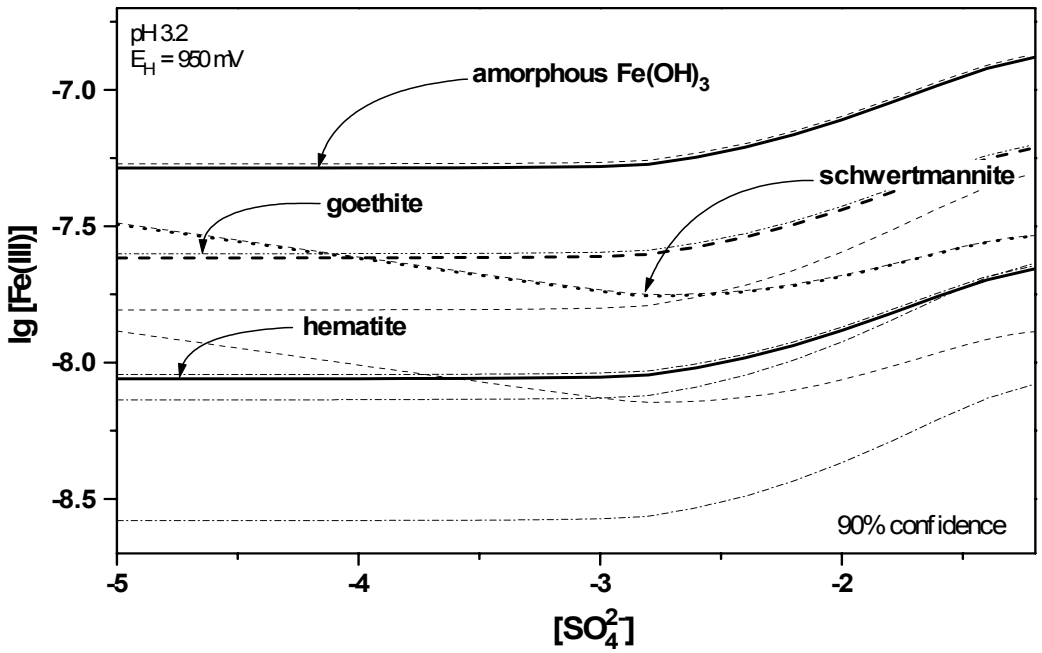

Figure 4: Solubility of amorphous $Fe(OH)_3$ (lg K_{sp} = 0.89), goethite (lg K_{sp} = 0.5), hematite (lg K_{sp} = 0.00) and schwertmannite ($Fe_8O_8(OH)_6SO_4$; lg K_{sp} = -8) as a function of the sulfate concentration. Dashed lines give 90% confidence limits.

Figure 4 illustrates another consequence of measurement uncertainty in trace element modeling. Processes in aqueous systems are strongly affected by mineral transformations and alterations. It has occured that schwertmannite compounds are present in AMD waters. Schwertmannites are sulfate containing iron oxyhydrates. Their formation in high-sulfate AMD waters generates about 2.7 H^+ ions per formula unit Fe(III). However, the stability region of schwertmannites is badly understood (SCHWERTMANN, BIGHAM & MURAD 1995). Considering only the mean values in the simulation fig. 4, it may be concluded that hematite is the most stable among the four phases considered while schwertmannite is more stable than amorphous $Fe(OH)_3$ at sulfate concentrations above 10—5 mol L^{-1}. The LJUNGSKILE simulation, however, explains that given the uncertainties in the formation constants of the Fe(III) hydrolysis species (uncertainty level I) no inambiguous statement can be made about the stability of schwertmannite $Fe_8O_8(OH)_6SO_4$ vs. either amorphous $Fe(OH)_3$, goethite or hematite – except perhaps that at low sulfate concentrations hematite may be more stable than schwertmannite. Taking into account the difficulty to assess solubility products of highly insoluble compounds like Fe(III) hydrates and oxyhydrates, the variability of chemical composition of these compounds and the variability of compositions (Schwertmann & Cornell 1991), the prediction becomes even more questionable. These latter uncertainties are not yet included in the uncertainty intervals in fig. 4.

References

CHALMERS, R.A. (1993): Space Age Analysis. Talanta 40: 121 – 126.

DE BIÈVRE, P. (1991): Reproducibility is never a proof of accuracy... Accred. Qual. Assur 4: 387

EKBERG, C., ÖDEGAARD-JENSEN, A. & MEINRATH, G. (2003): LJUNGSKILE 1.0: A Computer Program for Investigation of Uncertainties in Chemical Speciation. SKI REPORT 2003:03. Swedish Nuclear Power Inspektorate. Stockholm/S 2003.

EURACHEM (2000): Quantifying Uncertainty in Chemical Measurement (Ellison, Rösslein, Williams, eds.) EURACHEM.

GUM (1993): Guide to the Expression of Uncertainty in Measurement. ISO Genève/CH.

KELL, G.S. (1977): Nature 267: 665 – 667.

MARTIN, J.H. & FITZWATER, S.E. (1988): Iron deficiency limits phytoplankton growth in the north-east Pacific subarctic. Nature 331: 341 – 343.

MAY, P.M. & MURRAY, K. (1991): JESS – a joint expert speciation system I. Raison d'être. Talanta 38: 1409 – 1417

MEINRATH, G. (2000): Comparability of thermodynamic data – a metrological point of view. Fresenius J. Anal. Chem. 368: 574 – 584.

MEINRATH, G. & SPITZER P. (2000): Uncertainties in Determination of pH. Mikrochim. Acta 135: 155 – 168.

MEINRATH, G. (2001): Measurement uncertainty of thermodynamic data. Fresenius J. Anal. Chem. 369: 690 – 697

MEINRATH, G. & LIS, S. (2002): Applicationof cause-and-effect diagrams to the interpretation of UV-Vis spectroscopic data. Anal. Bioanal. Chem. 372: 333 – 340

MEINRATH, G., EKBERG, C. & STRÖMBERG, B. (2003): A retraceable method to assess uncertainties in solubility estimations exemplified by a few americium solids. 35: 55 – 66.

MILLERO, F.J., YAO, W. & AICHER, J. (1995): The speciation of Fe(II) and Fe(III) in natural waters. Mar. Chem. 50 (1995) 21 – 39.

PRICE, G. (2000): Pragmatic philosophies of measurement in chemistry? Chem. Australia. October 2000: 38 – 40

SCHWERTMANN, U., BIGHAM, J.M. & MURAD, E. (1995): The first occurence of schwertmannite in a natural stream environment. Eur. J. Mineralogy 7: 547 – 552.

SCHWERTMANN, U. & CORNELL, R.M. (1991): Iron Oxides in the Laboratory. VCH Verlagsgesellschaft Weinheim/FRG

SPITZER, P. & WERNER, B. (2002): Improved reliability of pH Measurement. Anal. Bioanal. Chem. 374: 787 – 795.

THOMPSON, M. (1993): Statistics – the curse of analytical classes. Analyst 119: 127N

VIM (1994): International Vocabulary of Basic and General Terms in Metrology. Beuth Verlag Berlin/FRG.

WIELGOSZ, R.I. (2002): International comparability of chemical measurement results. Anal. Bioanal. Chem. 374: 767 – 771

Anwendung von isotopenhydrologischen Methoden bei Einzugsgebietsuntersuchungen

Petra Schneider[1], Susanne Voerkelius[2], Karsten Osenbrück[2], Jürgen Meyer[3]

Hydroisotop-Piewak GmbH, Oberfrohnaer Str., 84, D-09117 Chemnitz

Hydroisotop GmbH, Woelkestr. 9, D-85301 Schweitenkirchen

Wismut GmbH, Jagdschänkenstr. 52, D-09117 Chemnitz

Einzugsgebietsstudien erfordern das hydraulische Verständnis der Fliessprozesse in der gesättigten und der ungesättigten Zone. In den Einzugsgebieten von Kohlungbach und Wiesenbach wurden isotopenhydrologische Untersuchungen mit dem Ziel der Ermittlung der mittleren Verweilzeiten, Austauschraten und Mischungsprozesse von Grund- und Oberflächenwasser durchgeführt. Hierfür kamen radioaktive und stabile Umweltisotope zur Anwendung (^{2}H, $^{16/18}O$, ^{3}H, ^{85}Kr, $^{14/15}N$, ^{34}S). Die isotopenhydrologischen Untersuchungen wurden mit konventionellen hydrologischen und hydrogeologischen Methoden kombiniert, um ein konzeptionelles Wasserhaushaltsmodell der beiden Einzugsgebiete zu entwickeln. Die Ergebnisse wurden in einem Einzugsgebietsmodell zusammengefasst und bilanziert.

1 Einführung

Die Anwendung von Umweltisotopen als hydrologische Tracer umfasst zwei Typen von Untersuchungsmethoden (KENDALL et al. 1998):

- Tracer des Wassers selbst : Isotopenhydrologie des Wassers,
- Tracer der im Wasser gelöste Stoffe: Isotopenbiogeochemie von gelösten Stoffen.

Die Untersuchungen am Wassermolekül können an Sauerstoffisotopen ($^{16/18}O$) und an Wasserstoffisotopen (Deuterium ^{2}H, Tritium ^{3}H) durchgeführt werden. Diese Isotope sind ideale Tracer der Wasserquellen sowie deren Bewegung und mischen sich konservativ.

KENDALL et al. 1998 beschreiben die wesentlichen Prozesse, denen Sauer- und Wasserstoffisotope in Einzugsgebieten unterliegen, folgendermaßen: (1) Phasenänderungen, die das Wasser über oder nahe dem Grundwasserspiegel beeinflussen (Verdunstung, Schmelzprozesse), und (2) einfache Mischungen über oder nahe dem Grundwasserspiegel. In Einzugsgebieten können stabile Sauerstoff- und Wasserstoffisotope genutzt werden, um die Beiträge junger (und alter) Grundwasserkomponenten zu ermitteln. Tritium und Krypton-85 können als Tracer genutzt werden, um Grundwasserverweilzeiten < 50 Jahre zu ermitteln und Mischungsprozesse aufzuklären.

Die Fließwege in einem Einzugsgebiet werden durch die Wechselwirkung der gesättigten mit der ungesättigten Zone bestimmt. Die Speisung des das Einzugsgebiet entwässernden Gewässers kann durch verschieden schnelle Wasserkomponenten erfolgen, die ihren Ursprung je nach geologischem Aufbau des Einzugsgebietes im Grundwasser oder in der ungesättigten Zone haben. In Abhängigkeit davon, ob Matrixfluss oder Kluftzuflüsse im Einzugsgebiet dominieren, können junge oder alte Wässer oberirdisch entwässern. Die Anforderung, die Fließwegedynamik genau zu kennen, zeigt sich beim Einbezug der geochemischen Prozesse in das Einzugsgebietsmodell: wenn die Hydrologie eines Einzugsgebietes unzureichend verstanden ist, kann auch die Beschreibung geochemischer Prozesse auf Einzugsgebietsebene nur unzureichend erfolgen.

2 Charakterisierung des Untersuchungsgebietes

Die Einzugsgebiete des Kohlungbaches und des Wiesenbaches befinden sich im Südwesten von Sachsen in der Nähe der Stadt Aue (vgl. Abbildung 1). Der Hauptvorfluter ist die Zwickauer Mulde mit einer mittleren Wasserführung von ca. 10 m^3/s. Der mittlere korrigierte Niederschlag für den Untersuchungsraum Aue wird mit 897 mm (45-jährige Messreihe) angegeben. Das Klein-

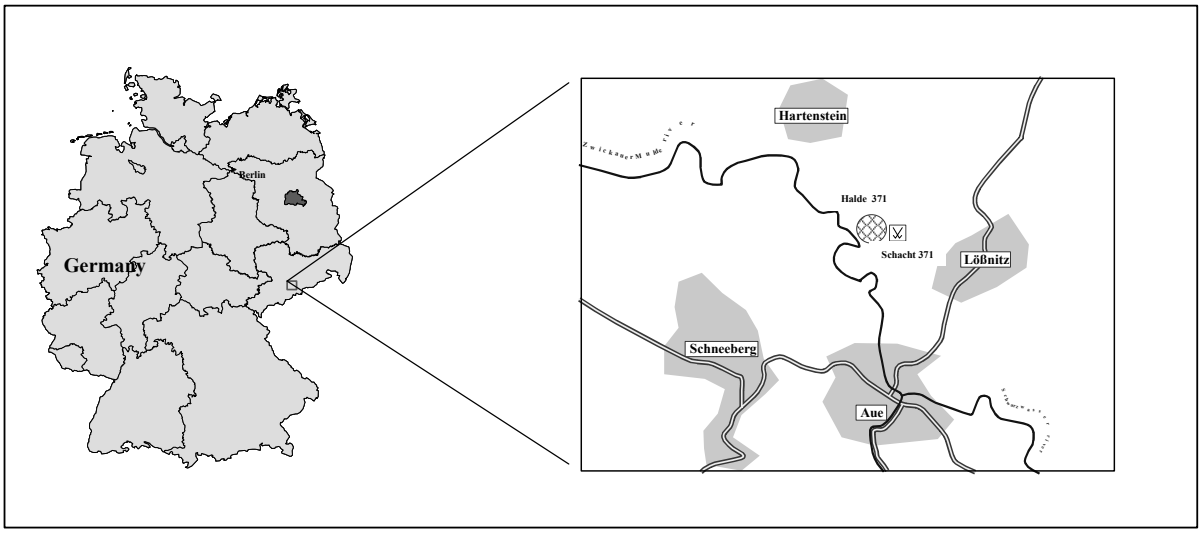

Abb.1: Lage des Untersuchungsgebietes.

klima im Untersuchungsgebiet kann als gemäßigt und niederschlagsreich für die unteren Lagen der Mittelgebirge eingestuft werden.

Der Kohlungbach drainiert eine Einzugsgebietsfläche von ca. 131 ha, wobei 59,5 % auf Wald, 3,9 % auf versiegelte Flächen, 2,2 % auf Wiesen und 34,4 % auf Bergematerial aus dem Uranerzbergbau (Halde 371/I der Wismut GmbH) entfallen. Der Wiesenbach drainiert eine Einzugsgebietsfläche von ca. 81 ha, wobei 22,9 % auf Wald, 3,7 % auf versiegelte Flächen, 44,1 % auf landwirtschaftliche Nutzfläche und 28,3 % auf Bergematerial aus dem Uranerzbergbau (Halde 371/II der Wismut GmbH) entfallen. Beide Bäche treten im oberen Teil des Einzugsgebietes in das grobkörnige Haldenmaterial ein, durchfließen es und treten im abstromigen Bereich des Einzugsgebietes wieder aus. Von dort entwässern die Bäche die einzugsgebietstypische Stofffracht in die Zwickauer Mulde.

Das Untersuchungsgebiet befindet sich nördlich der Lößnitz-Zwönitzer Zwischenmulde, die aus oberordovizischen, silurischen und devonischen Gesteinslagen besteht, die in die unterordovizischen Phyllite der Erzgebirgsnordrandzone eingefaltet sind. Das Gestein kann als Kluftaquifer mit Störungen beschrieben werden. Es unterliegt

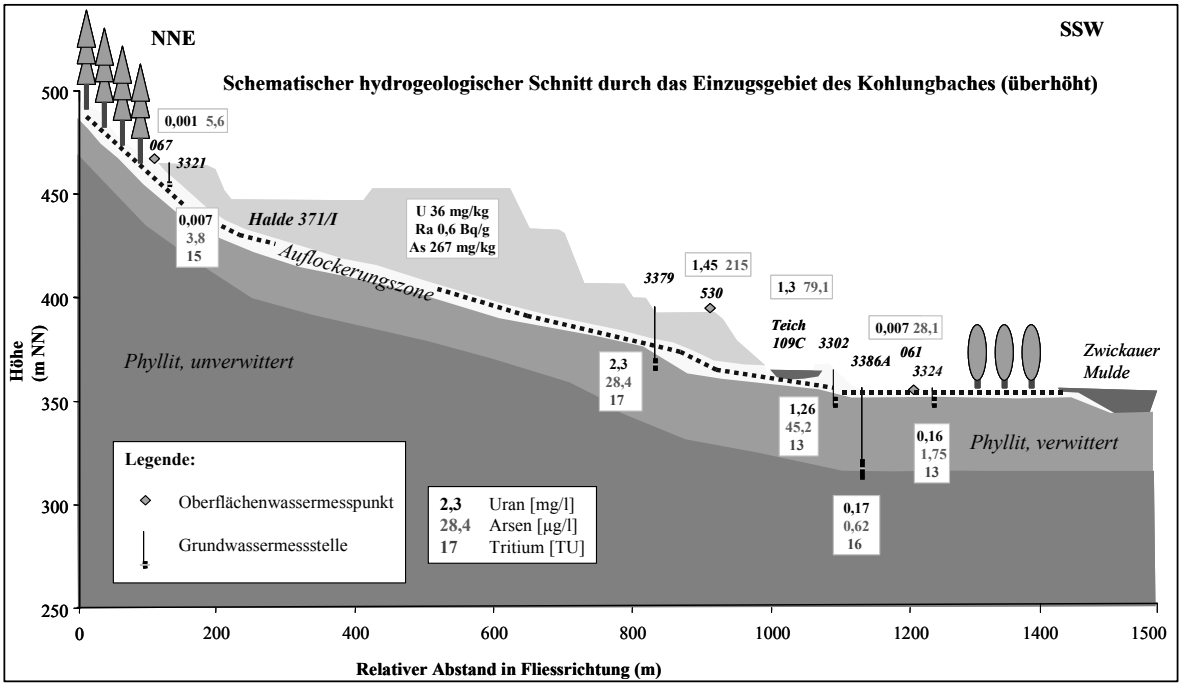

Abb. 2: Schematischer hydrogeologischer Schnitt durch das Einzugsgebiet des Kohlungbaches.

einer oberflächigen lehmigen Verwitterung bis in Tiefen von 2 m im Bereich von Hanglagen und bis zu 30 m im Bereich von Talsohlen. Grundwassermessstellen, die zur Aufklärung der hydraulischen Verhältnisse abgeteuft wurden, zeigen, dass sich der größte Teil des Grundwassers in der Verwitterungszone der Phyllite bewegt (vgl. Abbildung 2).

Die Verwitterungszone besteht aus einer Auflockerungszone des Festgesteines und einer überlagernden Lehmzone, die von Braunstaugleyböden bedeckt ist. In Pumpversuchen wurden in der Auflockerungszone mittlere hydraulische Durchlässigkeiten von 10^{-7} bis 10^{-8} m/s ermittelt, wobei erhöhte hydraulische Durchlässigkeiten von bis zu 10^{-5} m/s im Bereich tektonischer Strukturen angetroffen wurden. Die überlagernde Lehmzone hat eine hydraulische Durchlässigkeit im Bereich von 10^{-6} m/s. Das überlagernde Haldenmaterial ist überwiegend sandig/kiesig mit hohem Steinanteil beschaffen und ist daher mit hydraulischen Durchlässigkeiten von bis zu 10^{-2} m/s sehr gut durchlässig. Grundwasserneubildung im Einzugsgebiet findet im wesentlichen durch Infiltration an vertikalen Lekagen statt. Lokal findet man in der überlagernden Lehmzone einen Druckspiegel des Grundwassers.

3 Isotopenhydrologische Untersuchungsmethoden

Inhalt der Studie war die Einzugsgebietscharakterisierung mit dem Ziel der Ermittlung von Fliesswegen, Verweilzeiten und Stofftransporten. Dabei sollte auch die Prognose der Entwicklung der Stofftransporte berücksichtigt werden. Zu Beginn der Untersuchungen war über die Hydraulik der Einzugsgebiete nur wenig bekannt. Mit Hilfe konventioneller hydrogeologischer Methoden wurden die Schichtabfolgen und Aquiferdrücke ermittelt. Mit den isotopenhydrologischen Untersuchungen sollten spezielle Fragen zum Stofftransport und der hydraulischen Wirksamkeit der ermittelten Kluftwasserwegsamkeiten ermittelt werden. Eine spezielle Frage war die Ermittlung der Mittleren Grundwasserverweilzeiten, um die Grundwasserneubidlung im Einzugsgebiet abschätzen zu können. Folgende isotopenhydrologischen Untersuchungen wurden neben der hydrochemischen und hydraulischen Charakterisierung durchgeführt:

- Grundwasseraltersdatierung mittels Tritium (^{3}H) und Krypton-85,
- Sauerstoff-18/Deuterium-Untersuchungen,
- Sauerstoff-18-Zeitreihenuntersuchungen,
- Untersuchung der Gehalte von Schwefel-34 und Sauerstoff-18 am Sulfat,
- Untersuchung von Stickstoff-15 und Sauerstoff-18 am Nitrat.

Die hydrologisch-hydraulische Charakterisierung der Einzugsgebiete wurde außerdem mit klassischen hydrogeologischen und hydrochemischen Methoden vorgenommen (Hydrotopkartierung, hydrogeologische Bohrungen, Pump- und Versickerungsversuche, Erstellung von Grundwassergleichenplänen, Abflussmessung, Wasserhaushaltsbilanzierung, Hydrochemische und Gasgehaltsanalytik).

4 Isotopenhydrologische Charakterisierung der Einzugsgebiete

An den Grund- und Oberflächenwässern wurde die Bestimmung von Umweltisotopengehalten durchgeführt, um

- Aussagen zur Versauerungsproblematik abzuleiten,
- eine von hydrochemischen Ergebnissen unabhängige Klassifizierung der Wässer vornehmen zu können,
- Wässer unterschiedlicher Herkunft zu charakterisieren,
- Aussagen zur mittleren Verweilzeit der Wässer im Einzugsgebiet abzuleiten.

4.1 Sauerstoff-18/Deuterium-Untersuchungen

Die hydrologische Anwendung von Messungen des Gehaltes an den stabilen Isotopen ^{2}H und ^{18}O am Wassermolekül beruht im wesentlichen auf den in natürlichen Wässern auftretenden Konzentrationsunterschieden. Die verschiedenen Isotopeneffekte führen zu einer örtlich und zeitlich charakteristischen Markierung der Niederschläge und damit auch zu einer örtlich und zeitlich charakteristischen Markierung der verschiedenen Wasserkörper des Wasserkreislaufes. Die durch die Isotopeneffekte hervorgerufenen Schwankungen der Gehalte an den stabilen Isotopen ^{2}H und ^{18}O im Wasserkreislauf sind hauptsächlich durch Isotopenfraktionierungen bei Pha-

senumwandlungen (Verdampfung, Kondensation u.ä.) bedingt.

Wesentlich ist dabei, dass die Isotopenfraktionierung temperaturabhängig ist. Aus der Bestimmung der stabilen Isotope des Wassermoleküls Sauerstoff-18 und Deuterium in einer Wasserprobe lassen sich somit in erster Linie Rückschlüsse auf die klimatischen Bildungsbedingungen sowie die Höhenlage und geographische Lage bei der Wasserneubildung ziehen. Liegen die δ^2H-^{18}O-Meßwertpaare von Wasserproben im Bereich der Niederschlagsgeraden, kann daraus geschlossen werden, dass die Wässer meteorischer Herkunft sind. Dies ist in den Einzugsgebieten von Kohlungbach und Wiesenbach der Fall (vgl. Abbildung 3).

Die an Hand der Untersuchung der stabilen Isotope ermittelten Ergebnisse zeigen, dass alle in den Einzugsgebieten untersuchten Grund- und Oberflächenwässer Anteile junger Wasserkomponenten (< 2 a) enthalten. Auch die Oberflächenwässer werden von Anteilen junger holozäner Grundwässer gespeist. Dies ist für die Wasserhaushaltsbilanzierung der Einzugsgebiete wesentlich, da diese auf Klüften migrierende Komponente für den kurzfristigen Stofftransport, insbesondere nach Starkregenereignissen, verantwortlich ist.

4.2 Sauerstoff-18-Zeitreihenuntersuchungen

Sauerstoff-18-Zeitreihenuntersuchungen wurden an Kohlungbach und Wiesenbach in Anstrom und im Abstrom der Bergehalden durchgeführt. Ziel war es, die Zeitschiene des Stofftransportes im Haldenmaterial selbst zu ermittelten. Hierfür wurden z.T. in 14-tägigem Rhythmus, sowie während Starkregenereignissen täglich Sauerstoff-18-Proben entnommen und untersucht. Die Datierung über die ^{18}O-Gehalte beruht auf der jahreszeitlichen Schwankung dieser Isotopengehalte im Niederschlag und damit im neugebildeten Grundwasser. Soweit die ^{18}O-Schwankungen im Grundwasser noch messbar sind, lassen sich Grundwasserverweilzeiten im Bereich von Monaten bis Jahren angeben. Geht die ^{18}O-Variation im untersuchten Grundwasser über die Messgenauigkeit der Methode (± 0,15 ‰) hinaus, kann anhand des Ausmaßes der Dämpfung der ^{18}O-Variation sowie der zeitlichen Verzögerung gegenüber dem Niederschlags auf den Anteil und die mittlere Verweilzeit einer schnell zufließen-

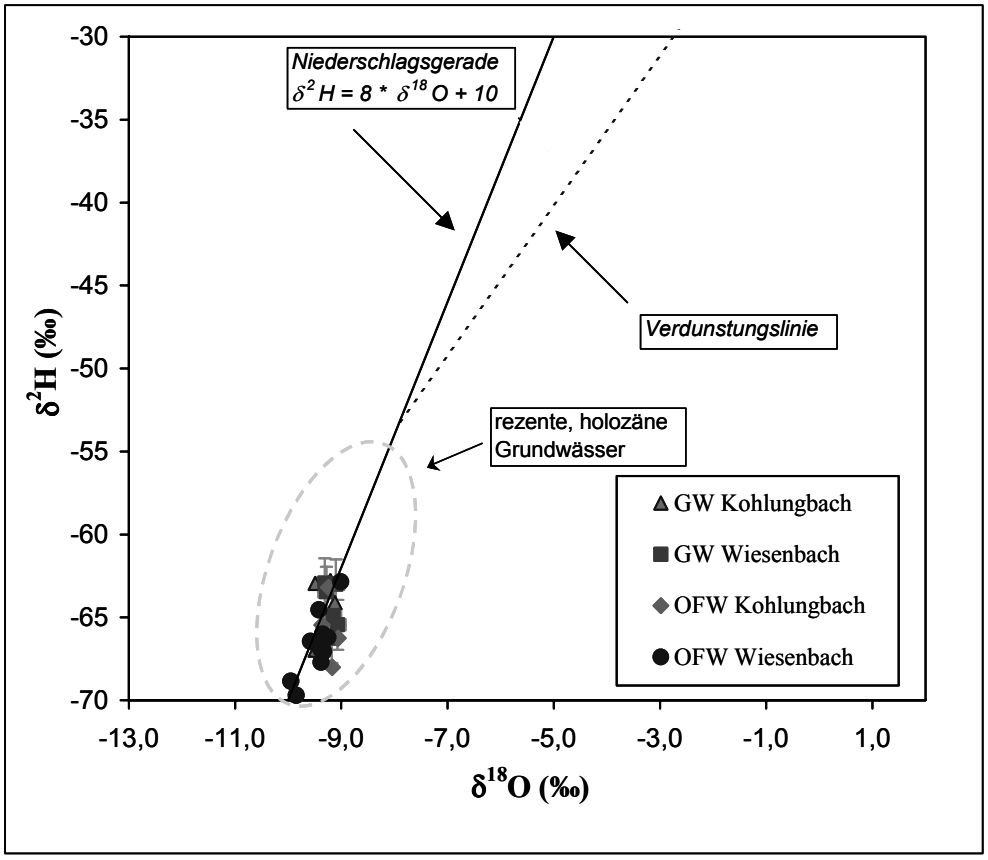

Abb. 3: Korrelation der Sauerstoff-18-Gehalte gegen die Deuteriumgehalte in den Einzugsgebieten von Kohlungbach und Wiesenbach (Werte des gesamten Einzugsgebietes).

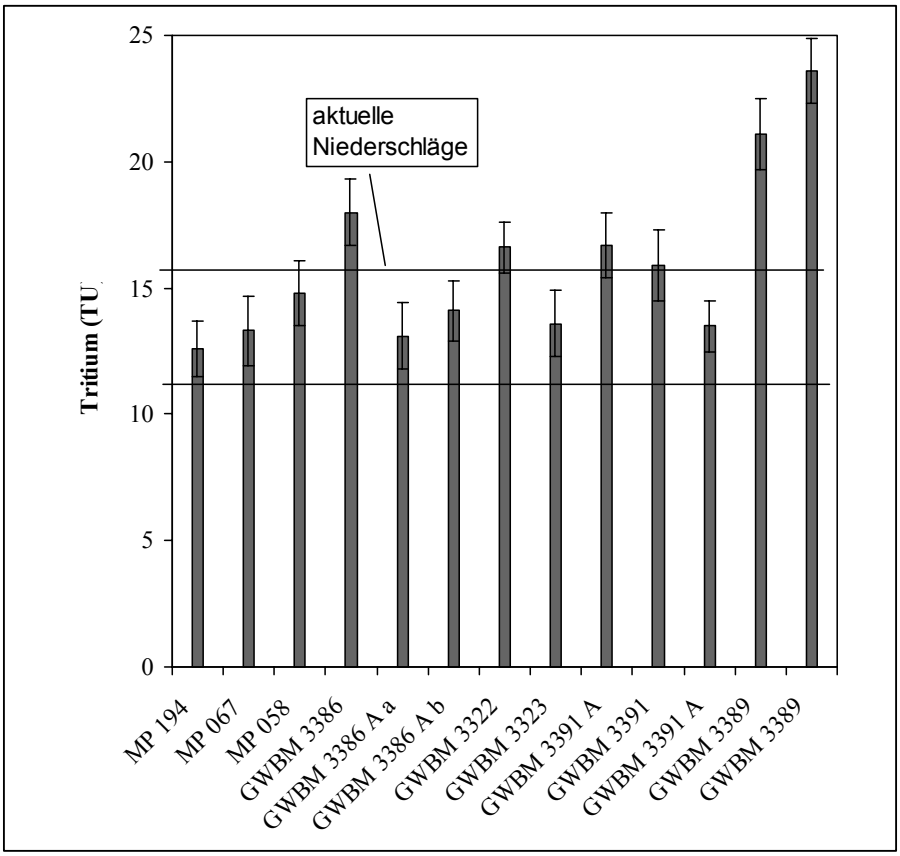

Abb. 4: Grafische Darstellung der Tritiumgehalte in den Einzugsgebieten von Kohlungbach und Wiesenbach (z.T. Mehrfachmessungen an Messstellen), Niederschlagswerte aus dem Einzugsgebiet (Zuordnung: Anstrom Wiesenbach: MP 194, GWBM 3389, GWBM 3323, Abstrom Wiesenbach: MP 058, GWBM 3322, Anstrom Kohlungbach: MP 067, Abstrom Kohlungbach: MP 058, GWBM 3386, GWBM 3386a, GWBM 3391).

den Grundwasserkomponente geschlossen werden. Ziel der ^{18}O-Zeitreihenuntersuchungen war die Bestimmung der Herkunft der Grund- und Sickerwässer im Haldenbereich und die Bestimmung der unterirdischen Abflussraten/Verweilzeiten in der Auflockerungszone sowie die nähere Untersuchung der Beziehung zwischen den Niederschlagsintensitäten und dem Zufluss schnell infiltrierender Komponenten.

Die durchgeführten Untersuchungen zeigten für die hypodermischen Wässer beider Einzugsgebiete etwa ein mit den Niederschlägen gleichsinnigen Verlauf der ^{18}O-Gehalte. Eine zeitliche Verzögerung zwischen der Input- (Niederschlag) und der Outputkurve lag im Prinzip nicht vor. Es wurde festgestellt, dass der Sauerstoff-18 – Jahresgang im Anstrombereich des Kohlungbaches die niedrigste mittlere Verweilzeit aufwies und eine gute Übereinstimmung mit dem Jahresgang des Niederschlags erkennen ließ. Peakmaximas und –minimas zeigten prinzipiell keine zeitliche Verschiebung. Im Einzugsgebiet des Wiesenbaches wurde dagegen eine deutliche Dämpfung festgestellt. Der tendenzielle Verlauf der Niederschläge ließ sich jedoch erkennen.

Die Ganglinien aus dem abstromigen Gebiet es Kohlungbaches zeichnete den tendenziellen Verlauf der Niederschläge nach. Das Alter der jung zufließenden Komponente ließ sich in den Outputkurven aufgrund fehlender Parallelität zum Verlauf der Inputkurve im Untersuchungszeitraum nicht ableiten. Eine mögliche Peakzuordnung war im Untersuchungszeitraum nur punktuell möglich. Eine mögliche Erkärung hierfür ist, dass das Wasser im Einzugsgebiet des Wiesenbaches eine Mischung aus zwei jungen Komponenten darstellt, die in etwa gleiche aber zeitlich versetzte Ganglinien aufwiesen. Hierdurch reagiert Sickerwasser in den Meßstellen nach einer längeren Trockenperiode zunächst unmittelbar auf ein Niederschlagsereignis, im folgenden ließ sich aber eine Peakabfolge nicht mehr der Niederschlagsganglinie zuordnen

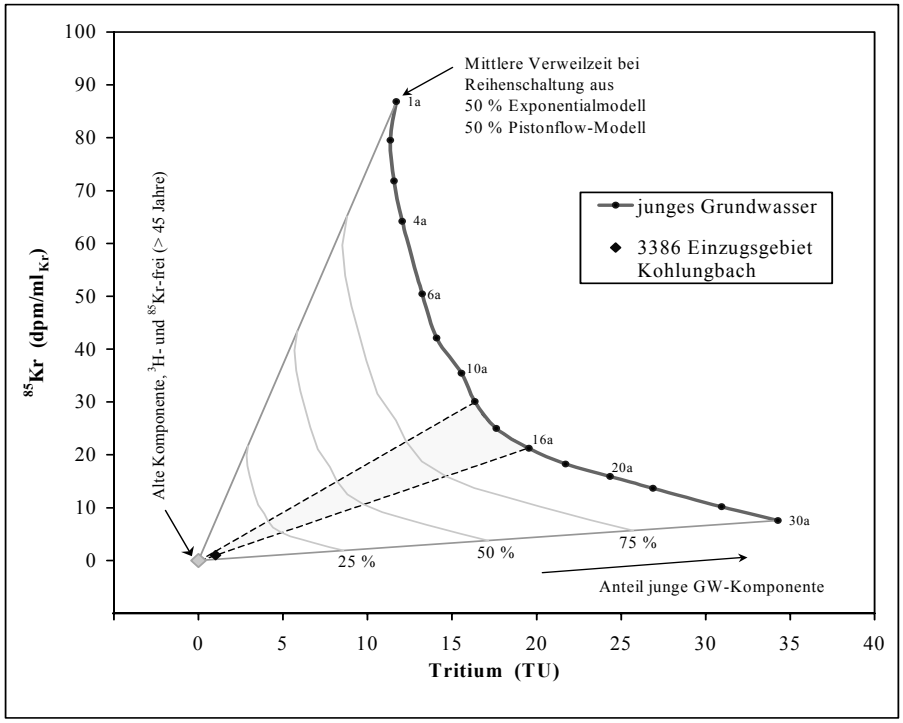

Abb. 5: Grafische Darstellung der Krypton-85-Gehalte in den Einzugsgebieten von Kohlungbach und Wiesenbach.

Aus dem Verlauf der ^{18}O-Gehalte ist abzuleiten, dass von Spätwinter bis Sommer nur lokal ein Zufluss einer schnell infiltrierenden Komponenten in der Auflockerungszone stattfindet. Hohe Niederschlagsmengen während Sommerniederschlägen führten allerdings flächendeckend in den gesamten Einzugsgebieten zum Zufluss einer schnell infiltrierenden Komponente in die Auflockerungszone, die an bevorzugte Fliesswege gebunden ist. Für diese Komponente wurde eine mittlere Verweilzeit von 2 bis 5 Monaten berechnet. Dabei konnte zwischen der mittleren Verweilzeit von 2 Monaten im Anstrombereich und 5 Monaten im Abstrombereich differenziert werden. Hieraus ist abzuleiten, dass der Stofftransport im Bergematerial eine Dämpfung erfährt. Der Anteil der schnell abfließenden Komponente im Oberflächenwasser schwankt in Abhängigkeit vom Witterungsgeschehen zwischen 20 und 50 %, und ist in der Auflockerungszone deutlich geringer.

4.3 Ermittlung der Grundwasserverweilzeit mittels Tritium und Krypton-85

4.3.1 Tritiumuntersuchungen

Mit dem Ziel der Altersbestimmung der Wässer wurde eine Untersuchung der Tritiumgehalte durchgeführt. Die Ergebnisse sind Abbildung 4 zu entnehmen. Die an den Grundwässern der verschiedenen Entnahmestellen analysierten Tritiumgehalte liegen in einem Bereich von 11 bis 24 TU. Für Grundwasserproben mit ^{3}H-Gehalten deutlich über 15 TU lässt sich mit dem Programm unter Annahme des Exponential-Modells mit Hilfe von MULTIS (RICHTER 1995) eine Mittlere Verweilzeit (MVZ) im Bereich von 10 bis 20 a berechnen. Alle Grundwasserproben mit ^{3}H-Gehalten unter 15 TU sind vermutlich jünger als 5-10 Jahre. Hydrogeologisch gesehen handelt es sich um einen Klufttransport.

4.3.2 Krypton-85

Das Edelgasisotop Krypton-85 (^{85}Kr, Halbwertszeit 10,8 Jahre) stammt hauptsächlich aus kerntechnischen Anlagen. Der Konzentrationsverlauf von ^{85}Kr in der Atmosphäre ist wegen des weltweit zunehmenden Kernbrennstoffverbrauchs seit Mitte der 50er Jahre monoton steigend. Die Aktivität von ^{85}Kr liegt derzeit bei ca. 90 dpm/mlKr (Kernzerfälle pro Minute und ml Krypton). Krypton löst sich im Niederschlagswasser und wird durch dieses in das Grundwasser eingetragen. Da der Input von ^{85}Kr gut bekannt ist und keine größeren regionalen Unterschiede auftreten, kann aus der Aktivität von ^{85}Kr in Grundwasserproben eine eindeutige Al-

tersangabe bzw. Aussage über die Verweilzeit des beprobten Grundwassers gemacht werden.

Liegen komplexere Grundwassersysteme vor, die sich aus Mischungen von Grundwasserkomponenten verschiedener Alter zusammensetzen, liefert die Bestimmung des ^{85}Kr-Gehaltes wegen der Eindeutigkeit des Inputverlaufes genaue Informationen über die Verweilzeit des Grundwassers bzw. seiner Komponenten.

Die ^{85}Kr-Gehalte der untersuchten Proben lagen im Bereich von 70 dpm/mlKr. und sind den aktuellen Eintragswerten zur Zeit der Probenahme vergleichbar (vgl. Abbildung 5). Dieser Messwert gibt einen Hinweis auf Grundwasser, welches unmittelbar aus den Niederschlägen neu gebildet wird. Aus den ^{3}H- Gehalten wurde unter Annahme des Exponential-Modells eine Mittlere Verweilzeit von etwa 15 Jahren berechnet. Aufgrund der vorliegenden Abweichung der Mittleren Verweilzeit, die über ^{85}Kr bzw. ^{3}H ermittelt wurde, muss davon ausgegangen werden, dass unterschiedliche Eintragsprozesse von Krypton-85 und von Tritium in das Grundwasser eine Rolle spielen. Derartige Vorgänge sind möglich, wenn eine mächtige ungesättigte Zone vorhanden ist, so dass sich aufgrund der langsamen Versickerung des Niederschlags ein zeitlicher Unterschied zwischen dem ^{3}H-Alter (Nullpunkt zu Beginn der Versickerung) und dem ^{85}Kr-Alter (Nullpunkt beim letzten Kontakt des Sickerwassers mit atmosphärischer Luft an der Basis der ungesättigten Zone) einstellt. Dies bedeutet für das Untersuchungsgebiet, dass im Haldenbereich, also oberstromig der untersuchten GWM ein Gasaustausch von Atmosphäre und Grundwasser möglich ist. Als Konsequenz für Stoffumsetzungsprozesse bedeutet dies, dass in der Halde aerobe Prozesse ablaufen.

5 Untersuchung spezieller Einzugsgebietseigenschaften

5.1 Hydrochemische Charakterisierung

Die untersuchten Grund- und Oberflächenwässer sind dem HCO_3-SO_4-Typ zuzuordnen. Entsprechend den im Gestein vorkommenden HCO_3-Gehalten werden die Wässer durch neutrale pH-Werte charakterisiert. Diese wirken auch puffernd gegenüber Versauerung, die im Waldeinzugsgebiet des Kohlungbaches zu verzeichnen ist. Die natürliche Mineralisation liegt bei etwa 0,4 mS/cm. Kontaminanten, die durch das Bergmaterial im Einzugsgebiet emittiert werden, sind Uran (0,8-2,5 mg/L) und Arsen (28-270 µg/L). Diese werden über die Oberflächenwässer und die Kluft-Wasserwegsamkeiten der Grundwässer transportiert.

5.2 Ergebnisse der Gehalte von Schwefel-34 und Sauerstoff-18 am Sulfat

Die Untersuchung der ^{34}S-Gehalte am Schwefel und am Sulfat werden für die Herkunftsbestimmung der im Wasser gelösten S-Komponenten eingesetzt. Die zusätzliche Bestimmung der ^{18}O-Isotopengehalte am Sulfat ermöglicht eine bessere Differenzierung der Sulfatquellen und erlaubt die Kontrolle von im Schwefelkreislauf ablaufenden Redoxreaktionen. Bei der Oxidation von Pyriten bzw. den damit immer vergesellschafteten, anderen metallhaltigen Sulfidmineralen werden beträchtliche Mengen an Säure gebildet. Diese führen bei der Erschöpfung des Puffervermögens karbonathaltiger Gesteine oder von Tonmineralien zur Versauerung von Haldensickerwässern und damit zur Mobilisierung der meisten Schwermetalle. Aufgrund der im neutralen Bereich liegenden pH-Werte der Sickerwässer sind die meisten Metalle bis auf z.B. Arsen immobil und werden nicht mit den Sickerwässern ausgetragen.

Ziele der Untersuchung war es, Aussagen zur Versauerungsproblematik bzw. Hinweise auf Reaktionsmechanismus der Pyritoxidation abzuleiten damit einen Beitrag zu einem besseren Verständnis der stattfinden hydrochemischen Reaktionen zu leisten. Des Weiteren sollte eine Charakterisierung der vorkommenden Schwefelverbindungen vorgenommen werden. Zur Charakterisierung der im Haldenkörper vorkommenden Schwefelverbindungen wurden die ^{34}S- und ^{18}O -Isotopengehalte am Sulfat in Sickerwasseraustritten sowie Bohrkernproben aus dem Bereich der Halde bestimmt. Die Ergebnisse sind in Abbildung 6 dargestellt.

Die analysierten Isotopengehalte des Schwefels aus den Bohrungen überstreichen einen Wertebereich von -6,2 bis +4,2 ‰ , der typisch für Pyrite/ Metallsulfide ist. Die im Sickerwasser gelösten Sulfate zeigen den gleichen ^{34}S -Wertebereich ($\delta^{34}S_{so4}$: -2,2 bis 2,0 ‰ $\delta^{18}O_{so4}$ -6,2 bis -2,0 ‰). Hieraus kann abgeleitet werden, dass die Schwefelverbindungen des analysierten Bohrguts auch die Quellen der gelösten Sulfate sind. Da das in den Sickerwässern analysierte Sulfat durch Oxi-

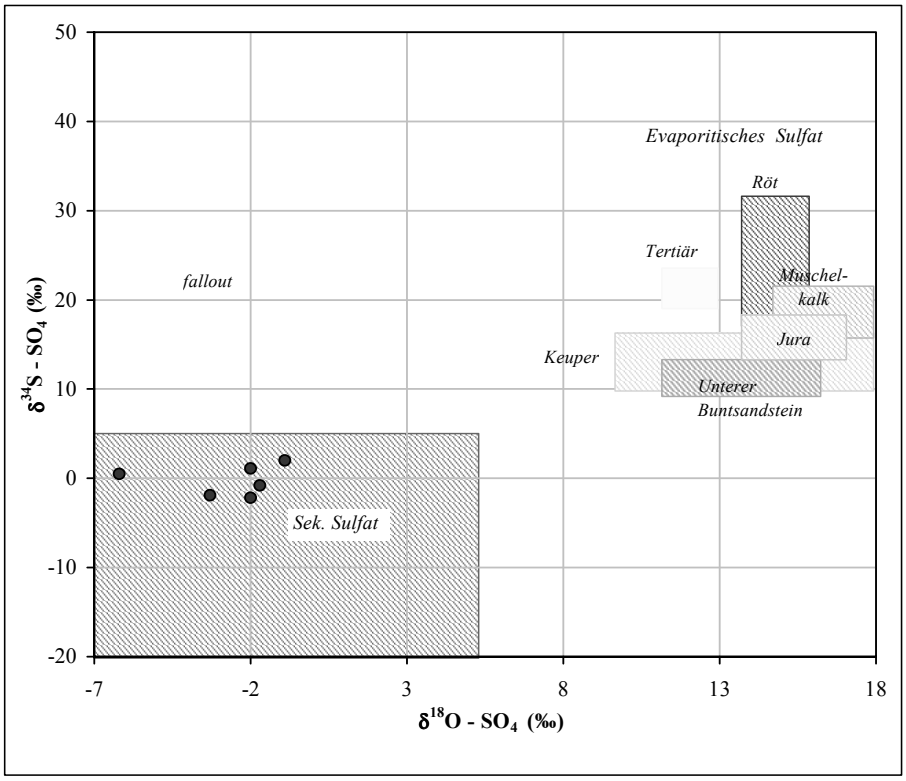

Abb. 6: Grafische Darstellung der Schwefelisotopengehalte in den Einzugsgebieten von Kohlungbach und Wiesenbach.

dationsreaktionen gebildet wurde, kann die sich bildende Säuremenge aus den Sulfatgehalten über die stöchiometrischen Reaktionsgleichungen abgeschätzt werden. Darüber hinaus gibt die gebildete Sulfatmenge Aufschluss über die tatsächliche Reaktionsgeschwindigkeit. Die Untersuchungen zum Reaktionsmechanismus geben den Hinweis auf einen vorwiegend abiotischen, oberflächenkatalytischen Mechanismus der Oxidation der Sulfide. Die sich bildende Säuremenge wird durch den Karbonatgehalt in der Halde abgepuffert, wodurch die meisten Schwermetalle immobilisiert werden.

5.3 Ergebnisse der Untersuchung von Stickstoff-15 und Sauerstoff-18 am Nitrat

Die Wässer im abstromigen Teil des Einzugsgebietes weisen zeitweise hohe Nitratgehalte auf, so dass sich die Frage nach der Quelle der Nitratgehalte stellte. Für die Herkunft von Ammonium- und Nitratgehalten in Wasserproben bildet die Stickstoff- und Sauerstoffisotopensignatur einen Quellenindikator. Mögliche Nitratquellen in den Untersuchungsgebieten sind:

- Nitrat aus organischer oder mineralischer Düngung (landwirtschaftliche Nutzflächen)
- Nitrat aus den forstwirtschaftlich genutzten Waldflächen
- Nitrat aus dem Niederschlag
- Ammonium/Nitrat aus den auf der Halde abgelagerten Kompost

Die Bestimmung der ^{18}O-Gehalte am Nitrat ermöglicht die Identifizierung von Nitrat aus Mineraldünger, aus den Niederschlägen und von Nitrat, welches durch Nitrifikation gebildet wurde. Eine weitere Differenzierung/Identifizierung von Nitratquellen ergibt sich über die zusätzliche Analyse der ^{15}N-Isotopengehalte. Diese gibt Aufschluss über die Herkunft von Nitrat, das durch Nitrifikation aus Mineraldünger, organischem Dünger bzw. Streu gebildet wurde.

Bei der Auswahl der Entnahmestellen wurden die in Frage kommenden Nitratquellen erfasst, deren Isotopensignatur bestimmt und diese mit der Signatur der Wässer im Abstrom des Einzugsgebietes verglichen. Die beprobten Nitratquellen waren die Messpunkte MP 067 (Wasser aus Waldeinzugsgebiet) und MP 194 (Wasser aus landwirtschaftlichen Nutzflächen). Die im

Tab. 1: $\delta^{15}N_{NO3}$ und $\delta^{18}O_{NO3}$–Werte am Nitrat der Wässer der Einzugsgebiete von Kohlungbach und Wiesenbach [Angabe der Messwerte im relativen Vergleich zum Internationalen Standard (AIR / SMOW) in der δ-Notation].

Messpunkt	**$\delta^{15}N_{NO3}$ [‰]**	**$\delta^{18}O_{NO3}$ [‰]**	**NO_3 [mg/l]**
Proben möglicher Nitrat-Quellen			
MP 194 (Landwirtschaft)	6,7	9,5	43,4
MP 067 (Forst)	1,0	44,7	5,2
Auslauf Kompost			1
Proben aus dem Abstrom			
MP 058	8,8	29,2	36
MP 113	9,1	28,1	37,2

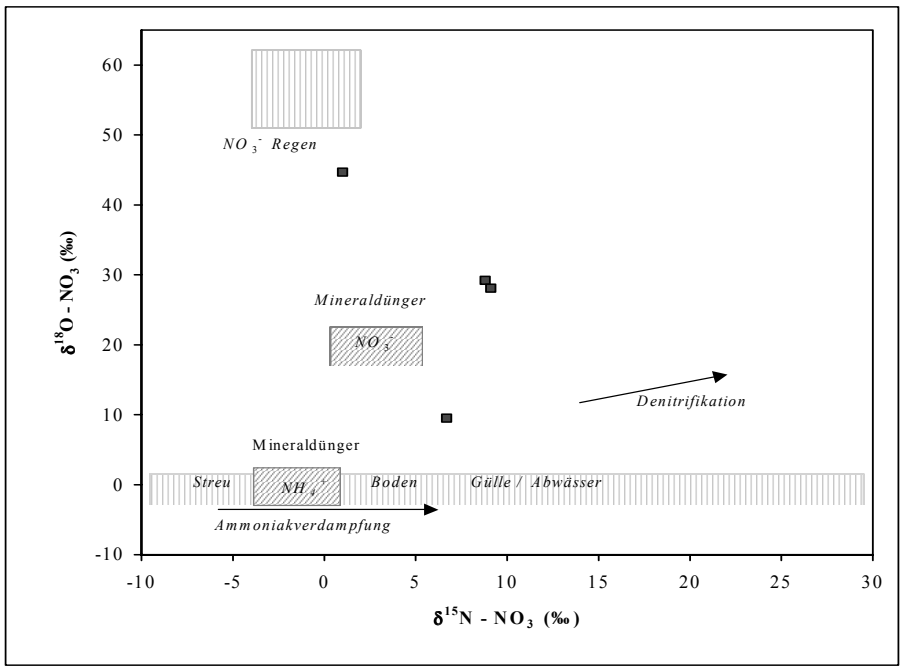

Abb.7: Grafische Darstellung der Nitratisotopengehalte in den Einzugsgebieten von Kohlungbach und Wiesenbach.

Abstrombereich beprobten Messstellen der Einzugsgebiete waren die Messpunkte MP 058 (Kohlungbach) und MP 113 (Wiesenbach). Die Ergebnisse sind in Tabelle 1 und Abbildung 7 dargestellt.

Die Ergebnisse zeigen für das Nitrat der Messstelle MP 067 (Forst) typische niedrige Werte für forstlich genutzte Einzugsgebiete und eine relative Nähe zu typischen Werten des Niederschlages. Hier spiegelt sich wider, dass Bäume durch die Auskämmung des Nitrates aus dem Niederschlag eine Erhöhung der Nitratgehalte bewirken können (SCHNEIDER et al. 2003). Die Signatur des Nitrats der Messstelle MP 194 ist typisch für Nitrat aus der Landwirtschaft mit einem hohem Anteil an organischem Dünger. Die Probe der Kompostflächen wies nur einen Nitratgehalt von 1 mg auf, weshalb die Bestimmung der Isotopengehalte nicht möglich war. Mögliche reduktive/denitrifizierende Prozesse spielen keine entscheidende Rolle. Daher bleibt die Isotopensignatur der Ausgangsquellen erhalten. Die Nitratgehalte im Abfluss zeigen dass eine Mischquelle vorliegt (aus Nitrat aus landwirtschaftlichen Bereich, Nitrat aus Niederschlägen). Somit findet keine sekundäre Erhöhung der Stickstoff- und Sauerstoffisotopengehalte durch die Kompostflächen statt.

6 Zusammenfassung der Ergebnisse

Die Ergebnisse der Isotopenuntersuchungen haben wesentliche Beiträge zum Systemverständnis der hydrologischen Prozesse in den Einzugsgebieten von Kohlungbach und Wiesenbach geliefert. Die aus den Isotopengehaltsmessungen ermittelten Ergebnisse und Interpretationen lassen

sich schwerpunktmäßig folgendermaßen zusammenfassen:

- anhand der isotopenhydrologischen Untersuchungen ist eine Klassifizierung bzw. Unterscheidung der Grund- und Sickerwässer entsprechend ihrer Herkunft möglich,
- die mittleren Verweilzeiten der Grundwässer in der Auflockerungszone liegen im Einzugsgebiet des Kohlungbaches zwischen 10 und 20 Jahren,
- nach Starkregenperioden ist der Eintritt von Sickerwasser durch den grundwasserhemmenden Verwitterungslehm in die Auflockerungszone möglich, wobei der Zustrom dieser jüngeren Komponente über den Zeitbereich von etwa zwei Monaten erfolgt,
- die am Haldenfuß austretenden Sickerwässer bilden ein Mischsystem (schnell infiltrierende Komponente und Grundwasser) und haben eine mittlere Verweilzeit im Bergematerial von zwei bis fünf Jahren,
- Niederschlagsereignisse lösen eine schnell infiltrierende Komponente im Bergematerial aus, deren mittlere Verweilzeit mit etwa zwei Monaten angegeben werden kann,
- aufgrund der vorliegenden Abweichung der Mittleren Verweilzeit, die über ^{85}Kr bzw. ^{3}H ermittelt wurde, muss davon ausgegangen werden, dass Bereiche der über dem Grundwasser liegenden ungesättigten Zone im Austausch mit der Atmosphäre stehen,
- aus der Bestimmung der Schwefelisotopengehalte der Haldensickerwässer kann abgeleitet werden, dass die Quelle des in den Wässern gelösten Sulfates ausschließlich auf die Verwitterung und Oxidation der im Haldenmaterial enthaltenen Metall-Sulfide zurückzuführen ist,
- reduktiv-denitrifizierende Prozesse finden wenn überhaupt, nur in geringem Umfang statt. Die Isotopensignatur der ursprünglichen Nitratquellen bleibt weitgehend erhalten und es ist nicht mit einer sekundären Erhöhung der Stickstoff- und Sauerstoffisotopengehalte zu rechnen.

Auf der Basis der ermittelten Fliesskomponenten mit verschiedenen Verweilzeiten und deren Jahreszeitabhängigkeit konnten Mischungsanteile berechnet, Fliesswege erkannt sowie die abfließenden Mengen bilanziert werden. Darüber waren wesentliche Beiträge zur Bilanzierung des Stofftransportes möglich.

Quellen

KENDALL, C., & MCDONNELL, J.J. (eds.): Isotope Tracers in Catchment Hydrology: Amsterdam, Elsevier, p. 611-646.

MEYER, J., JENK, U., SCHUPPAN, W. & KNAPPIK, R. (1998): Hydrogeochemical Aspects of the Aue pit Flooding. In: Merkel B, Helling C (eds.): Uranium-Mining and Hydrogeology, Ge-oCongress II, S. 124-129, Verlag Sven von Loga, Köln.

OSENBRÜCK, K., VOERKELIUS, S. & SCHNEIDER, P. (2000): Einsatz von Isotopenuntersuchun-gen zur unabhängigen Validierung hydrologischer und hydrochemischer Modellvorstellungen für die Erarbeitung von Monitoringkonzepten. In: Tagungsband „Internationale Konferenz Bergbausanierung - Technologien, Strategien, Revitalisierung“, Wismut GmbH, Schlema, Juli 2000.

REINCKE, H., HURST, S. & SCHNEIDER, P. (2002): Strategy Concept Elbe, in: Merkel B.J.; Planer-Friedrich, B.; Wolkersdorfer, C: Uranium in the Aquatic Environment, pp. 41-48, Springer Verlag.

RICHTER, J. & SZYMCZAK, P. (1995): MULTIS – ein Computerprogramm zur Auswertung isotopenhydrologischer Daten auf der Grundlage gekoppelter konzeptioneller Boxmodelle, Veröffentlichung der TU Bergakademie Freiberg, Lehrstuhl für Hydrogeologie.

SCHNEIDER, P., VOERKELIUS, S., OSENBRÜCK, K. & MEYER, J. (2002): Radioactive Contaminant Transport of Aue Mine Dump 371: A Geochemical and Isotopic Case Study, in: Merkel B.J.; Planer-Friedrich, B.; Wolkersdorfer, C: Uranium in the Aquatic Environment, pp. 841-847, Springer Verlag.

SCHNEIDER, P., NEITZEL, P., SCHAFFRATH, M. & SCHLUMPRECHT, H. (2003): Leitbildorientierte physikalisch-chemische Gewässerbewertung - Referenzbedingungen und Qualitätsziele, UBA Texte 15/03, Forschungsbericht 200 24 226, UBA-FB 000322, ISSN 0722-186X.

Hydraulic characteristics of constructed wetlands evaluated by means of tracer tests

Przemyslaw Wachniew[1], Piotr Czuprynski[1], Piotr Maloszewski[2],

[1]AGH University of Mining and Metallurgy, Mickiewicza 30, 30-059Krakow, Poland; wachniew@ftj.agh.edu.pl [2]GSF-Institute of Hydrology, Neuherberg, Germany

Use of tracers and mathematical modelling for evaluation of hydraulic characteristics of constructed wetlands is presented for two case studies representing two most common in Poland types of treatment wetlands: subsurface-flow system with *Phragmites* in Nowa Slupia *australis* and *Lemna* pond in Mniow. Instantaneously injected bromide and tritium were used to obtain residence time distributions (RTD) of wastewater in those wetlands. Flow components were identified and their hydraulic characteristics were derived from RTDs by fitting of the analytical solution of one-dimensional advection-dispersion equation to the experimental data.

1 Introduction

Knowledge of hydraulic properties is a prerequisite for studies of constructed wetlands functioning (WACHNIEW & ROZANSKI 2002). Hydraulic processes influence contaminant removal in wetlands in many ways and some aspects of these relationships remain undescribed. Efficiency of contaminant removal in wetlands is primarily related to the extent of contact between wastewaters and the reactive surfaces (substratum, plants, detritus) on which purification processes occur. Zones of stagnant flow as well as preferential and bypassing flows limit the opportunity for this contact. Apparent dispersion of solutes in wetlands is connected with various mixing and transport phenomena which can also influence wetland performance through redistribution of contaminants, oxygen and other gases and heat. In sub-surface flow systems mixing is related to physical phenomena that are specific for flow in porous medium while in ponds mixing is due to heat and momentum transfer and water density changes. Tracer technique is a valuable tool used to gain insight into wastewater flow phenomena in constructed wetlands. Examples of use of tracers to study hydraulics of constructed wetlands concern: mixing in wetlands (KADLEC 1994), influence of substratum clogging on transit times in gravel cells (TANNER ET AL. 1998), influence of pond properties on flow patterns (NAMECHE & VASEL 1998), testing of flow models (WERNER & KADLEC 2000). Residence time distribution (RTD) obtained as a breakthrough curve of a non-reactive tracer carries synthetic information on wetland hydraulic properties. Quantitative wetland characteristics are derived with help of an assumed model of wastewater flow. Use of tracers in studies of constructed wetlands is generally discussed by WACHNIEW & ROZANSKI (2002) and this work presents evaluation of hydraulic properties based on RTDs obtained in case studies representing two most commonly applied in Poland types of constructed wetlands: subsurface flow (SSF) systems and free water surface systems (FWS). The former type is represented by a gravel bed with common reed and the latter by a duckweed pond.

2 Study sites

2.1 Nowa Slupia

The constructed wetland system is located in the region of the Holy Cross Mountains (21°05' E - 50°52' N) at 250 m a. s. l. with an annual mean temperature of 8 ^{o}C and annual precipitation of 700 mm. It was built in 1995 in order to treat municipal wastewaters from both the Nowa Slupia sewage system and from septic tanks that are not connected to the sewage system. The wetland serves about 1500 inhabitants. The designed average diurnal flow rate to this system is 325 m^3/l and peak diurnal flow rate is 449 m^3/l.

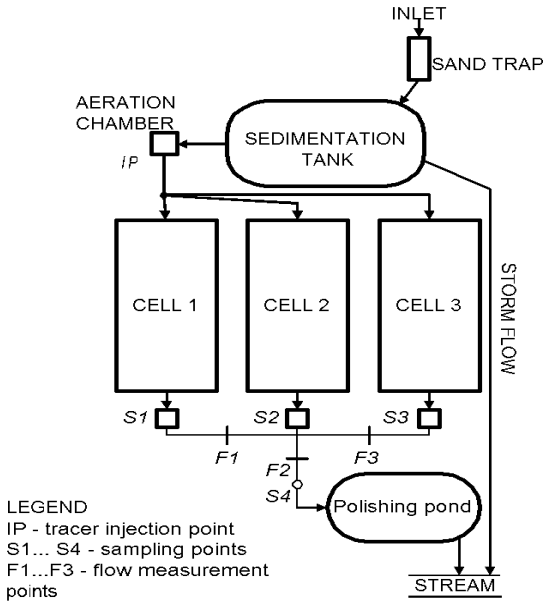

Figure 1: Constructed wetland system in Nowa Slupia.

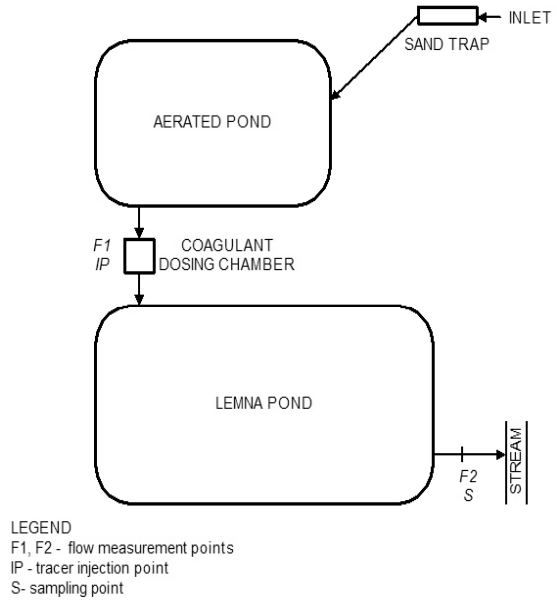

Figure 2: Wastewater treatment system in Mniow.

This subsurface horizontal flow system consists of three parallel gravel cells (78 m x 24 m x 1.2 m each), overgrown with common reed (*Phragmites australis*). Wastewaters are distributed across the width of each cell through perforated pipes. The cells have slope of 1% and are lined with 1 mm polyethylene. The wetland is flooded every spring to prevent growth of plant species other than *Phragmites australis*. The reeds are not harvested after the vegetation period. A sedimentation pond and an aeration tank provide primary treatment. Polishing pond (volume of 750 m^3) is used as a final treatment stage. Diagram of Nowa Slupia constructed wetland showing points of discharge measurements, tracer injections and sampling is presented in Fig. 1.

2.2 Mniow

The wastewater treatment plant is located west of the Holy Cross Mountains (20°29' E - 51°01' N) at 264 m a. s. l. with an annual mean temperature of 8 °C and annual precipitation of 700 mm. It was built in 1993 in order to treat municipal wastewaters from both the Nowa Slupia sewage system and from septic tanks that are not connected to the sewage system. The designed average diurnal flow rate of this system is 150 m^3/l and peak diurnal flow rate is 200 m^3/l. The treatment system consists of two ponds in series. First pond is aerated, second pond is free water surface constructed wetland with free-floating plants of the *Lemnaceae* family. The aerated pond and the duckweed pond have areas of 0.2 ha and 0.26 ha and depths of 3 m and 2.4 m, respectively. Floating plastic barriers are used in the second pond for control of duckweed. In order to remove phosphorous, especially in winter period, coagulant dosing chamber was constructed between the two ponds. Wastewaters leave the chamber through a pipe whose outlet is below the water surface in the duckweed pond. Diagram of Mniów wastewater treatment plant showing points of discharge measurements, tracer injection and sampling is presented in Fig. 2.

3 Tracer tests and estimation of hydraulic characteristics

Bromide ions (Br^-) injected in form of KBr solution were used as a tracer in all tests. In two cases tritium was used simultaneously with Br^-. Bromide is a commonly used tracer of water flow in environmental studies, including studies of constructed wetlands (WACHNIEW & ROZANSKI 2002) but there is some evidence of its non-conservative behaviour in wetland environment. Some studies suggest that bromide is taken up by plants (KUNG 1990; WHITMER et al. 2000). The question of bromide conservativity was addressed in this study by simultaneous use of bromide and tritium what allowed for comparison of their behaviour in the studied wetlands (see discussion below). Tritium constitutes a part of water molecule and as such is an ideal tracer of water flow. Tritiated water is generally not taken up selectively in any of physical, chemical

Table 1: Characterisitics of tracer tests in Nowa Slupia wetland.

Test	Amount of KBr (Br-) in kg	Average outflow from cells (1; 2; 3) in l/s	Test duration in hours	Number of samples from each cell
I - July 2001	30.0 (20.2)	1.6; 1.2; 1.4	94	36
II - November 2001	24.9 (16.7)	0.8; 0.6; 0.4	369	45; 45; 47
III – June - July 2002	24.0 (16.1) 25 mCi of ^3H	0.9; 0.7; 0.3	1013	39; 39; 38 50; 51; 53 (^3H)

Table 2: Characteristics of tracer tests in Mniow wetland.

Test	Amount of KBr (Br-) in kg	Average outflow in l/s	Test duration in days	Number of samples from each cell
I – June -September 2001	20.1 (13.5)	3.0	74	52
II – June - October 2002	24.9 (16.7) 25 mCi of ^3H	3.4	111	37 46 (^3H)

and biological processes that occur in wetlands. It is lost from wetland through the evapotranspirative pathway but tritium fractionation associated with this process is negligible. Bromide tracer was injected after dissolution of KBr in 80 l of wastewaters. This volume was necessary to completely dissolve required amounts of KBr. Due to low flow rates and technical difficulties injection of this amount of tracer solution in a strictly instantaneous manner was not possible. Injections were completed over 10 minutes in Nowa Slupia and 30 minutes in Mniow wetland. Given water transit times in both wetlands (see below) this mode of injection can be considered as practically instantaneous. The effluent was collected manually and discharges were measured at the same time by means of a calibrated vessel and stopwatch. Samples were collected to 0.2 l plastic bottles and stored in ambient temperatures.

Bromide concentrations in effluent samples were determined in the laboratory by use of bromide ion selective electrode with AgBr/AgS membrane (WTW Br 501), reference Ag/AgCl electrode (WTW R 502) and temperature probe (WTW TFK 325/HC). Electromotive forces and solution temperatures were measured by pH/mV meter (WTW pH 340/ION-SET). Calibration of the electrode with solutions containing known concentrations of bromide was not possible because of different ionic compositions of wastewaters and standard solutions and because of the presence of interfering ions in wastewaters (e. g. NH_4, HS^-, Cl^-). $Ni(NO_3)_2$ solution was added before measurements to remove sulphide ions from samples. The double standard addition method (CAMMANN 1973) was applied to derive bromide concentrations from electromotive force measurements. In this method electromotive force is measured three times: firstly for the sample with unknown concentration of Br- and then after each of two additions of a standard solution containing known concentration of bromide. Concentrations of bromide were calculated on the basis of the Nernst equation. Reproducibility of the method was 15% for background concentrations of bromide (ca. 0,8 mg/l) and less than 2% for concentration of bromide at the peak of breakthrough curves (ca. 25 mg/l). Tritium activities were measured by liquid scintillation spectrometry following standard procedures.

3.1 Nowa Slupia

Three tracer tests were performed in July 2001, November 2001 and June-July 2002. Bromide was used in all tests and in June 2002 tritium was injected simultaneously with bromide. Tracers were injected through the outflow pipe from the aeration chamber (IP in Fig. 1). Discharges were measured during all tests at points F1, F2, F3 (Fig. 1). Flow rates measured at points F1 and F3 corresponded directly to discharges from the respective cells. Discharge from cell 2 was calculated by subtraction of discharges from cells 1 and 3 from the total flow rate measured at point F2. In July 2001 only composite samples of the effluent were collected at point S4 (Fig. 1). Those samples represented the total outflow from the wetland. During two other tests effluents from each cell were sampled at points S1, S2 and S3. Table 1 presents information on amounts of injected tracers, average discharges, tests duration and sampling frequency.

Table 3: Hydraulic characteristics of Nowa Slupia wetland based on results of July 2001 tracer test.

flow component	mean transit time [h]	dispersion parameter	water volume [m^3]
I	25	0.03	95
II	40	0.02	175
III	74	0.02	635

Table 4: Hydraulic characteristics of Nowa Slupia wetland cells based on results of November 2001 and June – July 2002 tracer tests.

November 2001				June - July 2002		
Mean transit time [h]	dispersion parameter	water volume [m^3]		mean transit time [h]	dispersion parameter	water volume [m^3]
65	0.17	95	Cell 1	71	0.06	130
177	0.05	140	components	156	0.04	95
339	0.01	190		390	0.07	200
69	0.12	65	Cell 2	82	0.09	65
156	0.05	150	components	244	0.06	245
339	0.01	140		709	0.04	530
98	0.18	70	Cell 3	43	0.06	10
195	0.04	55	components	130	0.08	55
325	0.01	110		520	0.15	355

3.2 Mniow

Two tracer tests were performed in June - August 2001 and June – September 2002. Bromide was used in all tests and in June 2002 tritium was injected simultaneously with bromide. Tracers were injected into the coagulant dosing chamber (IP). Flow rates were measured at inlet and outlet at points F1 (inlet) and F2 (outlet). Discharges, water level in the pond and precipitation were measured daily in the morning. Table 2. presents information on amounts of injected tracers, average flow rates at outflow, tests duration and sampling frequency.

3.3 Estimation of hydraulic characteristics

Analyses of the obtained RTDs were based on an assumption that transport of wastewaters in both systems can be described by one-dimensional advection-dispersion equation. Solution of this equation in case of instantaneous injection and detection in fluid flux is given by the following equation (KREFT & ZUBER 1978):

$$C(x,t) = \frac{A}{Q}\frac{x}{\sqrt{4\pi D t^3}}\exp\left[-\frac{(x-Ut)^2}{4Dt}\right] \qquad (1)$$

where: C - tracer concentration, A – amount of tracer, Q – discharge, x - distance from injection point, D- dispersion coefficient, t - time from injection and U – mean water velocity. RTDs obtained in tracer tests correspond to solution (1) for a fixed distance from injection point corresponding to the sampling point. Preliminary values of mean transit time of tracer $\tau = x/U$ and dispersion parameter $P_D=D/Ux$ are calculated for the outlet point by the method of moments. These estimates are used as starting values for the fitting procedure by which equation (1) is iteratively fitted to the experimental RTD. Finally the procedure gives values of: τ, U, P_D and volume of mobile water in the system $V_m = \tau Q$ which can be compared to the nominal volume of water in the system in order to check for the occurrence of zones of stagnant flow.

4 Results and discussion

4.1 Nowa Slupia

Tracer recoveries calculated for each cell are roughly proportional to the respective discharges so the three flow components can be identified with separate cells. Components I, II and III correspond to cells 3, 2 and 1, respectively. Total volume of mobile water in the wetland is 905 m^3 what corresponds to 13% of the total wetland volume.

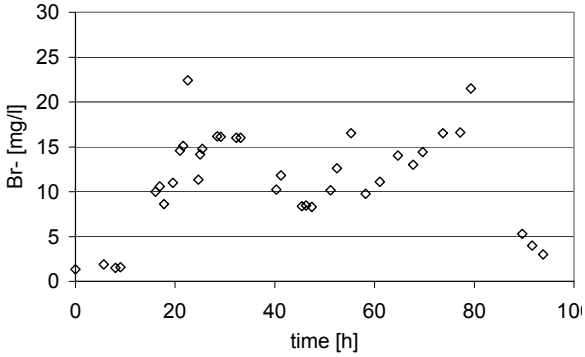

Figure 3: Bromide concentrations in outflow from Nowa Slupia wetland, July 2001.

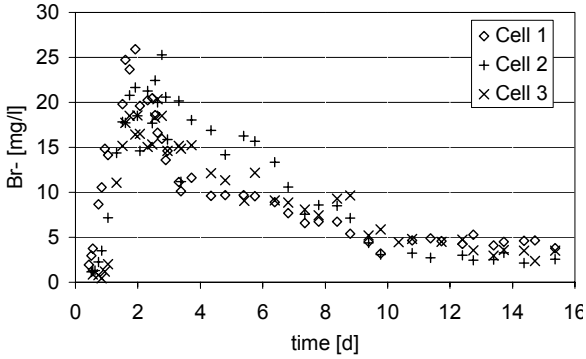

Figure 4: Bromide concentrations in outflow from Nowa Slupia wetland, November 2001.

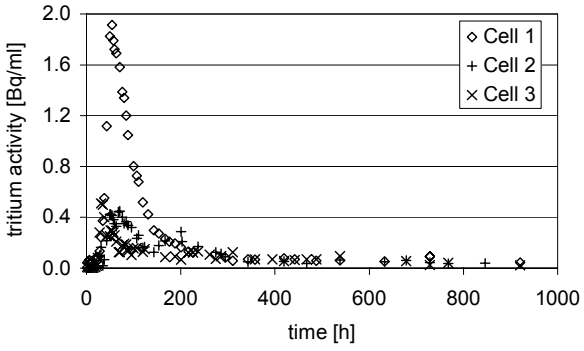

Figure 5: Tritium activities in outflow from Nowa Slupia wetland, June 2002.

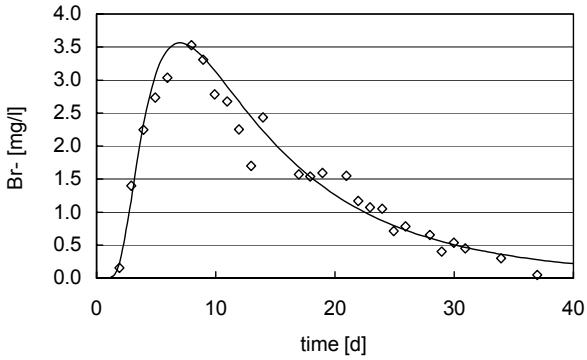

Figure 6: Bromide concentrations in outflow from Mniow wetland and the fitted curve, June – August 2001.

Figs 4 and 5 show breakthrough curves obtained separately for each cell in November 2001 and June – July 2002, respectively. Shapes of curves in Fig. 4 suggest that they might be a superposition of several components. Indeed, three flow components were identified in each of RTDs by sequential fitting of equation (1). Each of RTDs obtained during the 2002 test could be also separated in three components. Table 4 summarizes hydraulic characteristics derived from RTDs obtained during these two tests. Total volumes of mobile water vary between 235 to 840 m^3 what corresponds to 3 to 12% of the total wetland volume. Tables 3 and 4 show that three identical cells of the Nowa Slupia wetland reveal significant differences in their hydraulic properties. Moreover, hydraulic properties of each wetland cell changed over one year of observations. Differences between cells might result from differences in hydraulic loadings. Visual inspection of cell surfaces in summer 2002 revealed occurrence of bypassing flows and partial inundation of cells. These unfavourable from the viewpoint of wetland performance phenomena might be caused by clogging of the substratum with organic matter (TANNER ET AL. 1998; TANNER & SUKIAS 1998) and by operation practices (intentional flooding of cells). Correspondence between the above mentioned factors and quantitative hydraulic characteristics of wetland cells is, however, not obvious and requires further examination.

Results presented in Table 4 are arithmetic means of estimates based on tritium and bromide RTDs. It must be noted that tritium and bromide breakthrough curves have the same shapes and estimates of hydraulic characteristics based on both tracers agree within 10%. These findings suggest that behaviour of bromide tracer in the environment of constructed wetlands is similar to behaviour of tritium which is considered as the ideal tracer of water flow. Close correspondence of bromide and tritium breakthrough curves proves also reliability of the applied methodology of bromide concentration measurements by use of ion selective electrode.

4.2 Mniow

Fig. 6 presents results of the first tracer test performed in Mniow wetland in June – August 2001. Bromide concentrations are plotted together with a curve fitted to them. Following hydraulic characteristics were estimated: mean transit time – 15.8 days, dispersion parameter – 0.3, volume of mobile water – 3900 m^3. Actual volume of the pond is 5100 m^3 so 24% of pond volume was not active in throughflow. Second tracer test performed in Mniow with bromide and tritium in 2002 gave very flat breakthrough curves with low peak concentrations of tracers. This unexpected response of the system resulted from density effects associated with injection of high density solution of KBr to the pond. Fig. 7 presents plots of bromide concentration in three cross-sections three weeks after injections. These plots were obtained by extrapolation of bromide concentrations measured in six depth profiles. Locations of cross-sections and depth profiles are shown in the sketch. Cross-sectional activities of tritium show very similar picture with apparent vertical stratification of tracer in cross-section A. Tritium became attached to KBr solution because both tracers were injected simultaneously after dilution in the same volume of water. Development of density effects in constructed wetland ponds is favoured by flows characterized typically by low Reynolds numbers (SCHMID ET AL. 2003). Cross sections of bromide concentration presented in Fig. 7 show also general flow pattern in the pond and indicate possible zones of stagnant flow. Surprisingly the first test in Mniow was apparently not influenced by density effects despite the fact that KBr solutions of similar densities were injected in case of both tests. In June 2001 tracer was injected during passage of an atmospheric front which brought significant drop in air temperature, rain and strong wind. The meteorological phenomena could induce vertical mixing in the pond preventing formation of stable salt solution layer.

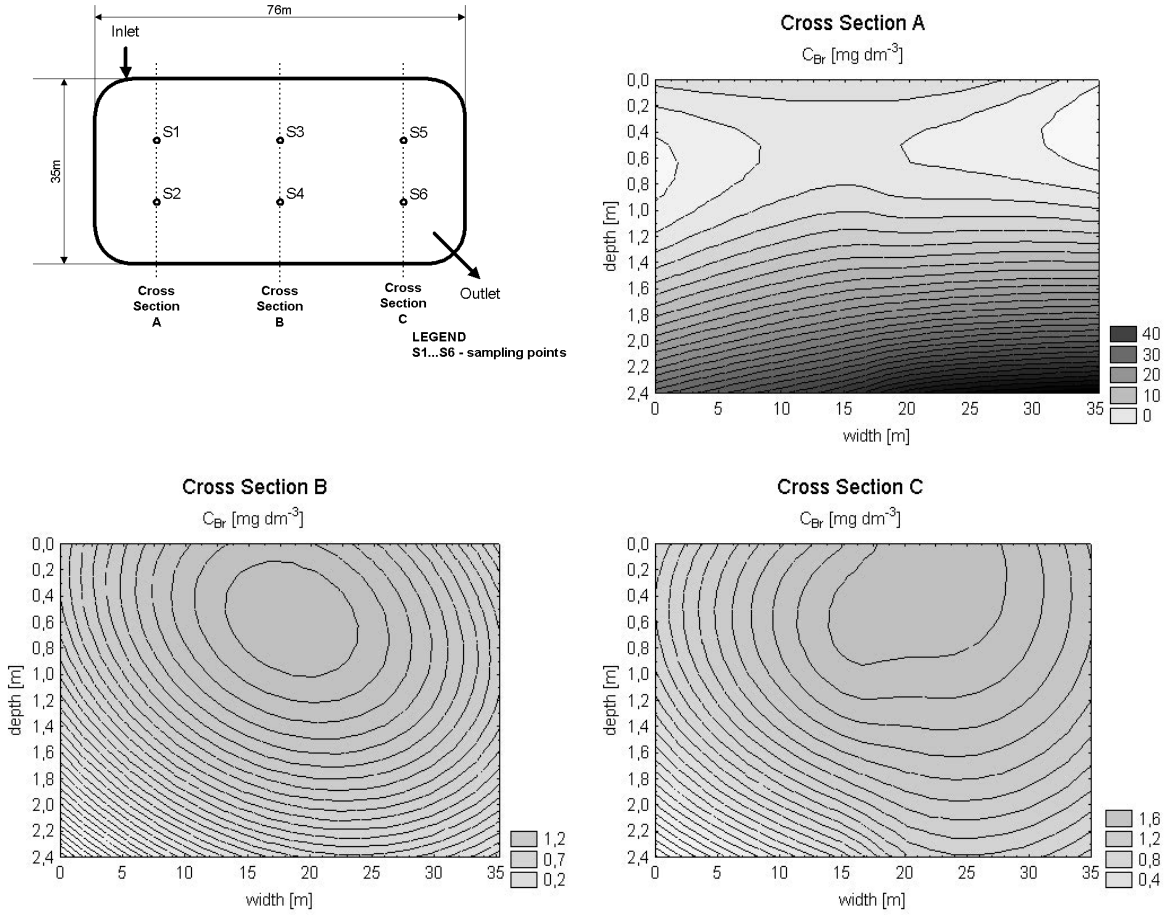

Figure 7: Bromide tracer distribution in three cross sections, Mniow, June 2002.

5 Conclusions

1. Bromide and tritium proved equally useful as tracers of wastewater flow in objects representing two types of constructed wetlands: the subsurface flow system with common reed and the free water surface system with duckweed.
2. Ion selective electrode can be used for reliable measurements of bromide concentrations in wastewaters.
3. Possibility of density effects must be considered when dissolved salts are used as tracers in ponds.
4. Wastewater flow through each of gravel cells of the Nowa Slupia wetland is apparently a superposition of three components. Their physical interpretation requires further studies.
5. Three identical cells of the constructed wetland reveal large degree of variability in quantitative hydraulic characteristics which might be related to uneven distribution of wastewaters between the cells and/or to other hydraulic phenomena like bypassing flows and inundation of cell surfaces with wastewaters.

Acknowledgments

This paper is a contribution to the project PRIMROSE within the 5th Framework Programme of Research, Technical Development and Demonstration of the European Union (project number: EVK1-CT-2000-00065).

References

CAMMANN, K. (1973): Das Arbeiten mit Ionselektiven Elektroden. Eine Einführung. Springer-Verlag Berlin, Heidelberg.

DOREGO, N.C. & LEDUC, R. (1996): Characterization of hydraulic flow patterns in facultative aerated lagoons. *Wat. Sci. Tech.*, 34, 99-106.

KADLEC, R.H. (1994): Detention and mixing in free water wetlands. *Ecol. Engng.*, 3, 345-380.

KING, A.C., MITCHELL, C.A. & HOWES, T. (1997): Hydraulic tracer studies in a pilot scale subsurface flow constructed wetland. *Wat. Sci. Tech.*, 35, 189-196.

KREFT, A. & ZUBER, A. (1978): On the physical meaning of the dispersion equation and its solutions for different initial and boundary conditions. *Chem. Eng. Sci.*, 33, 1471-1480.

KUNG, K.J.-S. (1990): Influence of plant uptake on the performance of bromide tracer. *Soil. Sci. Soc. Am. J.*, 54, 975-979.

NAMECHE, TH. & VASSEL, J.L. (1998): Hydrodynamic studies and modelization for aerated lagoons and waste stabilization ponds. *Wat. Res.*, 32, 3039-3045.

SCHMID, B.H., HENGL, M. & STEPHAN, U. (2003): Kriterien zur Beurteilung der Schichtungsneigung bei Markierversuchen in Oberflächengewäwassern. *Österr. Wasser- und Abfallwirtschaft*, 55, 19-26.

TANNER, C.C., SUKIAS, J. P. S. & UPSDELL, M. P. (1998): Organic matter accumulation during maturation of gravel-beds constructed wetlands treating farm dairy wastewaters. *Wat. Res.*, 32, 3046-3054.

TANNER, C.C. & SUKIAS, J.P.S. (1998): Accumulation of organic solids in gravel-bed constructed wetlands. *Wat. Sci. Tech.*, 32, 229-239.

WACHNIEW, P. & ROZANSKI, K. (2002): Tracers and isotopes in constructed wetland studies. *Wissenschaftliche Mitteilungen*. Technische Universitaet Bergakademie Freiberg, 19, 19-23.

WERNER, T.M. & KADLEC, R.H. (2000): Wetland residence time distribution modelling. *Ecol. Engng.*, 15, 77-90.

WHITMER, S., BAKER, L. & WASS, R. (2000): Loss of bromide in a wetland tracer experiment. *J. Environ. Qual.*, 29, 2043-2045.


BERGAKADEMIE
TECHNISCHE
UNIVERSITÄT
FREIBERG

Trace Elements in the Waters of Troy

Christian Wolkersdorfer, Claudia Blume, Claudia Weber

TU Bergakademie Freiberg, Lehrstuhl für Hydrogeologie, Gustav-Zeuner-Str. 12, 09596 Freiberg/Sachsen, E-Mail: c.wolke@web.de

Hydrogeological investigations were conducted within the Historical National Park Troia in northwestern Anatolia (Turkey). 131 springs, wells, caves, and surface waters have been sampled and 44 representative samples were analyzed in the laboratory. It was possible to deduce three water types which differ in their main ions and especially in conductivity. Some trace elements and main parameters in waters used for drinking exceed the EU standards which might need future actions. No clear indication for the source of the water in the Troyan spring cave and for the other waters in the area investigated could be found by now, which might be due to a lack of geological information.

1 Introduction

Troy (Troia, Troja, Truva, Illios, Illium) in Western Anatolia (Turkey) belongs to the most intensively investigated archaeological sites in the world. Since the time of Heinrich Schliemann, though not being the first one who excavated at the site, four archaeological teams excavated Troy and in 1988 Manfred Korfmann of Tübingen University and Brian Rose of Cincinnati University started the latest period of investigations. Besides the archaeological investigations, natural sciences were always an integral part of the research at the Hisarlık hill, were Troy is located (ARCHÄOLOGISCHES LANDESMUSEUM BADEN-WÜRTTEMBERG et al. 2001).

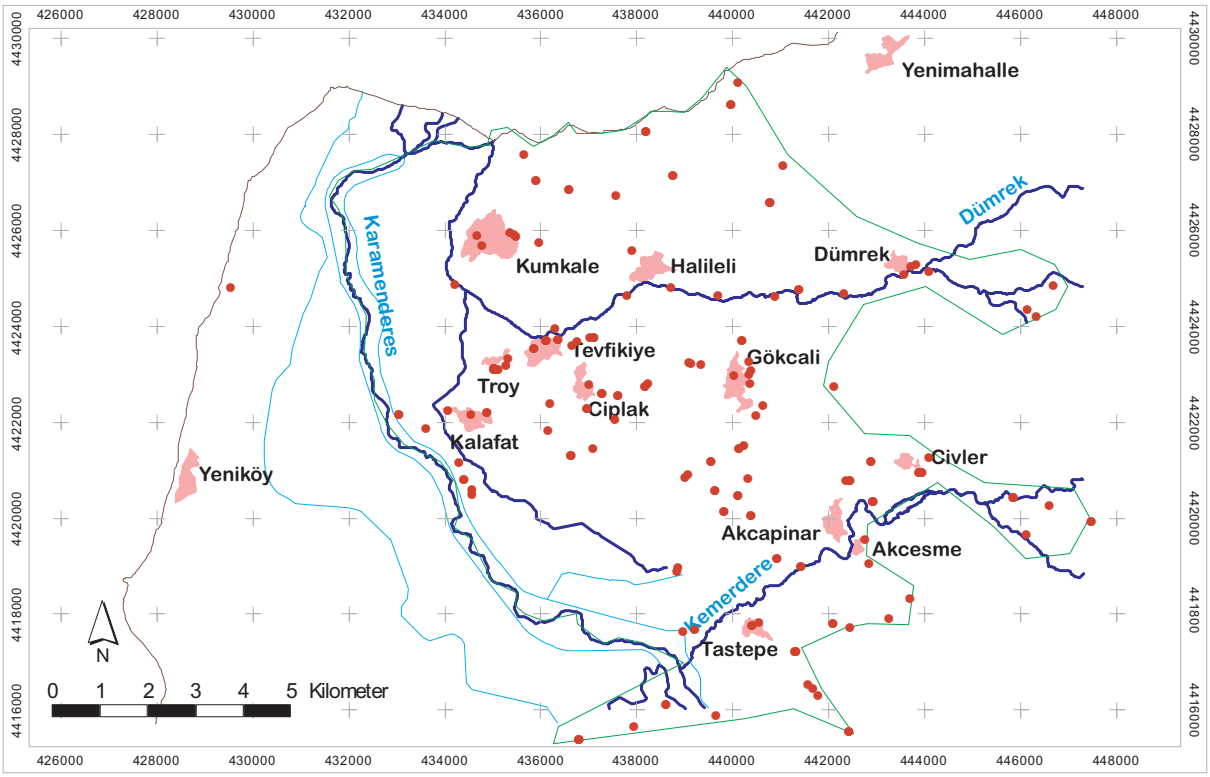

Figure 1: Area of the "Historical National Park Troia" and the locations sampled in 2001 and 2002 (darker dots). Map based on IKONOS data provided by the Troia-Team. Co-ordinates: UTM, WGS84.

Troy's importance dates back to the 8th century B.C., when Homer wrote down the Iliad and Odyssey, where he described the myths and the war that was fought in Troy's vicinity. Starting in the 17th century A.D. travellers and scientists tried to locate the place of the Troyan war and in 1863 Frank Calvert, after having studied Homer's descriptions, concluded that the Hisarlık must be the site of the historic Troy. Heinrich Schliemann, who visited the Troas at that time, started to excavate the hill in 1870 and he soon stated, that Hıssarlık was the place were the Troyan war took place. To understand the ongoing discussion of Troy's importance, three things must be distinguished: the place where the Troyan war happened, the place where Homer located his epic poem, and the place of today's Troy. Though the latter two are commonly seen to be identical, this must not necessarily be the case for all three of them. Therefore, every investigation should make clear which of the three Troys is meant. In this paper, Troy is seen as the place of the present archaeological excavations of the Tübingen/Cincinnati teams.

An important question about Troy is where the cold and hot springs described by Homer could have been located (Iliad, XXII v. 147). A set of springs which meet Homer's characteristics can be found near Pınarbaşi, but not only two, but more then eight water outlets near Miocene conglomerates can be found there – all of them bearing more or less the same hydrogeological parameters. One of the first systematic hydrogeological investigations to locate Homer's cold and hot springs was conducted by Rudolf Virchow in 1879. He measured the temperatures of several springs and rivers in the north-western Troas and discussed his findings (VIRCHOW 1879).

Since then no regional hydrogeological investigations were conducted in the National Park, though two deep wells are located north-east of Pınarbaşi: Pınarbaşi and Kokarna with average yields of 600—1500 and 50 Ls^{-1}, respectively (Yüzer 1997). Both wells are used for the water supply of Pınarbaşi and for irrigation purposes. Unfortunately, no more data is given for this water. Intensive hydrogeological and geothermal investigations are reported from the Çanakkale and the Ezine geothermal fields (e.g. MÜTZENBERG et al. 1992; BATTOCLETTI 1999). KAYAN (2000) focuses on the water supply of Troy without investigating the hydrogeological situation in the broader vicinity and the hydrogeochemical properties of the waters at all.

The whole investigation area is drained by two rivers: the Karamenderes, flowing from south to north, and the Dümrek flowing in an east—west-direction. Both rivers flow into the Çanakkale Boğazi (Dardanelles) north-west of Kumkale. YÜZER (1997) gives a catchment area of 1,584 km² and an average discharge of 12,900 $m^3 s^{-1}$ for the Karamenderes. A mean temperature of 15 °C and a mean annual precipitation of 600 mm is given for Çanakkale and the observation period 1990—2001 (pers. comm. Jeff Masters). Typical for the area is an extensive agricultural use by which the groundwater table was lowered to about 5 — 15 m below surface.

This paper describes the first findings of the hydrogeological investigations of the TU Bergakademie Freiberg. Since 2001 a total of 131 springs and surface waters were measured and 44 water samples taken to be analysed in the laboratory. Yet, no indication for a hot and cold spring near Troy could be found – which might not be surprising, as Strabo 2000 years ago describes in his Geographica, that the hot spring had already disappeared at the time of his visit (Geographica XIII 1,43).

2 Investigations

In summer 2001 and 2002 a total of 131 springs, bore holes and surface streams in an area of approximately 120 km² within the "Historical National Park Troia" have been visited, most of them twice (fig. 1). At each site the on-site parameters temperature, conductivity, redox-potential, oxygen, and pH-value were evaluated with a Myron P6 multi-parameter probe and the flow measured. Based on these results 44 representative locations including the historical sampling sites of Virchow were selected for water sampling. At each of those sampling points, four water samples were taken to be analysed for base- and acid-capacity (sample 1: 250 mL), NO_3^{2-}, NO^{2-}, PO_4^{2-}, and $Fe^{2+/3+}$ (sample 2: 250 mL, filtered through Sartorius 0.45 cellulose nitrate filter), main ions (sample 3: 250 mL, filtered through Sartorius 0.45 cellulose nitrate filter) and trace elements (sample 4: 50 mL, filtered through Sartorius 0.45 cellulose nitrate filter and acidified with ultra-pure HNO_3). Samples 1 and 2 were analysed on-site with a Hach Photometer DR 890 and a Hach Digital Titrator. Samples 3 and 4 were stored in a cool place within the Excavation House and analysed at the TU Bergakademie Freiberg for main anions (IC,

photometry, ion selective probe) and TU Dresden – Tharandt for trace elements (ICP-MS).

As the investigations described here were the first hydrogeological investigations of this kind in the National Park, we measured as many trace elements as possible, to find out, which of them could be used as natural tracers in the area: Li, Ni, Zn, Sr, Ba, Co, U, Rb, Tl, Sb, Ce, Cu, Mo, Eu, As, Sn, Cd, Pb, Bi, In, Cs, Mn, La, Tm, Lu, Cr, Nd, Ho, Ag, Er, Zr, Sm, Dy, W, Be, Pr, Hf, Gd, Tb, Yb, Th. In future studies this list will be reduced to the important parameters only (fig. 4).

In addition to the chemical parameters, three conductivity, pressure, and temperature probes were installed within the research area during the field investigations (fig. 3). Two of them still measure the parameter changes at Düden Spring near Calvert's Farm and at the outflow of the cave spring (squares tu 14/15). Furthermore, two tracer tests, one with sodium chloride, the other one with Na-fluorescein were conducted between shaft 4 and the cave spring's entrance.

3 First Results and Conclusions

All the waters in the National Park have a pH between 6.5 and 8.5 and are therefore well buffered in the range of the $CaCO_3$-buffer. Their temperature is between 16.4 and 31.9 °C, whereas the higher temperatures are an indication for shallow waters with lower residence times and the lower temperatures indicate ground water of deeper strata. Conductivity ranges between 360 and 5,560 µS cm^{-1} (fig. 2). Redox-potentials of natural waters are within a range of 60 and 430 mV, and the chlorinated waters from the deep well near Halileli between 710 and 900 mV (used as public water supply in Troy).

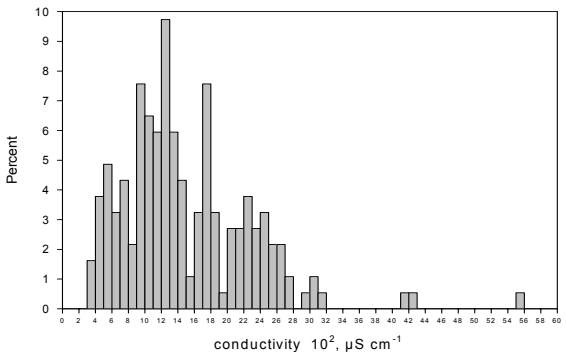

Figure 2: Histogramm of the conductivities in the Historical National Park Troia area (185 data sets).

Cluster analyses (average linkage) show, that the Troyan waters can be classified into three water types, with a total of eight subtypes. The detailed interpretation of those types is still under way, but the three main types can be interpreted as follows: Type 1 are waters with a conductivity range of 0.4—1.9 mS cm^{-1} (75 %), Type 2 waters range between 1.9 and 4 mS cm^{-1} (23 %),

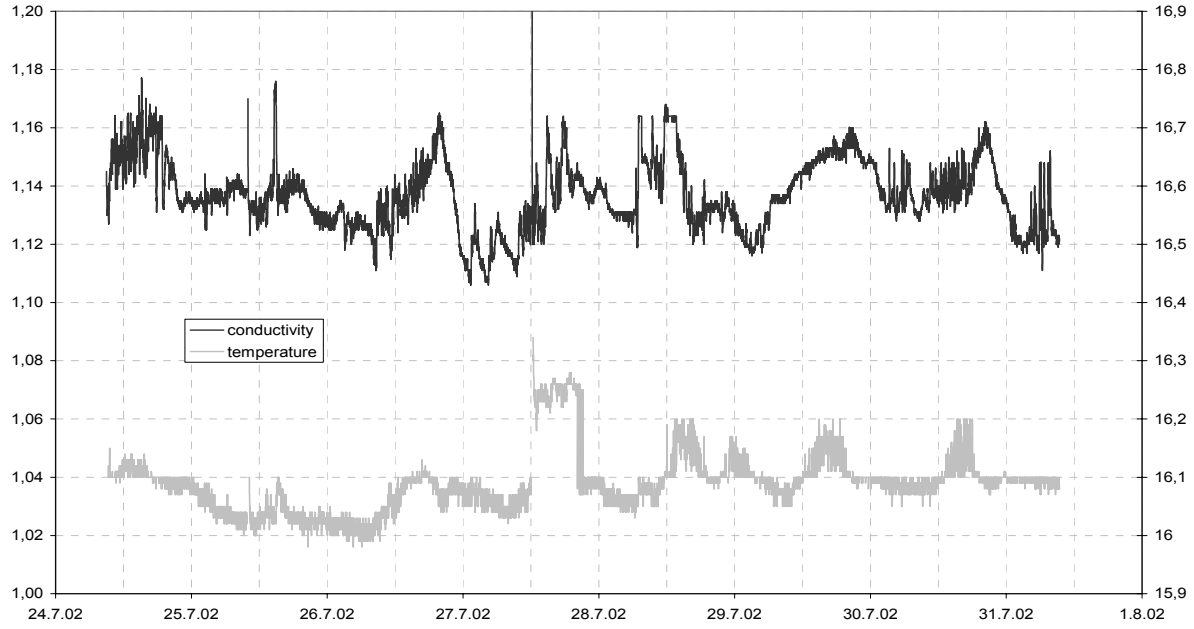

Figure 3: Temperature and conductivity distribution within the Troyan spring cave (conductivity: left scale, upper graph; temperature: right scale, lower graph).

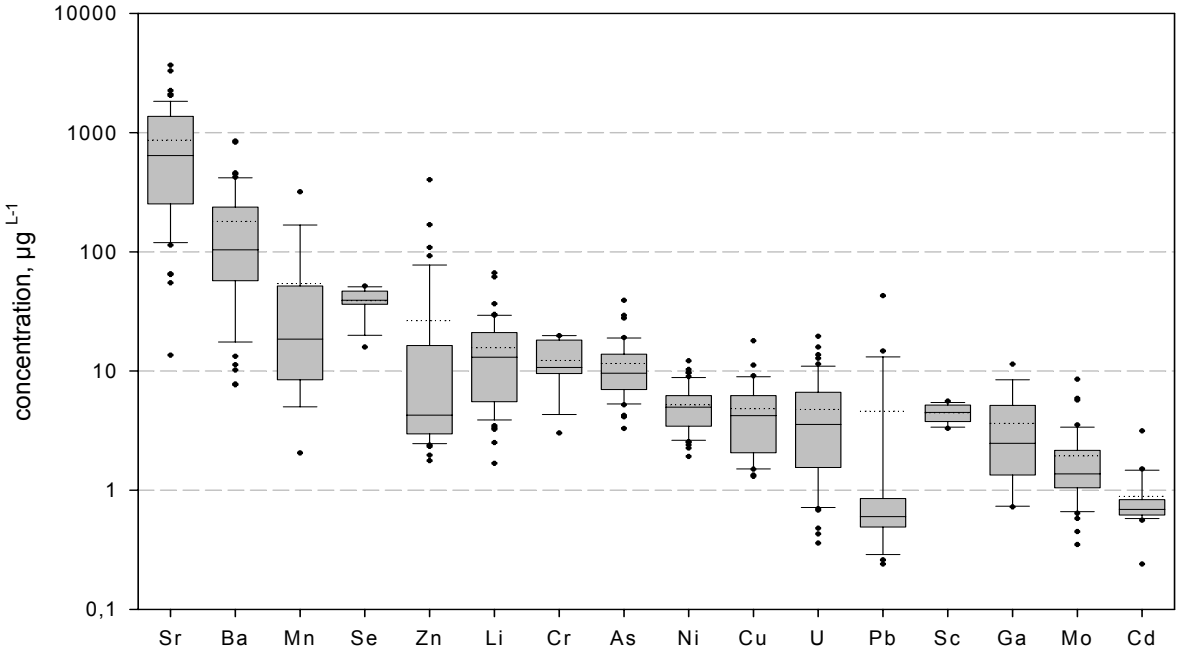

Figure 4: Box plot graph of trace elements in the Troyan waters. Dotted horizontal line: mean; solid horizontal line in box: median; 10th, 25th, 75th, and 90th percentiles. Outliers are given as crosses.

and Type 3 waters have conductivities above 4 mS cm^{-1} (2 %). Investigating the spatial distribution of those waters shows, that the volcanic and Mesozoic rocks in the south east of the area investigated, the surface waters and the wells in the alluvial plain mainly belong to type 1, while Type 2 and 3 waters are concentrated at the Troy ridge. A connection to the geological formations could not yet be established, but cannot be excluded from the first results. Very similar is the pH-distribution, with the lower pH-values generally related to higher and the higher pH-values related to lower conductivities.

Characteristic for many waters analysed in the National Park are the high NO_3^--contents of up to 330 mg L^{-1}. Most of those waters are used for drinking purposes, not necessarily as public water supply, and more than half of them exceed the recommended EU drinking water standard of 25 mg L^{-1}. A clear interpretation can be given for the extreme high NO_3-contents of the springs north of Tevfikiye and this situation might be seen as an indicator for the other height NO_3^--contents in the area as well. Above the springs the inhabitants have small farm lands with chicken, cattle, and goats. As the protective layer above the springs is only about 20 m thick and consist of limestone, sandstone, and siltstone, the animals' excrements pass through those sediments very quickly, resulting in the extreme NO_3^{2-}-mass concentrations.

One of the most important trace elements in the Troyan waters is Sr (fig. 4), as it is strongly liked to the three Troyan water types. Sr mass concentrations range between 14 and 3,690 µg L^{-1} with higher mass concentrations between Kumkale and Yenimahalle and south of a line between Gökçali and Çiplak. Rb/Sr ratios are not very selective, as they show a strong log-normal distribution, with the highest values at the spring cave and Düden spring. Interestingly, this shows that the rock's source for the Sr and Rb waters seems to be of a common origin, which can not be deduced from the mass concentrations of those two elements alone.

Zn, Cu, and Pb can easily be used to trace back tab waters. No correlations between the 3 water types and those heavy metals can be found, but to metal water pipes used. In the case of a well south of Çiplak, which was sampled in 2001 and 2002, this situation can be studied exemplified: in 2001 the well had a well head made of metal and a pipe containing Pb. In 2002 the well head was removed and the mass concentrations of Zn, Cu and Pb decreased significantly (Zn: 400 to 50; Cu: 18 to 7; Pb: 10 to 1 µg L^{-1}).

Arsenic seems to be a problematic element in the Historical National Park, because nearly 50 % of

the analysed waters exceed the EU drinking water limit of 10 µg L^{-1}. Those waters are used for irrigation, and cattle watering tanks. KNACKE-LOY (1994) already noticed that Troyan pottery contains unusually height arsenic contents. Thus, the arsenic in the Troyan water might reflect this local anomaly, too. Because there is no correlation between the three Troyan water types and the arsenic content, the sources for the arsenic in the water are not clear, yet.

Due to the high pH-values, most of the REEs analyzed are below the detection limit. With the sampling and analyzing technique used, they are therefore not selective for the Troyan waters. From the data presented above, it can be deduced, that future hydrogeological studies must include environmental isotopes, such as $\delta^{18}O$, $\delta^{2}H$, or $\delta^{14}C$ or Sr-isotope ratios. Such studies were not possible within the framework of these first investigations.

As a first result, it can be concluded, that some of the Troyan waters should not longer be used as drinking water due to the height NO_3^{2-} or metal contents. Furthermore, three different water types can be found in the Historical National Park Troia, which seem to be connected to the different geological strata of the Neogene, Quaternary and Palaeozoic as well as volcanic rocks. It is not clear yet, from where the water at the archaeological site of Troy (spring cave) comes from, but due to the low conductivity of the Troy waters, the source must be different from the shallow waters of the Troy ridge. Waters similar to those of the spring cave can be found near Paşa Tepe, north of Gökçali, and Düden spring.

4 Acknowledgements

The authors want to express their gratitudes to the Troia-Teams of Tübingen (Manfred Korfmann) and Cincinnati (Brian Rose), who gave us the chance to conduct our hydrogeological investigations. İlhan Kayan introduced us to the local quaternary geology and his students were of great help for the contact to the local inhabitants of the Historical National Park Troia. Having our Freiberg colleagues Katrin Bergmann and Pia Lippmann with us in Troy was of great help, because they mapped the area geologically and gave us many hints of where to find springs or bore wholes. Of great help were our laboratory assistants Peter Volke and Hajo Peter.

Special thanks to Ernst Pernička, who supported us in Freiberg and who opened up the gate to this interesting research area near Troy. Also special thanks to Jana Göbel, who gave us the results of her unpublished PhD-thesis and many literature references.

This work has been financed by the DFG Troia-Project, the "Friends of Troy", by the TU Bergakademie Freiberg and private sources of the authors.

5 Literature

ARCHÄOLOGISCHES LANDESMUSEUM BADEN-WÜRTTEMBERG, TROIA-PROJEKT DER EBERHARD-KALRS-UNIVERSITÄT TÜBINGEN, BRAUNSCHWEIGISCHES LANDESMUSEUM, HERZOG ANTON ULRICH-MUSEUM, KUNSTMUSEUM DES LANDES NIEDERSACHSEN & KUNST- UND AUSSTELLUNGSHALLE DER BUNDESREPUBLIK DEUTSCHLAND (2001): Troia – Traum und Wirklichkeit. – 1st ed., 487 p.; Stuttgart (Theiss).

BATTOCLETTI, L. (1999): Geothermal Resources of Turkey. – client: Idaho National Engineering & Environmental Laboratory; Alexandria (Bob Lawrence & Associates).

KAYAN, İ. (2000): The Water Supply of Troia. – Studia Troica, **10**: 135—145, 12 Abb.; Mainz.

KNACKE-LOY, O. (1994): Isotopengeochemische, chemische und petrographische Untersuchungen zur Herkunftsbestimmung der bronzezeitlichen Keramik von Troia. – Heidelberger geowissenschaftliche Abhandlungen, **77**: 193, 63 fig., 25 tab., 7 app.; Heidelberg.

MÜTZENBERG, S., BALDERER, W. & RAUERT, W. (1992): Environmental isotope study of saline geothermal systems in western Anatolia, Canakkale, Turkey. – Proceedings – International Symposium on Water-Rock Interaction, **7**: 1317—1320, 4 fig.; Edmonton.

STRABO & GROSKURD, C. G. (1988): *Geographica* – Erdbeschreibung in Siebzehn Büchern **1—3**. – reprint; Hildesheim (Olms).

VIRCHOW, R. (1879): Beiträge zur Landeskunde der Troas. – Abh. Königl. Akad. Wiss. Berlin Phys. Klas., **3**: 1—190, 2 app.; Berlin.

YÜZER, E. (1997): Hydrogeology of Northwestern Turkey. – In: SCHINDLER, C. & AKSOY, A. – p. 125—137, 2 fig., 10 app.; Zürich (vdf, Hochschulverl. an der ETH Zürich).


BERGAKADEMIE
TECHNISCHE
UNIVERSITÄT
FREIBERG